Conformational changes and complex formation in DNA mismatch repair

Inauguraldissertation

zur Erlangung des Grades

Doktor der Naturwissenschaften

- Dr. rer. nat. -

des Fachbereiches Biologie und Chemie, FB08

der Justus-Liebig-Universität Gießen

vorgelegt von

Dipl.-Biol. Andreas Daniel Marx

Gießen, 2013

Die vorliegende Arbeit wurde am Institut für Biochemie (FB08) der Justus-Liebig-Universität Gießen, zwischen März 2009 und Juni 2013, durchgeführt. Die Betreuung wurde von Prof. Dr. Peter Friedhoff übernommen. Gefördert wurde die Arbeit durch die Programme GRK 1384 (International Research Training Group) der Deutschen Forschungsgemeinschaft und FP7 HEALTH-F4-2008-223545 (mismatch2model) der Europäischen Union. Zusätzlich wurde die Arbeit durch das International Giessen Graduate Centre for the Life Sciences (GGL) unterstützt.

Dekan	**Prof. Dr. Holger Zorn** Institut für Lebensmittelchemie und Lebensmittelbiotechnologie, FB08 Justus-Liebig-Universität Gießen Heinrich-Buff-Ring 58, 35392 Gießen
Erstgutachter	**Prof. Dr. Peter Friedhoff** Institut für Biochemie, FB08 Justus-Liebig-Universität Gießen Heinrich-Buff-Ring 58, 35392 Gießen
Zweitgutachter	**Prof. Dr. Michael Niepmann** Biochemisches Institut, FB11 Justus-Liebig-Universität Gießen Friedrichstrasse 24, 35392 Gießen

Erklärung

Ich erkläre: Ich habe die vorgelegte Dissertation selbständig und ohne unerlaubte fremde Hilfe und nur mit den Hilfen angefertigt, die ich in der Dissertation angegeben habe. Alle Textstellen, die wörtlich oder sinngemäß aus veröffentlichten Schriften entnommen sind, und alle Angaben, die auf mündlichen Auskünften beruhen, sind als solche kenntlich gemacht. Bei den von mir durchgeführten und in der Dissertation erwähnten Untersuchungen habe ich die Grundsätze guter wissenschaftlicher Praxis, wie sie in der „Satzung der Justus-Liebig-Universität Gießen zur Sicherung guter wissenschaftlicher Praxis“ niedergelegt sind, eingehalten.

Gießen, den 07.06.2013 _____

(Andreas D. Marx)

Danksagung

Ich danke …

Professor Dr. Peter Friedhoff für die Betreuung und Förderung über all die Jahre.

Professor Dr. Pingoud für die freundliche Aufnahme am Institut für Biochemie und die unermüdliche Begeisterung für die Wissenschaft.

Professor Dr. Niepmann für die Übernahme des Zweitgutachtens.

Dr. Joyce Lebbink, Dr. Michele Cristovao und Nicolaas Hermans, M.Sc., für die Zusammenarbeit im Projekt mismatch2model und den herzlichen Empfang in Rotterdam.

Dr. Anja und Dr. Marika für das Korrekturlesen.

den derzeitigen und ehemaligen Mitarbeitern am Institut für das großartige Gemeinschaftsgefühl im Labor und in der Freizeit. Die Zeit mit Euch werde ich sehr vermissen.

meiner Familie für all die Unterstützung in den letzten 31 Jahren.

meinen Berliner und Gießener Freunden.

den Lacrossern aus Gießen und Marburg.

List of publications

1. Cristovao, M., Sisamakis, E., Hingorani, M.M., Marx, A.D., *et al*., *Single-molecule multiparameter fluorescence spectroscopy reveals directional MutS binding to mismatched bases in DNA.* Nucleic Acids Res, 2012. 40(12): p. 5448-64.
2. Xiao, Y., Jung, C.P., Marx, A.D., *et al*., *Generation of DNA nanocircles containing mismatched bases.* Biotechniques, 2011. 51(4): p. 259-62, 264-5.
3. Winkler, I., Marx, A.D., *et al*., *Chemical trapping of the dynamic MutS-MutL complex formed in DNA mismatch repair in Escherichia coli.* J Biol Chem, 2011. 286(19): p. 17326-37.

Publication in preparation

1. Marx, A.D., *et al*., *Visualizing unspecific binding of proteins to DNA with FRET*.

Table of contents

List of abbreviations

% (v/v)	percentage in volume to volume
% (w/v)	percentage in weight to volume
[a]	fluorescence acceptor
[d]	fluorescence donor
[b]	fluorescence donor and acceptor
a.u.	arbitrary units
ADP	adenosine diphosphate
ATP	adenosine triphosphate
bp	base pair
BSA	bovine serum albumin
cf	correction factor
cc	closed circle
Da	Dalton
DNA	deoxyribonucleic acid
DOL	degree of labeling
dNTP	deoxyribonucleotide triphosphate
ds	double-strand
DTT	dithiothreitol
E. coli	*Escherichia coli*
e.g.	*exempli gratia* (for example)
EDTA	ethylene diamine tetra acetic acid
FRET	Förster Resonance Energy Transfer
HEPES	4-(2-Hydroxyethyl)piperazine-1-ethanesulfonic acid
HPLC	high performance liquid chromatography
HPNCC	Hereditary nonpolyposis colon cancer
IDLs	insertion-deletion loops
IPTG	Isopropyl β-D-1-thiogalactopyranoside
kb	kilo base pair
L	linear DNA
MMR	DNA mismatch repair
ND	not determined
nt	nucleotide
OD	optical density
oc	open circle
PAGE	polyacrylamide gel electrophoresis
PCR	polymerase chain reaction
rpm	rounds per minute
RT	room temperature
sc	supercoiled
SFM	scanning force microscopy
SG	SYBR Green I
smMFD	single-molecule Multiparameter Fluorescence Detection
ss	single-strand
Tris	tris(hydroxymethyl)aminomethane
U	units
UV	ultraviolet

Summary

The DNA mismatch repair system (MMR) plays a crucial role in maintaining genomic stability. It is capable of detection and correction of errors that arise during replication, for example base substitution mismatches or insertion-deletion loops. Hereditary nonpolyposis colon cancer is the most frequent form of hereditary colon cancer in humans and is caused by mutations of proteins in the MMR. Despite intensive investigations of several laboratories, there is still uncertainty about the composition of protein and DNA complexes and the role of the conformational changes involved. Therefore, the aim of this thesis was to establish fluorescence-based assays which allow the analysis of initial sub-steps in MMR. As the MMR is highly conserved and well-studied in *Escherichia coli*, these assays were developed for the *Escherichia coli* system.

To observe complex formations in MMR the phenomenon of Förster Resonance Energy Transfer was used. By labeling one component of the MMR with a donor and another one with an acceptor fluorophore, it was possible to observe a complex formation between those two components. A similar setup was used to determine conformational changes of one MMR component that carried both, the donor and acceptor fluorophore. Both reactions could be followed by spectroscopic detection of the fluorescence signals. Several assays of this thesis required the generation and testing of suitable DNA constructs and fluorescence modification of different protein variants. For the fluorescent dye labeling of proteins, single-cysteine variants were selected from a set of variants which were originally generated for crosslinking studies. A possible disturbance of the protein activity by the fluorophores was excluded as the selected protein variants (MutS R449C D835R, MutL H297C, and MutH S85C) were not influenced in activity after fluorescent dye labeling.

Changes in fluorescence intensity as well as FRET efficiency were monitored during each assay to visualize involved conformational changes and complex formations. Fluorescence spectra were always recorded as a quality control to ensure that the observed intensity changes were due to FRET. The analyzed processes in MMR were MutS mismatch recognition, MutS bending DNA, MutS sliding clamp formation, MutS-MutL complex formation, MutL interaction with DNA, MutL-MutH complex formation, and MutH forming and leaving the incision complex. Kinetic data sets for selected sub-steps were collected and used for the development of a kinetic model for the whole MMR system in frame of the European FP7 project mismatch2model. With this collection of fluorescence assays it is now possible to gain new insights into the sub-steps of MMR which helps to understand the intricate MMR process in detail. Currently, the fully active, fluorescent dye labeled proteins which were generated in frame of this thesis are used in single-molecule studies of the MMR, for example in a magnetic tweezers setup combined with fluorescence detection.

Zusammenfassung

Das DNA-*mismatch*-Reparatursystem (MMR) spielt eine zentrale Rolle bei der Aufrechterhaltung der Stabilität des Genoms. Es ist in der Lage Replikationsfehler zu erkennen und zu korrigieren. Zu diesen Fehlern gehören Basenfehlpaarungen und Insertions-Deletions-Schleifen. Hereditäres nicht-polypöses kolorektales Karzinom ist die häufigste vererbbare Darmkrebserkrankung beim Menschen und wird durch Mutationen in Proteinen des MMRs ausgelöst. Trotz intensiver Forschungsarbeiten verschiedenster Labore bestehen immer noch Unklarheiten über die Zusammensetzung von Protein- und DNA-Komplexen und die Rolle der beteiligten Konformationsumwandlungen. Aus diesem Grund war das Ziel der vorliegenden Arbeit die Entwicklung und Etablierung fluoreszenzbasierter Analyseansätze, die eine Untersuchung der ersten Teilschritte des MMRs ermöglichen. Da das MMR hoch konserviert und in *Escherichia coli* gut untersucht ist, wurden diese Analyseansätze für das *Escherichia coli*-System entwickelt.

Um Komplexbildungen im MMR beobachten zu können, wurde das Phänomen des Förster-Resonanz-Energietransfers (FRET) ausgenutzt. Die Markierung einer Komponente des MMRs mit einem Donor- und einer anderen mit einem Akzeptorfluorophor ermöglichte die Beobachtung von Komplexbildungen zwischen diesen beiden Komponenten. Ein ähnlicher Versuchsaufbau wurde für die Untersuchung von Konformationsumwandlungen verwendet. In dem Fall trug eine Komponente des MMRs beide Fluorophore, den Donor und den Akzeptor. Beide Reaktionen konnten mittels spektroskopischer Detektion der Fluoreszenzsignale verfolgt werden. Einige Analyseansätze dieser Arbeit setzten die Herstellung und Überprüfung von passenden DNA-Substraten und die Fluoreszenzmarkierung verschiedener Proteinvarianten voraus. Für die Fluoreszenzmarkierung von Proteinen wurden Einzelcysteinvarianten aus einer Reihe von Varianten ausgewählt, die ursprünglich für *crosslinking*-Studien generiert wurden. Eine mögliche Störung der Proteinaktivität durch die Fluorophore konnte ausgeschlossen werden, da die verwendeten Proteinvarianten (MutS R449C D835R, MutL H297C und MutH S85C) nach der Fluoreszenzmarkierung keine Beeinträchtigung in ihrer Aktivität zeigten.

Änderungen der Fluoreszenzintensität sowie der FRET-Effizienz wurden während allen Analyseansätzen aufgezeichnet und visualisierten die beteiligten Komplexbildungen und Konformationsumwandlungen. Bei jedem Analyseansatz wurden zusätzlich Fluoreszenzspektren aufgezeichnet, um sicherzustellen, dass die beobachteten Effekte auf FRET basierten. Die untersuchten Prozesse des MMRs umfassten die MutS *mismatch*-Erkennung, MutS induzierte Biegung der DNA, MutS *sliding clamp*-Bildung, MutS-MutL Komplexbildung, MutL Interaktion mit DNA, MutL-MutH Komplexbildung und die Bildung des *incision complex* durch MutH. Es wurden kinetische Datensätze aus einigen Analyseansätzen ausgewählt und für die Erstellung eines kinetischen Modells des gesamten MMRs im Rahmen des europäischen FP7 Projektes mismatch2model verwendet. Mit dieser Sammlung von

fluoreszenzbasierten Analyseansätzen ist es nun möglich neue Einblicke in die Teilschritte des MMRs zu erhalten, die dabei helfen können die komplexen Abläufe besser zu verstehen. Die voll funktionstüchtigen, fluoreszenzmarkierten Proteine, welche im Rahmen dieser Arbeit generiert wurden, werden derzeit in Einzelmolekül-FRET-Studien zur Untersuchung des MMRs verwendet, zum Beispiel in einer fluoreszenzgekoppelten *magnetic tweezers*-Apparatur.

1. Introduction

DNA is the carrier of the genetic information of every organism. Its stability is constantly threatened by intrinsic and extrinsic factors. Environmental agents like the ultraviolet (UV) component of sunlight, ionizing radiation or genotoxic chemicals can cause alterations in DNA structure. Reactive oxygen species arising as by-products of normal cellular metabolism are a permanent enemy to DNA integrity [1]. Replication errors produced by the DNA polymerase may lead to miscoding or mutations, if unrepaired [2]. To ensure genomic stability, every organism possesses a variety of repair processes, each addressing different DNA damages. The most common DNA damages, with their source and possible repair pathway are summarized in Figure 1.1.

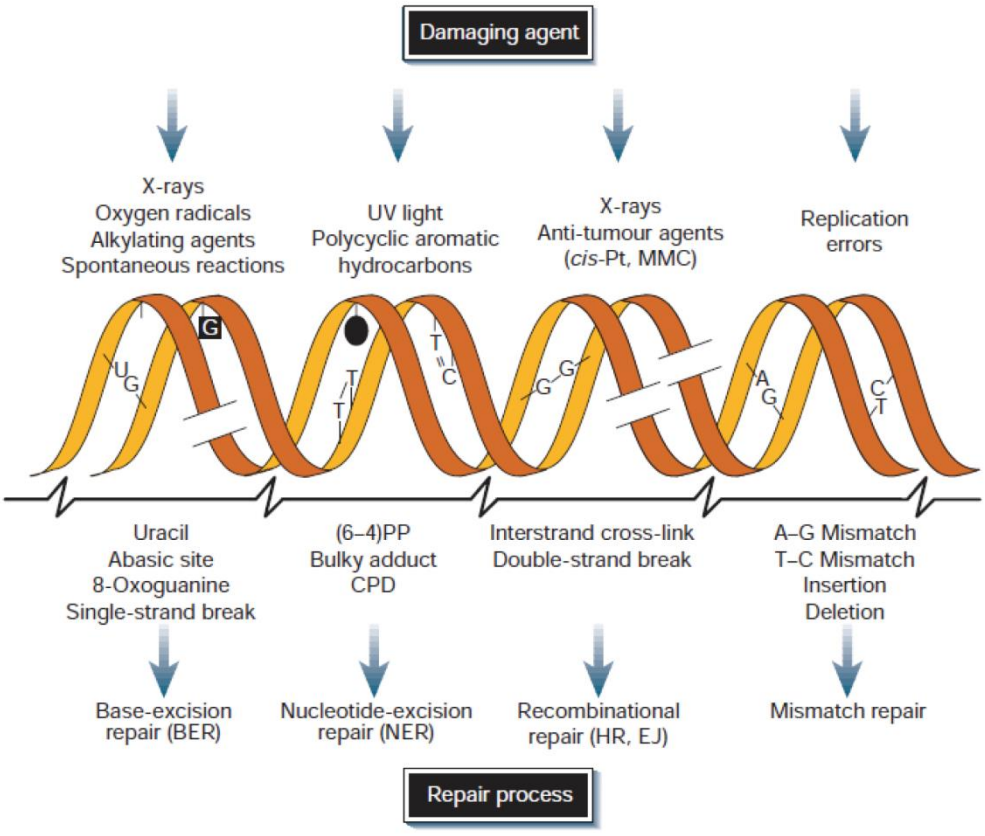

Figure 1.1: Common DNA damages and repair mechanisms
DNA damaging agents (top); examples of resulting DNA lesions (middle); and repair pathways to remove each lesion (bottom). The figure was adapted from Hoeijmakers, 2001 [1].

1.1 DNA mismatch repair

One of the systems that respond to DNA damages is the DNA mismatch repair system (MMR). It is capable of detection and correction of errors that arise during replication, for example base substitution mismatches or insertion-deletion loops (IDLs) [3] [4]. The MMR also affects the cellular processes of meiotic and mitotic recombination, DNA-damage signaling, apoptosis, immunoglobulin class switching, somatic hypermutation and triplet-repeat expansion [5]. The MMR system is highly conserved and mechanistically similar in prokaryotes and eukaryotes [6]. Inactivation of MMR leads to an increased mutability of 50-1000 fold [7]. In humans an inactive DNA mismatch repair system is the cause of hereditary nonpolyposis colon cancer (HNPCC) [8] [9].

1.2 DNA mismatch repair in *Escherichia coli*

In *Escherichia coli* (*E. coli*) the initiation of the MMR starts with the recognition of a mismatch or IDL by the protein MutS. After mismatch recognition MutS undergoes nucleotide dependent conformational changes and transforms into a sliding clamp [10] [11] [12]. This activated form of MutS is able to recruit the next key protein in MMR which is MutL [13]. The homodimeric MutL is also able to adopt different conformations coupled to different nucleotide bound states of the subunits [14]. In *E. coli*, MutL couples the mismatch recognition of MutS with the strand discrimination factor MutH [15] [16]. The MMR system is active shortly after replication when GATC sites remain transiently hemimethylated [17]. This hemimethylated DNA allows strand discrimination by endonuclease MutH as the protein is only able to cleave the newly synthesized, unmethylated DNA strand which harbors the error [18]. In downstream repair reactions, the nicked DNA is unwound by the helicase UvrD and stabilized by single-strand binding proteins. Exonucleases are able to digest the erroneous DNA strand beyond the misincorporated base and DNA polymerase III resynthesizes the gapping DNA part. The remaining nick is sealed by ligases [7]. Reactions of the MMR system are shown in Figure 1.2.

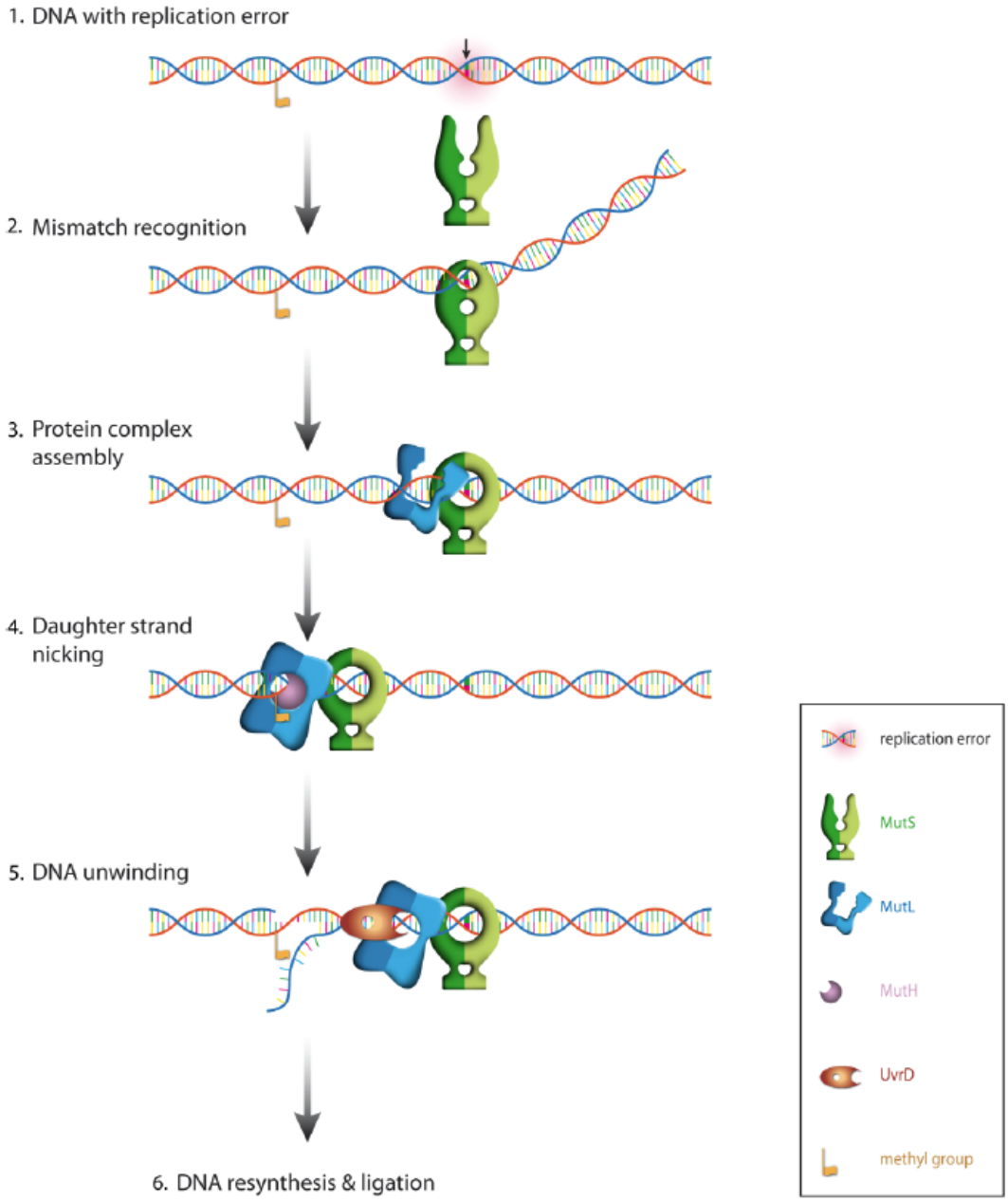

Figure 1.2: DNA mismatch repair in *Escherichia coli*
MutS (green) recognizes a mismatch and recruits MutL (blue). MutL enables endonuclease MutH (globular magenta) to bind and cleave its target site in the erroneous DNA strand. MutH is replaced by helicase UvrD (elliptical magenta) which unwinds the DNA to allow exonucleases the partially digestion of the erroneous DNA strand. The digested DNA is resynthesized and ligated. The figure was adapted from Lebbink, 2010 [19].

1.3 Coupling of mismatch recognition and strand discrimination

Despite intensive investigations of various groups, the coupling of mismatch recognition with the strand discrimination signal in MMR remains controversy [7] [20] [17]. There are different models proposing different mechanisms for the reaction. These models can be separated in models describing a *cis* or a *trans* activation of downstream factors like MutH. *Cis* activation is characterized by sliding [21] [22], polymerization [23], accumulation [24] or translocation [11] [25] of MutS and / or MutL along the DNA helix. Whereby *trans* activation is characterized by overcoming the distance between the mismatch and the strand discrimination signal via bending or looping of the DNA [26] [27]. A further separation can be performed by dividing these models in stationary models in which MutS and MutL remain bound to the mismatch or remain in the vicinity of the mismatch and mobile models which suggest a movement along the DNA. Three popular models are illustrated in Figure 1.3 (modified after Larrea *et al*., 2010 [6]).

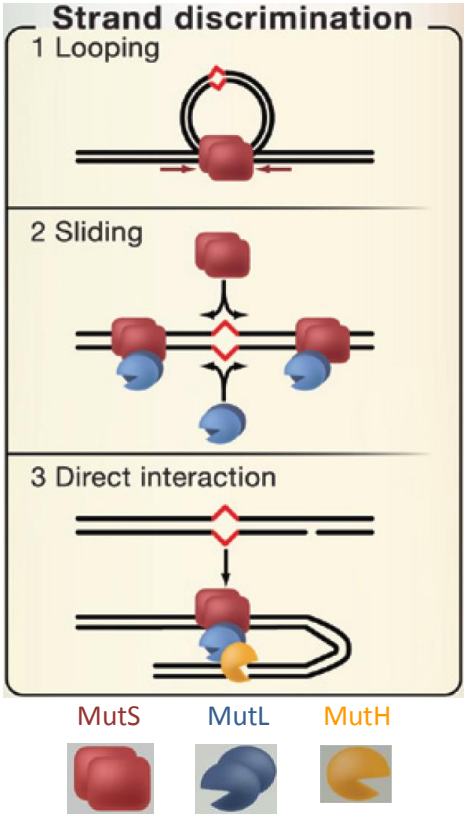

Figure 1.3: Models for coupling the mismatch recognition with strand discrimination
1 MutS is able to form DNA loops. Some models describe that this looping enables MutS to reach the GATC site and activate other components of the MMR. **2** MutS and MutL are able to facilitate conformational changes which are coupled to nucleotide exchanges. Some models describe that MutS transforms into a sliding clamp after mismatch recognition and verification and thus becomes competent to diffuse along the DNA helix and activate other components of the MMR. **3** MutS bends the DNA upon mismatch binding. Some models describe that this bending may help to bridge the distance between the mismatch and strand discrimination signal and thus enables activation of downstream MMR factors as MutH. The picture was modified after Larrea *et al*., 2010 [6].

1.4 MutS

MutS acts as a mismatch sensor and recognizes heteroduplex DNA [28] [29]. An ADP-bound, dimeric MutS is able to intercalate phenylalanine 36 into DNA upon mismatch binding and stabilizes the DNA-MutS complex [28] [29]. Following conformational changes coupled to nucleotide exchange in the subunits of MutS activate downstream repair factors like MutL [30]. The MMR-relevant form of MutS exists as a dimer as well as a tetramer, whereby the dimeric form alone is already able to facilitate the MMR reaction [31] [32]. The mutation D835R, used by Manelyte *et al*., leads to a disturbance in the tetramerization interface at the C-terminal domain. Proteins carrying this mutation cannot form tetramers anymore. In this thesis, all MutS variants used also contained the D835R mutation because it reflects a simplification of the MMR system as the biological function of the tetrameric form of MutS still remains elusive. The MutS variants used here were cysteine-free variants, in which all native cysteines had been mutated to serine, alanine or valine [33]. With an additional mutation, the arginine at position 449 was mutated to cysteine (R449C) [34] enabling fluorescent-dye labeling of MutS via a maleimide crosslinker [35]. The position 449 was chosen because an attached fluorophore was unlikely to disturb DNA binding or MutL-recruitment [36]. For investigations of the MutS-MutL-binding interface, the variant D246C was used in exchange for the R449C variant. The latter allowed a comparison of FRET efficiencies between different fluorophore positions in MutS in combination with a fixed fluorophore position in MutL [37]. Position 246 is nearby the DNA-mismatch-binding domain of MutS and a fluorophore attached to this position generates a high FRET signal to a MutL fluorescence labeled within the N-terminus.

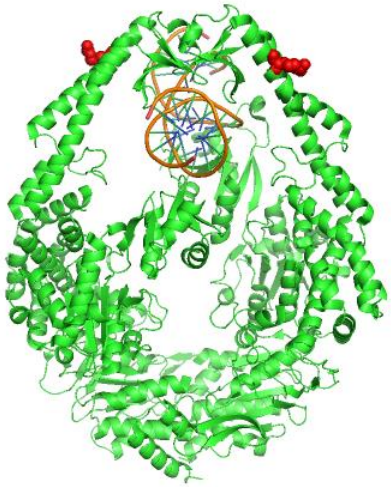

Figure 1.4: MutS dimer bound to DNA containing a G:T mismatch
PyMOL-modified cartoon view of the crystal structure of MutS dimer (green) with highlighted positions 449 (red spheres), where a cysteine enables fluorescent dye labeling via maleimide crosslinking. DNA (blue and orange). A truncated version of MutS had been used to allow the crystallization (residues 1-800). Modified after pdb code 1e3m [28].

1.5 MutL

MutL couples mismatch recognition by MutS with the strand discrimination of MutH [16]. In *E. coli*, MutL is a homodimer consisting of a N-terminal domain which is connected via a long, flexible linker to the C-terminal domain. A dimer is able to bind two nucleotides. MutL undergoes large conformational changes driven by an ATPase cycle [14] and can adopt open or condensed conformations [38]. As for MutS, MutL variants used in this thesis did not possess any native cysteine anymore [39]. Histidine at position 297 was mutated to cysteine (H297C) [34] to enable fluorescent dye labeling of MutL at the N-terminal domain [35] (Figure 1.5).

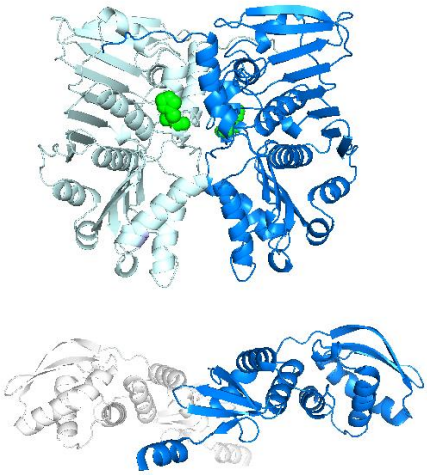

Figure 1.5: MutL dimer
PyMOL-modified cartoon view of the crystal structure of MutL. **Top:** N-terminal domains of a MutL dimer (light and dark blue) with highlighted positions 297 (green spheres) which carry the cysteine for later fluorescent dye labeling. **Bottom:** C-terminal domains of a MutL dimer (light and dark blue). Linker connecting N- and C-terminal domains are not shown. Modified after pdb code 1b63 [14] and 1x9z [40].

1.6 MutH

The endonuclease MutH of *E. coli* is a monomer and binds and cleaves hemimethylated and unmethylated GATC sequences [41]. In *E.* coli, newly synthesized DNA strands remain transiently unmethylated at GATC sequences until Dam-methyltransferase methylates the contained adenine [42]. The transiently hemimethylated status of the DNA serves as a strand discrimination signal as the newly synthesized and yet unmethylated DNA strand is cleaved by MutH [41]. The DNA binding ability of MutH at physiological relevant ionic strength (100 - 160 mM) [43] is so low that it needs to be recruited to DNA in a MutS, MutL, and mismatch dependent manner [44]. However, at low ionic strength MutH is able to cleave DNA without the assistance of MutS and MutL.

The only native cysteine in MutH was mutated to serine to create a cysteine free variant [45]. Serine at position 85 was mutated to cysteine (S85C) [46], which is placed in a loop structure of MutH, where a later attached fluorophore most likely is not disturbing the activity or interactions of MutH. The mutation of glutamic acid to alanine at position 77 in MutH leads to a catalytically inactive protein, which is still able to bind DNA [47] [48]. This variant of MutH was used to analyze MutH binding to DNA without cleaving the DNA.

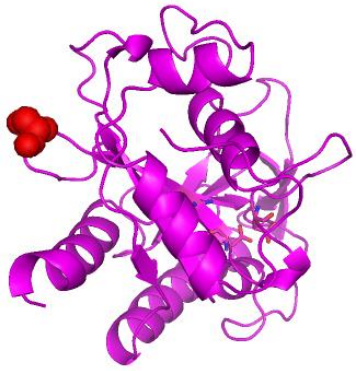

Figure 1.6: MutH
Modified cartoon view of the crystal structure of MutH in PyMOL. An introduced cysteine in a loop region at position 85 is highlighted (red spheres). This position enables later fluorescent-dye labeling of the protein via maleimide crosslinking. Modified after pdb code 1azo [49].

1.7 Aim: Visualization of sub-steps in MMR

The MMR was heavily studied for decades but the composition of protein and DNA complexes and the role of involved conformational changes remains still elusive. To understand the intricate MMR in detail it was essential to take a closer look at the individual sub-steps involved. Therefore, the aim of this thesis was to develop fluorescence-based assays that allow a visualization and analysis of these sub-steps, beginning with the mismatch recognition by MutS and ending with the formation and dissociation of the incision complex by MutH.

To enable the observation of complex formations and conformational changes the phenomenon of FRET was used. Different components of the MMR needed to be labeled with a donor and/or an acceptor fluorophore for this purpose. Therefore, the first objective was to find suitable positions in the MMR proteins for a possible attachment of a fluorophore and to test the activity of these variants after fluorescence dye labeling. The second objective was the generation of suitable DNA substrates which were required for the formation of certain sub-steps in MMR. As some of the analyzed complex formations were highly dynamic, a circular DNA needed to be generated which also contained a mismatch to initiate the MMR reaction. To monitor a MutS- and MutL-dependent recruitment of MutH and therefore the formation of the incision complex, another DNA was required which additionally possessed a fluorophore. Finally, the generated DNA constructs and the fluorescence labeled protein variants needed to be selected and combined within a suitable fluorescence setup for each individual FRET assay to allow the observation of conformational changes and complex formations.

2. Experimental Procedures

All standardized molecular biological procedures had been performed after *Current Protocols in Molecular Biology* [50]. Schematic views of reactions in chapter 3 were drawn with the software Adobe Illustrator. Statistical and mathematical calculations were performed with the software Microsoft Excel, OriginPro 8.5 and GraphPad QuickCals.

2.1 Materials

Table 2.1: protein and DNA markers

Marker	Manufacturer
Page ruler unstained protein ladder	Thermo Scientific
pUC8 Mix Marker	Thermo Scientific
GeneRuler 1 kb DNA ladder	Thermo Scientific
GeneRuler Ultra low range DNA ladder	Thermo Scientific

Table 2.2: DNA and protein purification kits

Kit	Manufacturer
Wizzard Plus SV Minipreps	Promega
Wizzard Plus SV Midipreps	Promega
Wizzard SV Gel and PCR clean-up system	Promega
Zeba Desalting spin columns 0.5 ml	Pierce
Zeba Desalting spin columns 5 ml	Pierce

Table 2.3: Proteins

Protein	Manufacturer
BSA	New England Biolabs
BamH1	Thermo Scientific
ExonucleaseI	Thermo Scientific
ExonucleaseIII	New England Biolabs
Lambda Exonuclease	New England Biolabs
MutS / MutL / MutH	(own production)
Nb.BtsI	New England Biolabs
Nt.BspQI	New England Biolabs
Pfu-Polymerase	(own production)
Pfusion-Polymerase	Thermo Scientific
Proteinase K	Thermo Scientific
$RecJ_F$	New England Biolabs
TaqI-Methyltransferase	New England Biolabs
T4 Ligase	Thermo Scientific
T4 DNA Polymerase	Thermo Scientific

Table 2.4: Reagents

Reagent	Manufacturer
Acetic acid	Roth
Acrylamide/Bis-acrylamide 40%, 29:1	AppliChem
Adenosine-5´-diphosphate	Sigma
Adenosine-5´-triphosphate	Sigma
Alexa Fluor^{R}-maleimide	Invitrogen
Aluminium sulfate	AppliChem
Agarose (Ultra PURE^{TM})	AppliChem
Ammonium persulfate	Merck
Ampicillin	AppliChem
Benzamidine	Sigma
Bromphenolblue	Merck
Coomassie brilliant blue (G250)	AppliChem
Coomassie InstantBlue	Expedeon
Dimethyl sulfoxide	Merck
Dithiothreitol	AppliChem
dNTPs	Roth
Ethanol	Roth
Ethidiumbromide	Merck
Ethylenediaminetetraacetic acid	Roche
Glycerol	AppliChem
Glycine	Roth
HEPES	AppliChem
Hydrochloric acid	AppliChem
Imidazole	AppliChem
InstantBlue Coomassie	Expedeon
Isopropyl-β-D-1-thiogalactopyranoside	AppliChem
Magnesium chloride	Merck
2-Mercaptoethanol	Merck
Ni-NTA-Agarose	Qiagen
Oligodeoxyribonucleotides	IBA, Eurogentec and Purimex
Phenylmethanesulfonyl fluoride	AppliChem
Phosphoric acid	Roth
Potassium chloride	Roth
Potassium hydroxide	Merck
Sodium chloride	AppliChem
Sodium dodecyl sulfate	Roth
Sucrose	Merck
Tetracycline	AppliChem
Tetramethylethylenediamine	Merck
Tris	AppliChem
Tris-(2-carboxyethyl)-phosphine	Merck
Tween 20	Merck

Table 2.5: Buffers
The pH was adjusted at RT.

MutS/L binding buffer (pH 7.9)

Tris-HCl	20 mM
NaCl	1 M
Imidazole	5 mM
Glycerol	10 % (v/v)

MutH binding buffer (pH 7.9)

Tris-HCl	20 mM
NaCl	1 M
Imidazole	5 mM

MutS/L washing buffer (pH 7.9)

Tris-HCl	20 mM
NaCl	1 M
Imidazole	20 mM
Glycerol	10 % (v/v)

MutH washing buffer (pH 7.9)

Tris-HCl	20 mM
NaCl	1 M
Imidazole	20 mM

MutS/L elution buffer (pH 7.9)

Tris-HCl	20 mM
NaCl	1 M
Imidazole	200 mM
Glycerol	10 % (v/v)

MutH elution buffer (pH 7.9)

Tris-HCl	20 mM
NaCl	1 M
Imidazole	200 mM

MutS/L HPLC buffer (pH 8.0)

HEPES-KOH	10 mM
EDTA	1 mM
KCl	200 mM
Glycerol	10 % (v/v)

MutH HPLC buffer (pH 8.0)

HEPES-KOH	10 mM
EDTA	1 mM
KCl	500 mM

Fluorescence buffer FB125 (pH 7.5)

HEPES-KOH	25 mM
KCl	125 mM
$MgCl_2$	5 mM
Tween 20	0.05 % (w/v)

Fluorescence buffer FB000 (pH 7.5)

HEPES-KOH	25 mM
$MgCl_2$	5 mM
Tween 20	0.05 % (w/v)

Fluorescence buffer FB000-$MgCl_2$ (pH 7.5)

HEPES-KOH	25 mM
Tween 20	0.05 % (w/v)

STE buffer (pH 8.0)

Tris-HCl	10 mM
NaCl	100 mM
EDTA	0.1 mM

TPE buffer (pH 8.2)

Tris-H_3PO_4	100 mM
EDTA	2 mM

SDS electrophoresis buffer (pH 8.3)

Tris	25 mM
Glycine	190 mM
SDS	0.1 % (w/v)

AAP (5x) Agarose loading buffer (pH 8.0)

EDTA	250 mM
Sucrose	25 % (w/v)
SDS	1.2 % (w/v)
Bromphenolblue	0.1 % (w/v)

AAP (5x) without dye (pH 8.0)

EDTA	250 mM
Sucrose	25 % (w/v)
SDS	1.2 % (w/v)

SDS loading buffer (5x) (pH 6.8)

Tris-HCl	160 mM
SDS	2 % (w/v)
Glycerol	40 % (v/v)
2-Mercaptoethanol	5 % (v/v)
Bromphenolblue	0.1 % (w/v)

Coomassie staining solution

Coomassie G250	0.1 % (w/v)
Phosphoric acid	2 % (v/v)
Aluminium sulfate	5 % (w/v)
Ethanol	10 % (v/v)

Buffer yellow (pH7.5)

Tris-HCl	10 mM
$MgCl_2$	10 mM
BSA	0.1 mg/ml

Deposition buffer (pH 7.5)

HEPES-KOH	10 mM
$MgCl_2$	10 mM

T4 DNA Ligase buffer (pH 7.5) (NEB)

Tris-HCl	50 mM
$MgCl_2$	10 mM
Dithiothreitol	10 mM
ATP	1 mM

ExoI buffer (pH 7.5) (Thermo Sci.)

Tris-HCl	50 mM
KCl	50 mM
EDTA	1 mM
Triton X-100	0.05 % (v/v)

NEBuffer 2 (pH 7.9) (NEB)

Tris-HCl	10 mM
NaCl	50 mM
$MgCl_2$	10 mM
Dithiothreitol	1 mM

NEBuffer 4 (pH 7.9) (NEB)

Tris-HCl	20 mM
Potassium acetate	50 mM
Magnesium acetate	10 mM
Dithiothreitol	1 mM

Table 2.6: Oligonucleotides
Oligonucleotides were purchased from the companies IBA, Purimex, and Eurogentec.

Name	Length [nt]	Sequence	Modifications
BBseq B111	19	TCA TCC TCG GCA CCG TCA C	
BBseq B111-P	19	TCA TCC TCG GCA CCG TCA C	5´-Phosphate
BBseq A302	21	ATC TTC CCC ATC GGT GAT GTC	
BBseq A302-P	21	ATC TTC CCC ATC GGT GAT GTC	5´-Phosphate
A-H-Nb.BtsI-F40236	35	CTC AAG CTT CAC TGC ATC GCA GAA ATC AAA GCT AA	-
A-X-Nb.BtsI-F40236	35	CTC GAG CTT CAC TGC ATC GCA GAA ATC AAA GCT AA	-
A2-X-Nb.BtsI-R41146	35	AAG CTC GAG CAC TGC TTG CTC CAT TAG CCA GAG CA	-
MutH GATC12 Beacon	36	TGC GGA TCC GGC TTT TTT TTT TTT GCC GGA TCC GCA	5´-HEX 3´-Black Hole Quencher1
G-XhoI	42	TAT TAA TTT CGC GGG CTC GAG AGC TTC ATC CTC TAC GCC GGA	-
G-XhoI-A594_T9	42	TAT TAA TTX CGC GGG CTC GAG AGC TTC ATC CTC TAC GCC GGA	X = position 9 Alexa594 coupled to T
T-HindIII	42	TCC GGC GTA GAG GAT GAA GCT TTC GAG CCC GCG AAA TTA ATA	-
T-HindIII-A488_T	42	TCC GGC GXA GAG GAT GAA GCT TTC GAG CCC GCG AAA TTA ATA	X = position 8 Alexa488 coupled to T
GATC45_oben	45	CCT TTC GGG CTT TGT TAG CTG AGG GAT CCT CGA GCA TAT GGC TCA	-
GATC46_unten-A647+T	46	TGA GCC ATA TGC XCG AGG ATC CCT CAT GCT AAC AAA GCC CGA AAG G	X = position 13 Alexa647 coupled to T
GATC46_oben	46	CCT TTC GGG CTT TGT TAG CAT GAG GGA TCC TCG AGC ATA TGG CTC A	-
untenZirkel+10	48	CAG ATT ACG CGC GGA AAA AAA GGA TCT CAA GAA CAX CCT TTC ATC TTT	5´-Phosphate X = position 36 Alexa647 coupled to T
obenZirkel	48	AAA GAT GAA AGG ATG TTC TTG AGX TCC TTT TTT TCT GCG CGT AAT CTG	X = position 24 modified with N6-Methyl-dA
untenZirkel-5	49	CAG ATT ACG CGC GGA AAA XAA AGG ATC TCA AGA ACA TCC TTT CAT CTT T	5´-Phosphate X = position 19 Alexa647 coupled to T

Table 2.7: Fluorophores

Fluorophores were purchased from the companies Invitrogen, Sigma-Aldrich, and IBA. Spectra of Alexa Fluor dyes, SYBR Green I and HEX were obtained from the Invitrogen homepage. Structures of Alexa Fluor dyes were also obtained from the Invitrogen homepage except for Alexa Fluor 647 which was adapted from [51]. The SYBR Green I structure was adapted from [52]. Structures and spectra of Atto dyes were obtained from the Atto-tec homepage.

Alexa Fluor 350 C_5-maleimide

Structure:

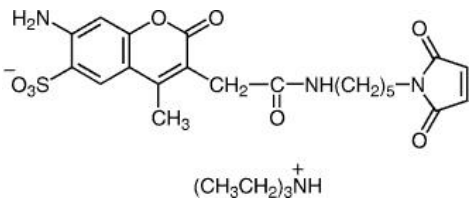

Excitation and emission spectrum:

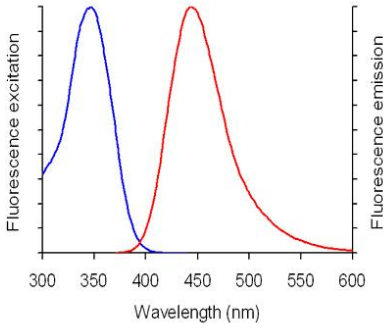

Absorption maximum	346 nm
Emission maximum	442 nm
Extinction coefficient	19,000 cm^{-1} M^{-1}
Correction factor 260 nm	0.25
Correction factor 280 nm	0.19

Alexa Fluor 488 C_5-maleimide

Structure:

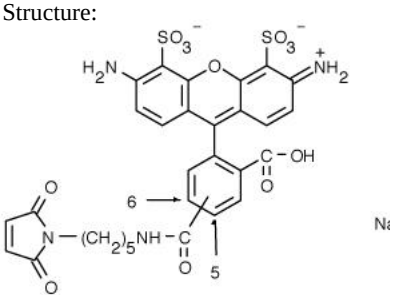

Excitation and emission spectrum:

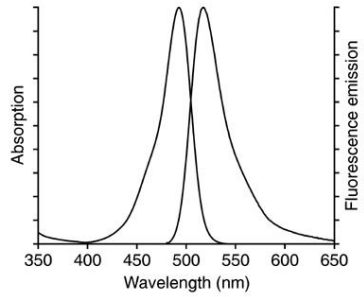

Absorption maximum	495 nm
Emission maximum	519 nm
Extinction coefficient	71,000 cm^{-1} M^{-1}
Correction factor 260 nm	0.30
Correction factor 280 nm	0.11

Alexa Fluor 594 C_5-maleimide

Structure:

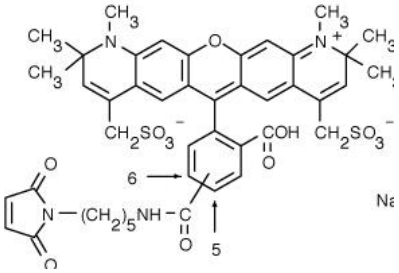

Excitation and emission spectrum:

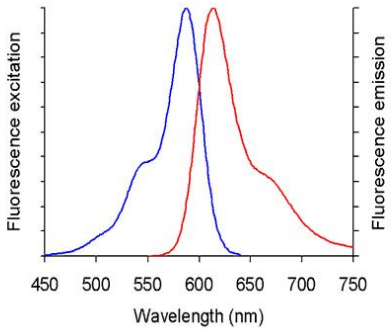

Absorption maximum	590 nm
Emission maximum	617 nm
Extinction coefficient	73,000 cm^{-1} M^{-1}
Correction factor 260 nm	0.43
Correction factor 280 nm	0.56

Alexa Fluor 647 C_2-maleimide

Structure showing C_5-maleimide:

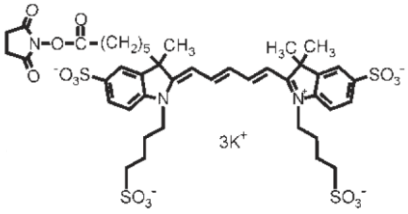

Excitation and emission spectrum:

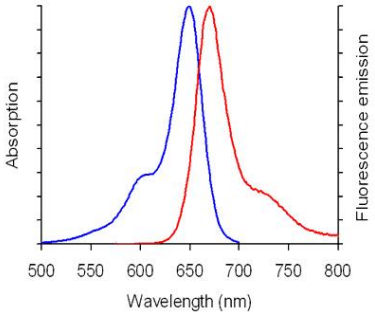

Absorption maximum	650 nm
Emission maximum	668 nm
Extinction coefficient	239,000 cm^{-1} M^{-1}
Correction factor 260 nm	0.00
Correction factor 280 nm	0.03

Atto 390 C_2-maleimide

Structure showing carboxy derivative without maleimide:

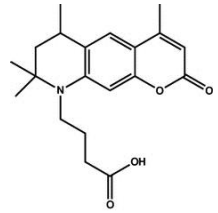

Excitation and emission spectrum:

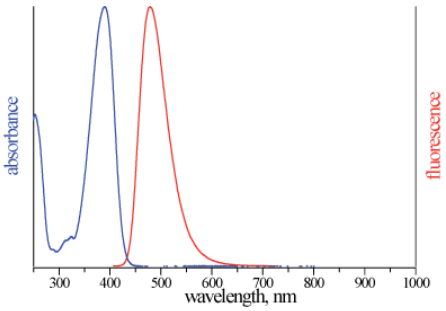

Absorption maximum	390 nm
Emission maximum	479 nm
Extinction coefficient	24,000 cm^{-1} M^{-1}
Correction factor 260 nm	0.52
Correction factor 280 nm	0.08

Atto 488 C_2-maleimide

Structure showing carboxy derivative without maleimide:

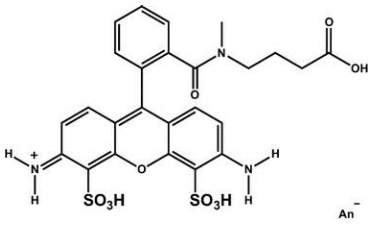

Excitation and emission spectrum:

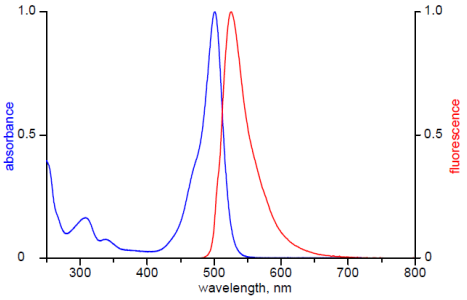

Absorption maximum	501 nm
Emission maximum	523 nm
Extinction coefficient	90,000 cm^{-1} M^{-1}
Correction factor 260 nm	0.25
Correction factor 280 nm	0.10

SYBR Green I

Structure:

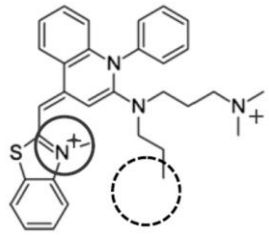

Excitation and emission spectrum of dsDNA-bound SYBR Green I:

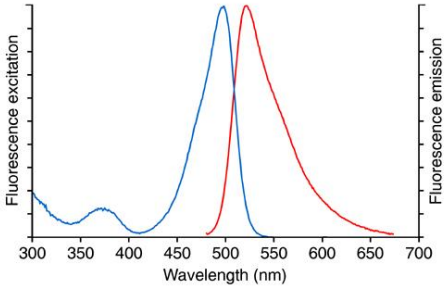

Absorption maximum	497 nm
Emission maximum	520 nm
Extinction coefficient	73,000 cm^{-1} M^{-1}
Correction factor 260 nm	0.23
Correction factor 280 nm	0.16

5´-Hexachlorofluorescein (HEX)

Structure:

Structure not available

Excitation and emission spectrum:

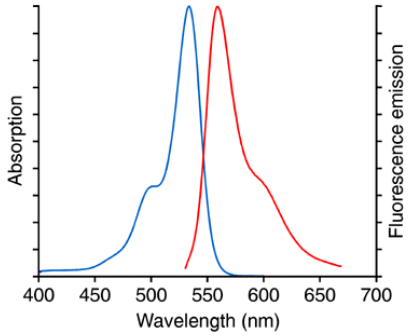

Absorption maximum	535 nm
Emission maximum	555 nm
Extinction coefficient	96,000 cm^{-1} M^{-1}
Correction factor 260 nm	ND
Correction factor 280 nm	ND

2.2 Nomenclature of fluorescence measurements

In this thesis, the nomenclature of Berney [53] and Gordon *et al*. [54] is used to describe varying fluorescence set-ups.

2.2.1 Channels

The term channel describes the fluorescence filter combinations for excitation and emission.

- Donor channel D: excitation of the donor and detection of the donor emission
- Acceptor channel A: excitation of the acceptor and detection of the acceptor emission
- FRET channel F: excitation of the donor and detection of the acceptor emission

2.2.2 Samples

The term sample describes the fluorescent dyes which are present in a sample during a measurement.

- Sample d: donor only
- Sample a: acceptor only
- Sample b: both dyes are present

An attachment of fluorescent dyes to proteins or DNA is indicated by square brackets after the name of the protein or DNA.

- Protein[d]: donor attached to the protein
- Protein[a]: acceptor attached to the protein
- Protein[b]: both dyes are attached to the protein

2.2.3 Signals

Signals are the combination of samples measured in a certain channel and therefore consist of a two letter code. The capital letter describes the channel while the small letter describes the dyes which are present in the sample. This nomenclature allows the occurrence of nine different cases: Dd, Da, Db, Ad, Aa, Ab, Fd, Fa and Fb.

2.3 Determination of concentrations and the degree of labeling (DOL)

The concentration of fluorophores and proteins was determined via the Lambert-Beer law (equation 1), where c resembles the concentration, A the absorbance at the absorbance maximum, l the path length, and ε the extinction coefficient.

$$c = A / \varepsilon \cdot l \qquad \text{equation 1}$$

To determine the fluorophore concentration equation 1 can be directly applied (equation 2).

$$c_{fluorophore} = A_{fluorophore} / \varepsilon_{fluorophore} \cdot l \qquad \text{equation 2}$$

Equation 1 can also be used to determine the protein concentration but requires a correction if a fluorophore is present in the sample (equation 3). In this case, the absorption of a fluorophore at 280 nm is subtracted from the protein absorption by the term - ($A_{fluorophore} \cdot cf_{280}$), where cf_{280} is the correction factor (cf) describing the absorbance efficiency of the fluorophore at 280 nm compared to its maximal absorbance. The correction factors used in this thesis were calculated manually or if available after the supplier's description.

$$c_{protein} = A_{280} - (A_{fluorophore} \cdot cf_{280}) / \varepsilon_{protein} \cdot l \qquad \text{equation 3}$$

Certain proteins used in this thesis were labeled with a fluorescent dye (chapter 2.6.3). The procedure ended with a majority of proteins in a sample being labeled. To describe the ratio of unlabeled to labeled proteins the term degree of labeling (DOL) is used. To determine the DOL, the concentration of proteins was compared to the concentration of fluorophores (equation 4).

$$DOL = c_{fluorophore} / c_{protein} \qquad \text{equation 4}$$

The DOL was also determined for DNA carrying fluorescent dyes. In this case, A_{280} is replaced by A_{260}, for the fluorophore cf_{260} was used instead of cf_{280}, and the extinction coefficient for the DNA was used.

2.4 Förster Resonance Energy Transfer (FRET)

Förster Resonance Energy Transfer (FRET) describes the phenomenon of a radiation free transfer of energy from an exited donor fluorophore to an acceptor fluorophore. Excitation of the donor results from absorbance of a photon and the subsequent FRET is enabled by dipole-dipole interactions between the donor and acceptor [55]. A detailed description of FRET parameters is given by Lakowicz [55]: "The rate of energy transfer depends upon the extent of spectral overlap of the emission spectrum of the donor with the absorption spectrum of the acceptor, the quantum yield of the donor, the relative orientation of the donor and acceptor transition dipoles, and the distance between the donor and acceptor molecules. […] The distance at which RET is 50 % efficient is called the Förster distance, which is typically in the range of 20 to 60 Å. The rate of energy transfer from a donor to an acceptor $k_T(r)$ is given by" equation 5, in which τ_D represents the lifetime of the donor in the absence of an acceptor, R_0 the Förster distance, and r the mean distance between donor and acceptor fluorophore.

$$k_T(r) = 1 / \tau_D \, (R_0 / r)^6 \qquad \text{equation 5}$$

The strong distance dependence of FRET (proportional to r^{-6}) allows observation of relative distance changes and was used in this thesis to visualize complex formations between components of the MMR.

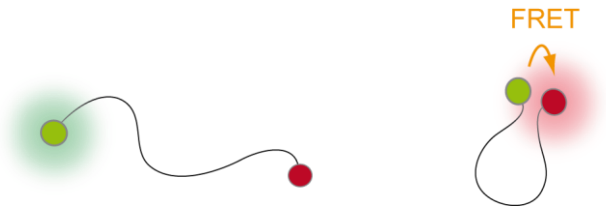

Figure 2.1: Distance dependence of FRET
An excited donor fluorophore (green) can transfer energy to an acceptor fluorophore (red) without radiation (orange arrow). This process is called FRET and depends strongly on the distance between donor and acceptor fluorophore. The picture was drawn with the software Adobe Illustrator.

2.5 Fluorescence anisotropy

A vivid explanation of fluorescence anisotropy (r) is given by Lakowicz [55]: "Anisotropy measurements reveal the average angular displacement of the fluorophore that occurs between absorption and subsequent emission of a photon. This angular displacement is dependent upon the rate and extent of rotational diffusion during the lifetime of the excited state. The rate of rotational diffusion depends on the viscosity of the solvent and the size and shape of the rotating molecule. […] For most experiments the sample is excited with vertically polarized light. The electric vector of the excitation light is oriented parallel to the vertical or z-axis. The intensity of the emission is measured through a polarizer. When the emission polarizer is oriented parallel ($_{II}$) to the direction of the polarized excitation the observed intensity is called I_{II}. Likewise, when the polarizer is perpendicular ($\perp$) to the excitation the intensity is called $I\perp$. These intensity values are used to calculate the anisotropy:"

$$r = (I_{II} - I\perp) / (I_{II} + 2I\perp) \qquad \text{equation 6}$$

"The anisotropy is a dimensionless quantity that is independent of the total intensity of the sample. This is because the difference ($I_{II} - I\perp$) is normalized by the total intensity, which is $I_T = I_{II} + 2I\perp$. The anisotropy is an intensity ratio-metric measurement. In the absence of artifacts the anisotropy is independent of the fluorophore concentration."

2.6 Expression, purification and fluorescent dye labeling of proteins

2.6.1 Expression

MutS and MutL proteins were expressed in *E. coli* HMS174(DE3) cell strains while MutH proteins were expressed in *E. coli* XL1-Blue cell strains. The HMS174(DE3) cells contained a derivate of the plasmid pET-15b encoding an N-terminal his-tag and either the *mutS* or *mutL* gene under control of a T7 promoter. The XL1-Blue cells contained a derivate of the plasmid pBAD18 encoding for the *mutH* gene under an arabinose-inducible promoter. An ampicillin resistance gene was encoded within the plasmids. 100 ml LB medium containing ampicillin was inoculated with the cells and incubated over night at 37 °C. 15 - 25 ml were taken from the overnight culture and given into four times 500 ml LB medium also containing ampicillin. The cells were grown at 37 °C until they reached an OD_{600} of 1.0 - 1.2. A 1 ml aliquot was taken from each culture. 5 ml 0.1 M IPTG was used for MutS and MutL cultures and 25g/1 arabinose for MutH cultures to induce protein expression. The temperature was decreased to 28 °C. After 4 h, another 1 ml aliquot was taken and the cultures were transferred into centrifuge tubes, thereby pooling two cultures together in one tube. The cultures were centrifuged for 15 min at 4200 rpm in a Beckman J6-HC centrifuge, supernatant removed and the pellet frozen at -20 °C for later protein purification steps.

2.6.2 Purification

The cell pellets were thawed on ice and 30 ml MutS/L binding buffer containing PMSF and benzamidine added. The mixture was resuspended until the pellet was completely dissolved. Sonification was performed 12 times for 30 s with 30 s pause for each cell pellet. The suspension was given into centrifuge tubes and centrifuged for 30 min at 20000 rpm and 4 °C in a Beckman J2-HS centrifuge. During centrifugation, two 50 ml falcon tubes had been filled with 35 ml MutS/L binding buffer and 750 ml Ni-NTA agarose bead suspension, resuspended and incubated for 30 min in the cold room on a rolling table. The Ni-NTA suspension was centrifuged for 5 min at 800 rpm and at 4 °C afterwards and supernatant was removed. After centrifugation of the sonificated cells, the supernatant was transferred into the falcon tubes containing Ni-NTA. The tubes were inverted a few times and incubated for 1 h in the cold room on the rolling table. The suspension was centrifuged for 5 min at 800 rpm and at 4 °C in a Beckman J6-HC centrifuge. 1 ml aliquot was taken and the supernatant removed. The pellets were washed with 35 ml MutS/L washing buffer, inverted a few times, and centrifuged for 5 min at 800 rpm and at 4 °C. Another 1 ml aliquot was taken and the supernatant removed. This washing and centrifuging was repeated two additional times. After the last washing and centrifugation step, 5 ml of Ni-NTA suspension and supernatant was kept and transferred into a

BioRad column in the cold room. After the Ni-NTA agarose beads settled down, the washing buffer was removed letting it run out of the column. A 1 ml aliquot of this washing buffer was kept. 500 µl MutS/L elution buffer was added and the beads were again allowed to settle down. Afterwards the fraction was collected in an Eppendorf tube and 500 µl elution buffer was added again to the Ni-NTA beads on the column. The elution step was repeated two additional times and in total three protein fractions were collected. Protein concentration of each fraction was determined and the fractions were either snap-frozen in liquid nitrogen for temporal storage at -80 °C and later purification or directly prepared for size exclusion chromatography. 10 mM DTT were added to the fractions, incubated for 20 min, and centrifuged at 13000 rpm in the cold room. Supernatant was applied to a size exclusion column coupled to a HPLC setup (LaChrom Elite from VWR-Hitachi). The running buffer for the HPLC was MutS/L HPLC buffer and the flow rate 0.5 ml per min. Fractions were collected corresponding to the protein and the protein concentration was determined. Afterwards the protein fractions were snap-frozen or prepared for the following fluorescence labeling.

2.6.3 Fluorescent dye labeling of proteins

Single cysteine variants of proteins were site-specifically labeled with a fluorescent dye. The reaction is illustrated in Figure 2.2.

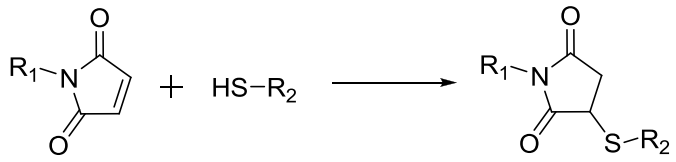

Figure 2.2: Coupling fluorescent dyes with proteins
Maleimide groups attached to fluorophores react with thiol groups of cysteines in proteins. A covalent bond is formed (drawn with the software ChemDraw Ultra 12.0).

The protein was incubated with 10 mM DTT for 20 min and purified via size-exclusion chromatography. Concentration of the fractions was determined. The amount of dye needed to label the protein was calculated (four times excess dye over protein) and appropriate fluorophore stocks were prepared by dissolving them in DMSO. Protein and fluorophore were incubated for 30 min on ice. Meanwhile Pierce Zeba 5 ml spin columns were prepared, equilibrating them with storage buffer: washing three times with 2.5 ml buffer and centrifuging each time for 2 min at 1600 rpm (1000 x g). Two columns were used for each protein fraction.

The protein was loaded on the first column and centrifuged as before. Flow-through was loaded on the second column and centrifuged again. Flow-through of the second column was transferred into an Eppendorf tube and centrifuged at 13000 rpm for 10 min (15000 x g). The supernatant was transferred into a new Eppendorf tube and snap-frozen in liquid nitrogen (storage in -80 °C).

2.6.4 Influence of fluorescent dye labeling on protein activity

Kinetics comparing unlabeled proteins with fluorescence labeled proteins had been performed with the GT932 DNA substrate. Generation of the substrate is described in 2.7.2. Two master mixes were prepared for the MMR reaction. One master mix contained 12.5 nM GT932 and 125 nM MutS in 1 x FB125 buffer. The other mix contained 5 mM ATP, 1 µM MutL, and 250 nM MutH in 1 x FB125 buffer. Both mixes were pre-incubated for 3 min at 37 °C. The reaction was started by pipetting 24 µl of the ATP-MutL-MutH mix into 96 µl of the DNA-MutS mix. Final reaction conditions were therefore 10 nM GT932, 100 nM MutS, 100 nM MutL, 50 nM MutH, 1 mM ATP, and 1 x FB125 buffer. The experiment using single cysteine, fluorescence labeled proteins was prepared as described for the unlabeled proteins and contained MutS variant R449C labeled with Alexa 647, MutL variant H297C labeled with Alexa 488, and MutH variant S85C labeled with Alexa 488. The DOL for all labeled proteins was higher than 95 %. After different time points, 10 µl of the reaction were removed and transferred into 2.5 µl of 5 x AAP buffer which stopped the reaction by denaturing the involved proteins. 0.1 U of Proteinase K were added to each time point sample afterwards and incubated for 10 min at 37 °C. The mixture of the time point samples was loaded onto a 2 % agarose gel prestained with ethidium bromide. The gel was prepared by adding 20 µg ethidium bromide to 50 ml of heated agarose.

After the run, the gel was illuminated at 302 nm and photographed with a BioDocAnalyze setup from Biometra. Intensities of bands were determined with the software GelAnalyzer. Intensities of closed circles (cc) were normalized by setting the intensity in fraction 0 min to 100 %. The experiment was performed three times with unlabeled proteins and three times with fluorescence labeled proteins. Reduction of uncleaved cc over time (k_1) was fitted with Origin software using the function ExpDec1.

2.7 Modified DNA substrates for DNA mismatch repair

2.7.1 Linear DNA substrates

For some of the complex formation assays, a linear DNA substrate was sufficient to enable the reaction. The linear DNA substrates used in this thesis are listed in Table 2.8.

Table 2.8: Linear DNA substrates
Linear DNA was generated by annealing single-stranded oligonucleotides (from Table 2.6)

DNA	Oligonucleotide 1	Oligonucleotide 2
Molecular beacon	MutH-GATC12_Beacon	-
GT42	G-XhoI	T-HindIII
GT42[d]	G-XhoI	T-HindIII-A488_T
GT42[b]	G-XhoI-A594_T9	T-HindIII-A488_T
+T46[a]	GATC45_oben	GATC46_unten-A647+T
AT46[a]	GATC46_oben	GATC46_unten-A647+T
GATC-5 oligo	untenZirkel-5	obenZirkel
GATC+10 oligo	untenZirkel+10	obenZirkel
GT100	G100_GATC	T100_GATC

The generation of GT484 was different as it originates from two separate PCR fragments. Both fragments possessed one 5´-phosphorylated DNA strand which was digested by lambda exonuclease. The two resulting single-stranded DNAs were complementary except for one position. Annealing those two single-stranded DNAs generated a 484 bp duplex DNA containing a G:T mismatch [56] [37].

2.7.2 Generation of DNA circles (GT932)

A standard circular DNA substrate with 932 bp length was generated to analyze nicking activities of modified and unmodified protein variants. This substrate was also used to enable DNA-dependent protein-protein complex formation. It is known that MutS has the capability to move along the DNA and may fall off DNA ends [57]. To stabilize formed protein complexes the DNA substrate needed to be circular. An additional requirement to investigate sub-steps in MMR was the integration of a mismatch into this DNA circle to enable MutS binding. The generation process of the substrate was developed by our group [58].

2.7.2.1 Nicking and cleavage of GT932 by the MMR

Nicking of GT932 leads to open circles. A second nick in the opposite DNA strand linearizes the circles. In this thesis, only the nicking activity was addressed. The reaction is comparable to the reaction described in 2.2.1.4, but other protein and DNA concentrations were used and the reaction was started by addition of only MutH. A 50 µl master mix was prepared containing 400 nM DNA, 500 nM MutS, 250 nM MutL, 1 x buffer yellow, and 150 mM KCl. The mix was pre-incubated at 37 °C for 3 min and started by addition of 500 nM MutH. The reaction was stopped at different time points by transferring 10 µl into 2.5 µl of 5 x AAP buffer. Analysis of bands in the gel was identical to the procedure in 2.2.1.4.

2.7.2.2 Visualizing GT932 with scanning force microscopy (SFM)

A solution of GT932 was diluted in 20 µl deposition buffer and transferred onto a mica surface. After 1 min the mica was moistened with distilled water and dried with air afterwards. Imaging was performed with a Nanoscope III (Digital Instruments, Santa Barbara, CA, USA) in tapping mode. The scan size was 2.000 µm, scan rate 1.969 Hz and the data scale 3.000 nm.

2.7.3 Generation of fluorescent-dye labeled DNA circles (1GATC[a])

Generation of the DNA is based on a protocol from Baerenfaller *et al*. [59] and was modified to enable integration of a fluorescent dye into the DNA circle (Nicolaas Hermans, unpublished data). The protocol was further modified in this thesis and the DNA single-strand production via phages was replaced by enzymatic reactions. The template to generate a single-stranded circular DNA is a derivate of the plasmid pGEM and was kindly provided by Nicolaas Hermans. It is 3197 bp long and is called 1GATC[a] as it contains one GATC site and was expressed in *E. coli* HMS174(DE3) cells. For cell cultivation, LB medium containing ampicillin was used as an ampicillin resistance gene is encoded on the plasmid. The plasmid was purified with the PureYield Plasmid Midiprep System from Promega. To incorporate an IDL and a fluorophore into the circle a five-step reaction was performed. The reaction started with nicking the plasmid in the bottom strand (Table 2.9).

Table 2.9: Reaction mix for the nicking of 1GATC plasmids

component	stock concentration	final concentration	volume
1GATC plasmid		290 µg	
Nt.BspQI	10 U/µl	2.5 U/µg DNA	72.5 µl
NEBuffer 3	10 x	1 x	145 µl
water	add to a volume of 1450 µl		

The reaction mix was incubated for 1 h at 50 °C and inactivated with 20 min at 80 °C. In the following step, Exonuclease III was used to digest the bottom strand (Table 2.10). The reaction mix was split and given into two Eppendorf tubes, each containing 725 µl.

Table 2.10: Reaction mix for Exonuclease III digestion

component	stock concentration	final concentration	volume
reaction mix			725 µl
ExoIII	100 U/µl	17 U/µg DNA	25 µl
NEBuffer 1	10 x	1 x	145 µl
water	add to a volume of 1450 µl		

Incubation time was 15 min at 30 °C and inactivation was 10 min at 70 °C. After inactivation the ss-plasmid-DNA was purified with the Wizard® SV Gel and PCR Clean-Up System from Promega. In the next step a complementary oligonucleotide was annealed to the remaining top strand (Table 2.11). This oligonucleotide carried a fluorophore and possessed an additional thymine in the sequence which generated the IDL after annealing.

Table 2.11: Reaction mix for annealing

component	stock concentration	final concentration	volume
ss-plasmid-DNA	needs to be determined	all	approx. 250 µl
Oligo (-5)	100 U/µl	0.075 µl/µg DNA	
NEBuffer 2	10 x	1 x	50 µl
water	add to a volume of 500 µl		

Annealing started on a heating block which was set to 95 °C for 5 min and then switched off. When the block cooled down to 40 °C the temperature was kept stable at 40 °C. The next step was a primer extension and ligation reaction which led to a double-stranded closed circle (Table 2.12). The reaction mix was split and given into two Eppendorf tubes, each containing 250 µl.

Table 2.12: Reaction mix for primer extension and ligation

component	stock concentration	final concentration	volume
reaction mix			250 µl
BSA	100 x	1 x	5 µl
dNTPs	2 mM	0.2 mM	50 µl
NEBuffer 2	10 x	0.5 x	25 µl
ATP	110 mM	1 mM	4.6 µl
T4 Pol (Fermentas)	5 U/µl	1 U/µg DNA	
T4 Ligase	400 U/µl	30 U/µg DNA	
water	add to a volume of 500 µl		

Incubation was for 1.5 h at 37 °C and inactivation for 10 min at 75 °C. Finally an exonuclease mixture of Exonuclease I, Exonuclease III, and RecJF digested remaining oligonucleotides which had been used in excess to the top strand of the circle in the annealing step (Table 2.13).

Table 2.13: Reaction mix for ExoI/III, RecJF digestion

component	stock concentration	final concentration	volume
reaction mix			500 µl
ExoI	20 U/µl	4 U/µg DNA	
ExoIII	100 U/µl	10 U/µg DNA	
RecJF	30 U/µl	6 U/µg DNA	

Incubation was for 15 min at 30 °C and inactivation for 10 min at 80 °C. Afterwards the fluorescent dye labeled 1GATC[a] circle was purified two times with the Wizard SV Gel and PCR Clean-Up System from Promega. In a vacuum centrifuge, remaining ethanol was removed by centrifuging 45 min at 55 °C. The concentration of GT932 was determined and the purity analysed on a 1.25 % agarose gel. Before the gel was stained with ethidium bromide, fluorescence of the 1GATC[a] circles was observed by exposing the gel to monochromatic light at wavelength 630 nm in a fluorescence imaging setup called *VersaDoc*.

2.8 Visualizing complex formation in MMR

All FRET assays and anisotropy measurements had been performed with the Fluoromax 4 spectral photometer manufactured by Horiba. The reactions were kept thermostatically stable at 20 °C. Calculations were done with the software Microsoft Excel and Origin by OriginLab Corporation. Fluorescence emission spectra were normalized to let the highest value be 1.

2.8.1 MutS binding DNA

Visualization of MutS binding DNA was achieved in two different assays which are described below. Both assays were established in cooperation with Michele Cristovao [36].

2.8.1.1 Site-specific DNA binding of MutS

An acceptor fluorophore labeled MutS will give a FRET signal upon binding to a donor labeled oligonucleotide containing a mismatch. In this case, the acceptor was Alexa 594 which was coupled via maleimide crosslinking to a cysteine residue at position 449 in MutS. The DNA substrate was generated by annealing the oligonucleotides T-HindIII and G_XhoI-A594_T9. The annealed DNA called GT42[d] contained a G:T mismatch and 12 bp away the donor fluorophore Alexa 488 coupled to a thymine in DNA. Reaction was started with 50 nM GT42[d] and 1 mM ADP in the 1x buffer FB125 at 20 °C. Excitation of the donor fluorophore was at 470 nM and the emission spectrum was measured from 490 - 800 nm. Addition of 100 nM MutS[a] was the second step and addition of 2 µM competitor DNA the final step. After step 2 and 3 the emission spectra had been measured as in step 1 and additionally the acceptor emission had been measured by exciting at 575 nm and measuring from 595 - 800 nm.

2.8.1.2 MutS bending DNA

This assay is similar to the site-specific binding of MutS but here two fluorophores on the DNA had been used to analyze the binding orientation of MutS. The setup for the assay was established before [36] [60]. Again Alexa 488 was used as acceptor and Alexa 594 as donor. The DNA substrate was therefore called GT42[b]. It also contained a mismatch and was generated by annealing the oligonucleotides T-HindIII-A488_T and G_XhoI-A594_T9. Step 1 in the assay started with 50 nM of GT42[b] and 1 mM ADP in the 1x buffer FB125. Step 2 was the addition of 200 nM MutS variant R449C D835R. And step 3 was the competition for MutS with addition of 2 µM of the unlabeled DNA GT42. In each step the emission spectra were

recorded for the donor and acceptor fluorophore as performed in the site-specific DNA binding of MutS assay (2.8.1.1).

2.8.1.3 Determination of MutS binding orientation at mismatches

The DNA-bending assay was additionally used to determine the MutS binding orientation at different mismatches. MutS was titrated to 10 nM donor labeled DNA (GT[d]). This reaction was repeated with double labeled DNA (GT42[b]). The reaction started with 10 nM DNA, 1 mM ATP, and 1 x FB125 buffer. In the next step, 1000 nM MutS variant R449C D835R was added. Half of this reaction mix was discarded and replaced by an equal volume of the starting reaction mix not containing MutS. With the MutS dilution steps, it was possible to vary MutS concentrations from 1000 nM to 1 nM. After each step, anisotropy of the fluorophores was determined, exciting Alexa 488 at 470 nm and Alexa 594 at 575 nm. Emission was recorded at 517 nm and 617 nm. The experiment was repeated three times for each DNA containing G:T, T:G or G:G mismatches or G:C homoduplex DNA. Recorded emission maxima as well as anisotropy values were averaged afterwards.

2.8.2 Monitoring MutS sliding clamp formation

MutS can be transformed into a sliding clamp on DNA which is ATP- and mismatch-dependent. On oligonucleotides, this sliding clamp falls off at the ends. To analyze kinetics of the sliding clamp formation, the following assay was developed. To enable a stable FRET between MutS as a sliding clamp and DNA, circular DNA was used. The circular DNA (GT932) contained a single G:T mismatch and its generation process was described before [61] [58]. SYBR Green I (SG) is a fluorescent dye which associates with double-stranded DNA. The fluorescence emission of SG is dramatically increased upon binding to double-stranded DNA. In this assay SG was associated with GT932 and acted as fluorescence donor. Alexa 647 coupled to MutS variant R449C D835R acted as acceptor MutS[a]. A FRET was generated when the labeled MutS[a] bound to the labeled DNA[d]. It started with 100 nM SG and 1 µM ADP in the 1x buffer FB125. Following steps were the stepwise addition of 100 nM MutS[a], 10 nM GT932, 1 mM ATP, and 1 µM of unlabeled MutS as competitor for the labeled MutS[a]. Time traces of the kinetics were observed during the reaction by exciting the donor fluorophore SYBR Green I at 470 nm and recording emission of the acceptor Alexa 647 at 670 nm. For determination of kinetic rate constants, the time traces had been analyzed with the software Origin and each phase was fitted separately with the equitation ExpDec1. The reaction was performed two times and determined kinetic rate constants were averaged.

2.8.3 MutS-MutL complex formation

To visualize and analyze the interaction between MutS and MutL, a FRET assay was developed. For this, the fluorophores Alexa 488 and Alexa 594 had been chosen as FRET pair. One fluorophore was covalently attached to the single cysteine MutS (variant D835R R449C or D835R D246C) and the other to the single cysteine variant of MutL H297C. When those two labeled proteins formed a complex, a FRET arose. The complex formation and dissociation of MutS and MutL was observed in fluorescence spectra of Alexa 488 and Alexa 594 where the fluorescence donor Alexa 488 was excited while the emission of the fluorescence acceptor Alexa 594 was measured. To analyze the dissociation reaction of the MutS-MutL complex, an excess of an unlabeled MutL variant H297C was used to compete for the binding of MutS. The resulting decrease in FRET was observed in the fluorescence spectra. Further conditions for the reaction were described before [37].

2.8.4 MutL binding DNA at low ionic strength

MutL possesses a weak ability to bind directly to DNA. At physiological salt conditions one cannot observe an interaction without the help of MutS. By lowering the salt concentration it is possible to record a FRET signal between an Alexa 488 labeled MutL variant 297 (MutL[d]) and a 46 bp long oligonucleotide containing Alexa 647 as acceptor fluorophore (DNA[a]). To investigate the influence of heteroduplex DNA on the binding of MutL, the reaction was performed with heteroduplex DNA created by a missing adenine in the bottom strand leaving an unpaired thymine in the top strand (0T46[a]) and compared to homoduplex DNA (AT46[a]). The reaction started with 400 nM MutL[d] and 1 mM ATP in 1x buffer FB000. Step 2 was the addition of 400 nM DNA[a]. And the final step was an increase in salt concentration to 200 mM by adding KCl. Fluorescence emission spectra for Alexa 488 and Alexa 647 were observed for each step the same way as described in 2.8.1.3. Calculation of FRET effects were performed by dividing maximal acceptor emission through maximal donor emission of not normalized spectra. Acceptor emission which derived from direct excitation of the acceptor fluorophore by excitation light for the donor fluorophore (signal Fd) was subtracted from the spectra of +DNA[a] and +KCl. Emission maxima of three independent experiments with 0T46[a] and three experiments with AT46[a] were averaged. MutL binding to DNA visualized by anisotropy was performed slightly different compared to the FRET-based assay. The reaction was started with 1 mM ATP, 1 x FB000 buffer, and 50 nM DNA (0T46[a]) labeled with Atto 488. 300 nM of unlabeled MutL was added followed by an increase in KCl concentration to 200 mM. Anisotropy was recorded during each phase of three independent experiments by using excitation at 470 nm and emission at 517 nm. Anisotropy values were averaged afterwards.

2.8.5 MutH binding DNA without MutS and MutL at low ionic strength

MutH possesses a weak ability to bind DNA which is inhibited at physiological salt conditions. To enable analysis of direct DNA binding by MutH the low salt buffer FB000 was used. The catalytically inactive MutH variant E77A allowed observation of a stable FRET by avoiding the MutH cleavage of its DNA substrate. The assay was started with 100 nM 1GATC-5[a] double-stranded oligonucleotide in 1 x FB000 buffer. Addition of 400 nM MutH[d] allowed complex formation between MutH[d] and DNA[a] which was reversed by addition of 125 mM KCl. Fluorescence emission spectra of Alexa 488 and Alexa 647 were recorded after each step. The spectra were normalized for the donor to be 1. As there was no donor within the first reaction step, the emission in this step was divided through the same normalization factor as used for step 2. Acceptor fluorescence of not normalized emission spectra was determined for all three reaction steps. A control with donor only was used to subtract overlapping donor fluorescence from the acceptor emission in step 2 and 3.

2.8.6 MutH cleaving DNA without MutS and MutL at low ionic strength

The experiment was performed with 50 nM of a molecular beacon in low salt buffer 1x FB000 in a fluorescence plate reader (Infinite F200 Pro from Tecan) with the software *i-control*. The Hex fluorophore was excited at 535 nm and its emission detected at 590 nm. Reaction was started by addition of 1 µM MutH variant C96S S85C. The experiment was repeated three times and the fluorescence normalized to be 1 at its maximum. For each measurement the MutH nicking rate (initial slope) was determined, averaged and fitted with the software Origin (using the function ExpDec1).

2.8.7 MutH recruitment to DNA at high ionic strength (incision complex)

First step in the reaction was a pre-incubation of 5 nM 1GATC-5[a] circle with 1µM ADP, 200 nM MutS, 200 nM MutL, and 100 nM of the catalytically inactive variant E77A of MutH[d] in 1 x FB125 buffer. The reaction was started by the addition of 1 mM ATP. Addition of 500 nM unlabeled and also catalytically inactive MutH resulted in a competition in the reaction. Fluorescence emission spectra of Alexa 488 and Alexa 647 were recorded after each step. After addition of MutH competitor, fluorescence kinetics were recorded by exciting Alexa 488 at 470 nm and measuring Alexa 647 emission at 670 nm. The donor was normalized to be 1 in the emission spectra. Maximal acceptor fluorescence during the reaction steps was determined at 670 nm. Changes in acceptor fluorescence were used for the quantitative analysis.

3. Results

3.1 Expression, purification and fluorescent dye labeling of proteins

3.1.1 Protein expression

In this thesis, the analysis of complex formations in MMR was monitored by FRET. A requirement for most of the FRET-based assays, described in this thesis, were fluorescent dye labeled proteins. Protein expression, purification, and fluorescent dye labeling are depicted in Figures 3.1-3.4. The procedure is illustrated here for MutL and was performed similarly with different variants of MutS and MutH.

Addition of IPTG to *E. coli* cultures lead to an induction of the *lac* operon. The *mutL* gene in the used *E. coli* strains was encoded on a plasmid under the control of a *lac* promoter. With induction of the *lac* operon the expression of MutL proteins was upregulated. MutL expression is demonstrated in Figure 3.1.

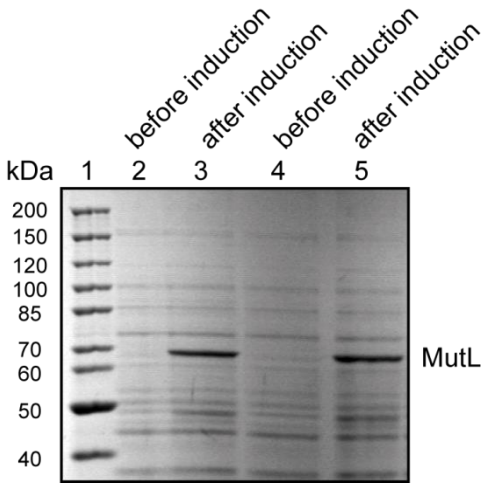

Figure 3.1: Expression of MutL in *E. coli*
Cell lysate of *E. coli* cultures before induction of MutL expression (lane 2 and 4) was compared to cell lysate after induction (lane 3 and 5). The fractions were analyzed on a 8% SDS-PAGE stained with Coomassie brilliant blue and the marker is PageRuler unstained protein ladder.

A strong band arrised after induction (lane 3 and 5). The molecular mass of approximately 70 kDa correlates with the molecular mass of MutL.

3.1.2 Protein purification

The expressed MutL protein was purified via affinity chromatography followed by size exclusion chromatography. Increasing MutL purity at different purification steps is visualized in Figure 3.2.

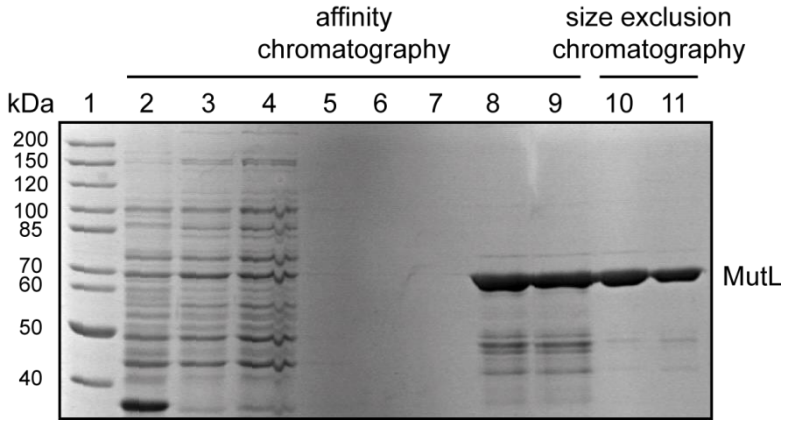

Figure 3.2: Purification of MutL
MutL was purified from cell lysate via Ni-NTA affinity chromatography (lane 2-9) and size exclusion chromatography (lane 10 and 11). Cell lysate can be seen in lane 2 and the supernatant after centrifugation of two different preparations in lane 3 and 4. Supernatants after each centrifugation in three following washing steps are indicated in lane 5-7. Fraction 1 and 2 of the elution step during the affinity purification are in lane 8 and 9. These elution fractions were pooled and further purified via size exclusion chromatography. Lane 10 and 11 show the 22 min and 23 min fractions of MutL after size exclusion chromatography. The samples were loaded on a 8% SDS-PAGE stained with Coomassie brilliant blue and the marker is PageRuler unstained protein ladder.

Lanes 2-4 demonstrate the presence of different proteins in the cell lysate before purification. A prominent band at approximately 70 kDa represents MutL which has a molecular mass of 70 kDa. Lanes 5-7 indicate that no MutL was eluted during washing steps and remained bound to the Ni-NTA agarose beads. The elution steps of the affinity purification (Figure 3.2, lane 8 and 9) show the purified MutL which still contained some other protein bands. To increase the purity of the samples, a size exclusion chromatography was performed which further increased the purity of the protein preparation (Figure 3.2, lane 10 and 11). The chromatogram is shown in Figure 3.3. The elution profile of MutL (red line) shows a major fraction of intact MutL which elutes at 23 min. Another fraction eluting at 28 min corresponds to degraded MutL (data not shown).

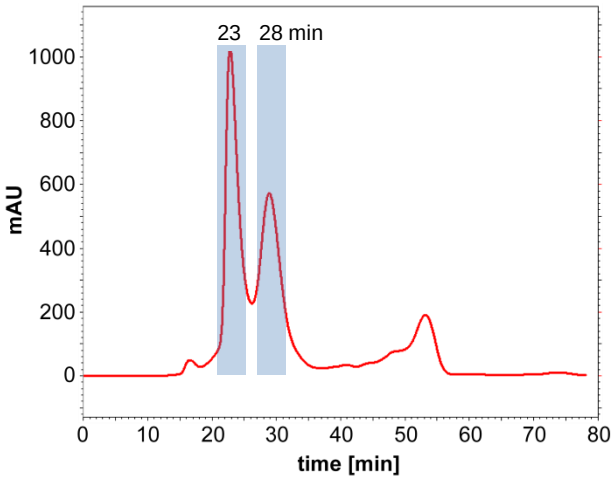

Figure 3.3: MutL purified by size exclusion chromatography
Eluates of the affinity purification were supplied to a size exclusion column coupled to a HPLC setup (LaChrom Elite from VWR-Hitachi) for further purification of MutL. MutS/L HPLC buffer was used with a flow rate of 0.5 ml / min. The protein elution profile was measured by absorption at 280 nm (red line) and its intensity in mAU reflects the amount of protein in each eluting fraction. The peak at 23 min corresponds to intact MutL while later eluting proteins resemble degraded MutL and other proteins.

3.1.3 Fluorescent dye labeling of proteins

The purified MutL was labeled with an Alexa or Atto fluorophore. This reaction was enabled by a maleimide group which was attached to the fluorophore. Maleimide reacted with the sulfhydryl group of a cysteine exposed on the protein surface which resulted in the formation of a stable carbon-sulfur bond [62].

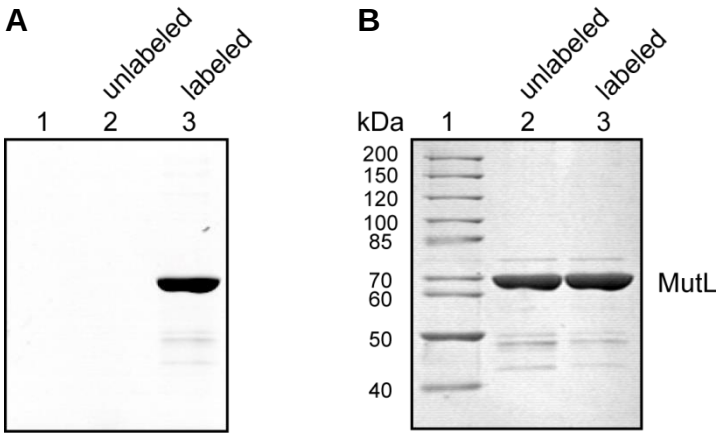

Figure 3.4: Fluorescence labeling of MutL
A MutL before fluorescence labeling (lane 2) and after labeling with Alexa 488 (lane 3) on an unstained 8% SDS-PAGE illuminated at 302 nm in a BioDocAnalyze setup from Biometra. 2 µg of protein were loaded for each sample. **B** The same gel after staining with InstantBlue Coomassie. The marker is PageRuler unstained protein ladder.

Success of the fluorescence labeling reaction of MutL can be seen in the comparison of the protein gel before and after staining (Figure 3.4). The unlabeled MutL (A, lane 2) does not show any fluorescence under illumination at 302 nm while a clear band arose after labeling MutL with Alexa 488 (A, lane 3). Gel staining with Coomassie brilliant blue revealed that the observed band has a molecular mass of approximately 70 kDa (B Lane 3) which correlates to the molecular mass of MutL. The degree of labeling was determined as described in 2.3.

3.1.4 Influence of fluorescent dye labeling on protein activity

Most assays in this thesis analyzing the complex formation of components of the MMR are based on FRET effects. To exclude the possibility that the fluorescent dyes at the proteins disturb interactions or reactions of the MMR system, enzyme kinetics had been performed to compare DNA nicking reactions of unlabeled proteins with kinetics of labeled proteins. Unmethylated DNA circles (GT932) served as a substrate in these reactions. Generation of GT932 is demonstrated in chapter 3.2.1. The conversion from closed circles (cc) to open circles (oc) and finally to linear products is explained and schematically illustrated in Figure 3.5 and Figure 3.10, A. A representative gel showing the nicking activity of MMR proteins is shown in Figure 3.5.

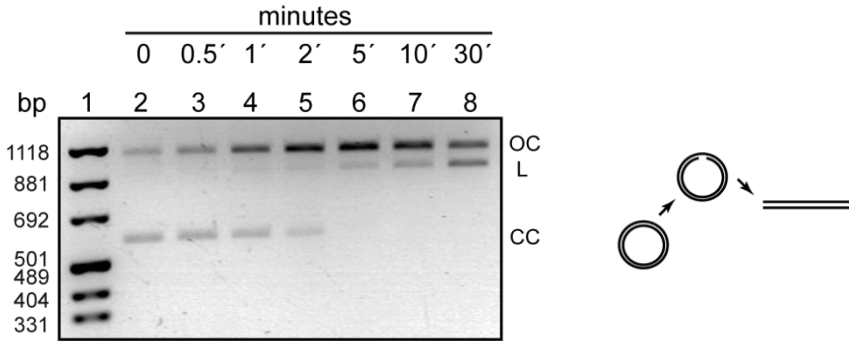

Figure 3.5: DNA nicking reaction showing activity of MMR proteins
DNA circles (GT932) were nicked and cleaved by MMR proteins at 37 °C. The reaction was stopped at different time points and analyzed on a 2% agarose gel prestained with ethidium bromide. MMR activity led to a conversion from closed circles (cc) to open circles (oc) and linear products (L). cc bands are less intense compared to oc and L because of a reduced incorporation of ethidium bromide into closed circles. The marker is pUC8 Mix Marker.

Intensities of uncleaved cc at different time points were determined with GelAnalyzer software and a single exponential function was used to fit the data with Origin software. Data points and the corresponding fit for unlabeled MMR protein activity can be seen in Figure 3.5, A, while

data points and the fit for fluorescent dye labeled MMR protein activity can be seen in Figure 3.5, B.

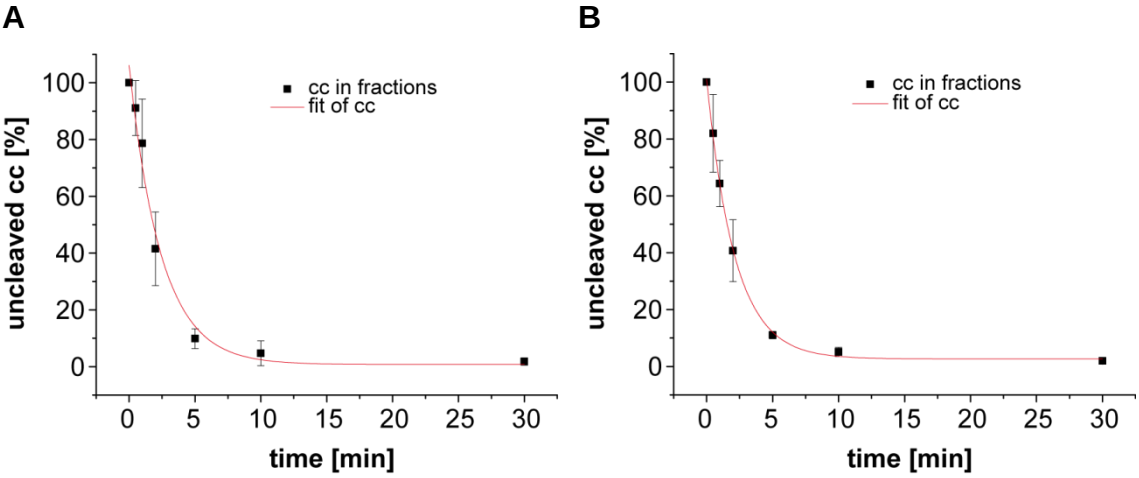

Figure 3.6: DNA nicking activity of unlabeled and fluorescent dye labeled MMR proteins
Activity of **A** unlabeled and **B** fluorescent dye labeled MMR proteins. Reduction of closed circles (cc) over time was determined to address the activity of MMR proteins. Intensities of bands were determined with GelAnalyzer software and a single exponential function was used to fit the data with Origin software. Data points for each step were averaged and are symbolized by black squares and the fit is indicated by a red line. Error bars are the standard deviation from n = 3 independent experiments. Proteins used in the experiment were single cysteine variants of MutS variant R449C D835R, MutL variant H297C, and MutH variant S85C. MutS carried the fluorescent dye Alexa 647, MutL and MutH the dye Alexa 488. The DOL for all labeled proteins was higher than 95 %.

Fitting of the cc reduction over time (Figure 3.6) allowed determination of MMR nicking rates (k_1). Nicking rates of unlabeled and fluorescent dye labeled MMR proteins are compared in Table 3.1.

Table 3.1: DNA nicking rates of unlabeled compared to fluorescent dye labeled proteins
The reduction of uncleaved cc during the MMR reaction was fitted and nicking rates were determined according to the unlabeled and fluorescent dye labeled MMR proteins. The error derived from n = 3 independent experiments.

protein modification	$t_{1/2}$	k_1
Unlabeled	150 ± 25 s	0.007 ± 0.001 s^{-1}
Labeled	130 ± 5 s	0.008 ± 0.0003 s^{-1}

There is no significant difference (p = 0.25, unpaired t-test) between the DNA nicking rates of unlabeled and fluorescence labeled MMR proteins (0.007 ± 0.001 s^{-1} and 0.008 ± 0.0003 s^{-1}). This reveals that the fluorophores at the selected positions on the proteins do not disturb the MMR system.

3.2 Modified DNA substrates for DNA mismatch repair

Analysis of MutS sliding clamp formation, the complex formation of MutS and MutL and other sub-steps in DNA mismatch repair requires suitable DNA substrates. For some sub-steps it is sufficient to use linear DNA derived from annealing of oligonucleotides or PCR fragments. To enable observation of site-specific DNA binding of proteins in these reactions, the DNA can carry a fluorophore close to the binding site of a protein. Other sub-steps in MMR require circular DNA substrates to avoid complex dissociation at DNA ends. Those circular substrates are called GT932 and their generation is demonstrated in 3.2.1. For observation of site-specific DNA binding on circular DNA, a third category of DNA substrates was generated, the 1GATC[a] circles. The generation of 1GATC[a] circles is shown in 3.2.2.

3.2.1 Generation of DNA circles (GT932)

DNA circles (GT932) were generated using a protocol we developed [58]. GT932 possessed a single GATC site, can be produced in high amounts, and can contain a single mismatch. Furthermore, the circular structure enables a more stable complex formation of MMR proteins as end-dependent dissociation of the proteins is not possible. Combined with a SYBR Green I (SG)-based FRET assay, it is possible to analyze protein binding events at any place of the circle (chapter 3.3.2.). The generation process included a PCR reaction, nicking, ligation, and a purification step with either exonuclease digestion or gel extraction (Figure 3.7).

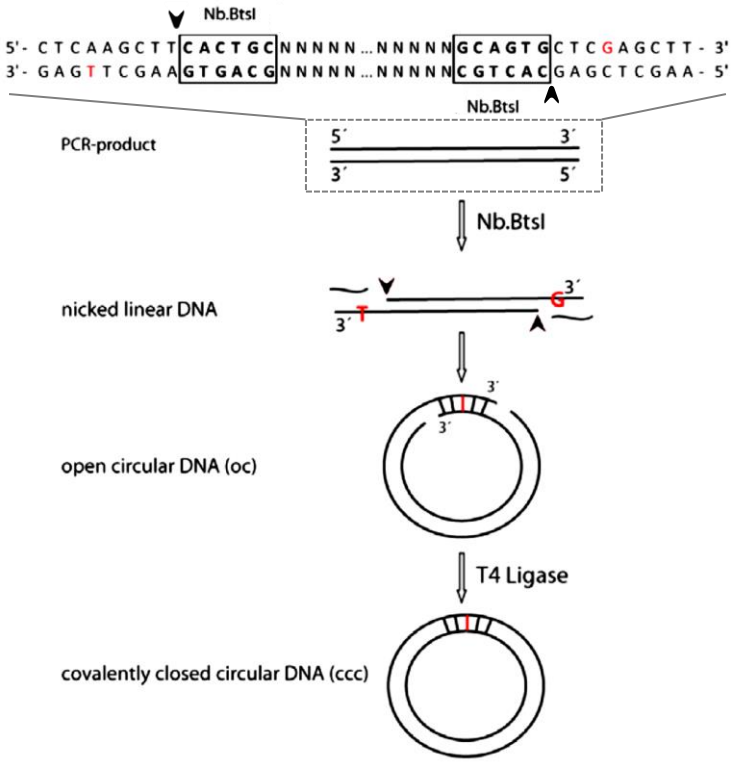

Figure 3.7: Schematic view of the generation of GT932
Linear DNA was nicked 5´ to a CACTGC sequence with Nb.BtsI to create 3´-overhangs. These complementary, 9 bp overhangs enabled the formation of open circles via self-annealing. Ligation generated closed circular DNA and exonucleases digested side products. Using varying primers for the synthesis of the linear top- and linear bottom-strand allowed the formation of a G:T mismatch within the final circle (indicated in red).

The natural DNA substrate within the incision step in *E. coli* MMR reaction is a hemi-methylated GATC site. A newly synthesized DNA strand containing an error remains unmethylated for some time and is therefore incised by MutH. To achieve a hemimethylated situation for the single GATC site in GT932, the DNA circles had been methylated by TaqI-Methyltransferase. GT932 contained a hybrid sequence of the recognition sites for TaqI-Methyltransferase and MutH. Both sites shared an adenine in one DNA strand while the other strand contained two distinct adenines for the recognition sites. Methylation of the TaqI site led to a methylated adenine in the GATC sequence of one DNA strand. The adenine in the GATC site of the opposite DNA strand remained unaffected, hence a hemimethylated GATC site was generated (Figure 3.8).

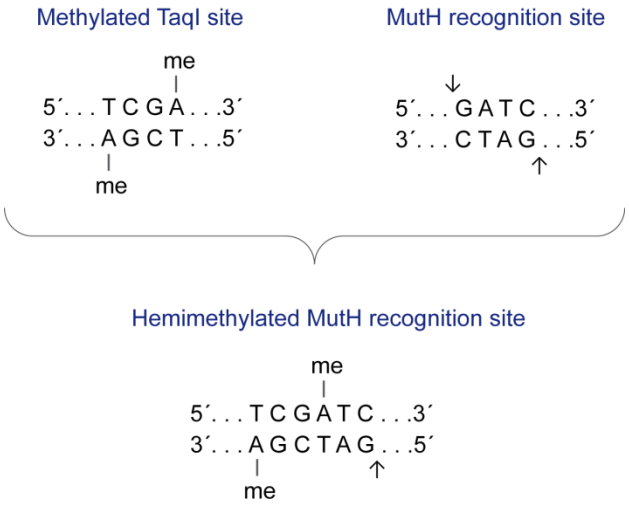

Figure 3.8: Generation of a hemimethylated GATC site
A methylated TaqI site (top left) together with a GATC site (top right) allows the formation of a hemimethylated GATC site in a hybrid sequence of both (bottom).

The generation process of GT932 is depicted in Figure 3.9. Products of the sub-steps migrated differently in an ethidium bromide prestained agarose gel. Linear PCR fragments are shown in lane 2. The nicking step, which led to 3´-overhangs, is indicated in lane 3. These overhangs were complementary except for a single mismatch and allowed formation of open circles which migrated slower in the gel. As these annealed overhangs were short and unstable, there was a mixture of fragments still in the linear form and some that already formed open circles. Ligation led to closure of open circles (lane 4). Therefore, the open circular band disappeared and a new faster migrating band appeared together with oligomers which migrated slower. ExoI / III treatment digested side products that contained nicks or DNA ends (lane 5) and only closed circles remained, indicated by a single band in this lane. Methylation of the TaqI site did not change the migration behavior of the circles (lane 6).

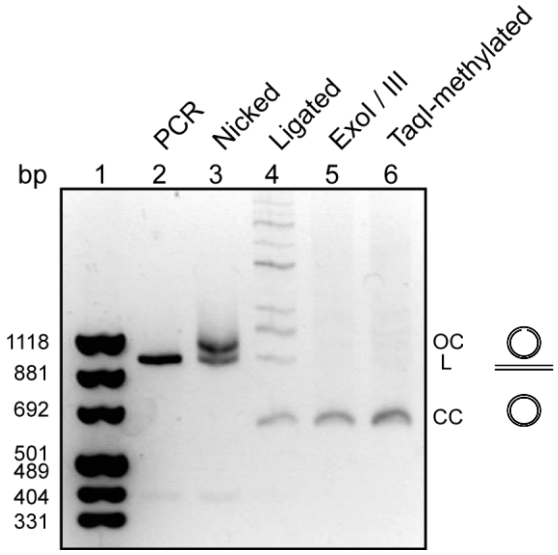

Figure 3.9: Generation of GT932 (DNA circles)
Different sub-steps of the circle-generation are visualized in a 2% agarose gel prestained with ethidium bromide. **PCR** A linear PCR fragment (L). **Nicked** Nicking of the linear PCR fragment led to the formation of open circles (oc). **Ligated** Open circles were transformed to closed circles (cc) via ligation. **ExoI / III** Closed circles were separated from side products via exonuclease digestion. **TaqI-methylated** Methylation of a TaqI site in the closed circle generated a hemimethylated GATC site. The marker is pUC8 Mix Marker.

The status of methylation in a GATC sequence is crucial for the MMR reaction. A fully methylated site cannot be cleaved by MutH. A hemimethylated site allows more efficient cleavage of one DNA strand by stabilizing the binding pocket of MutH with the methyl group in the uncleaved DNA strand [63] [41] [64]. Cleavage of unmethylated GATC sequences by MutH depends on the sequence context and leads in a two-step reaction to double-strand cleavage. Cleavage of hemimethylated GT932 was compared to cleavage of unmethylated GT932 (Table 3.2). Each reaction was repeated 3 times and the nicking rates were averaged. The reaction process is schematically illustrated in Figure 3.10, A and a representative gel is shown in Figure 3.10, B.

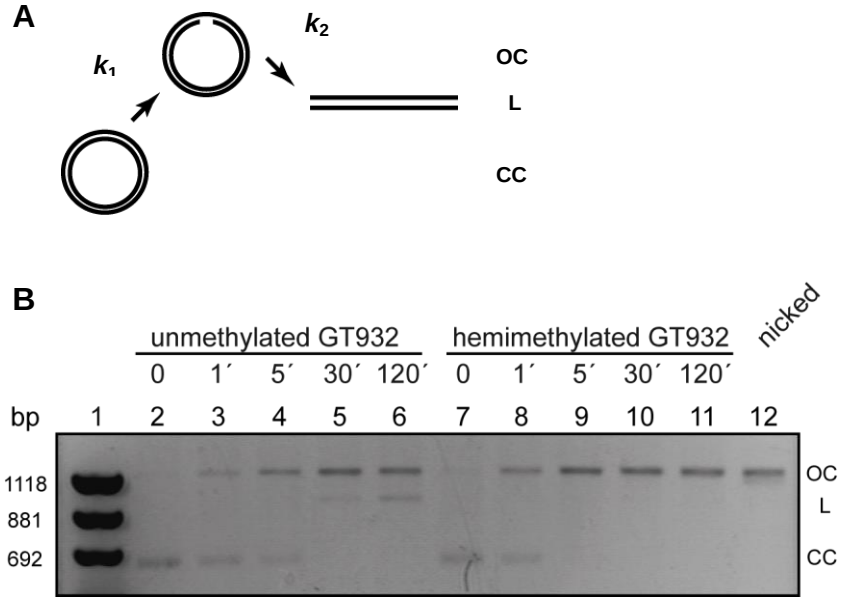

Figure 3.10: Cleavage of un- and hemimethylated GT932 by MMR proteins
A schematic view of the reaction. The covalently closed DNA circle (cc) was first nicked by MMR proteins (k_1). The resulting open circles (oc) could also be nicked in the second DNA strand if the GT932 was unmethylated (k_2). This second nicking step linearized the circle (L). In this work, the linearization activity was not addressed. **B** Conversion from cc to oc was analyzed in a 2% agarose gel prestained with ethidium bromide. Unmethylated (left) and hemimethylated (right) GT932 were incubated with MMR proteins. Decrease of cc reflected nicking and therefore protein activity (k_1). GT932 nicked by Nb.BtsI (nicked) was a control to visualize running of oc in the gel. The marker is pUC8 Mix Marker.

Averaged nicking rates (k_1) in Table 3.2 revealed a 4-fold faster nicking of hemimethylated GT932 compared to unmethylated ones which is statistically significant ($p < 0.05$, unpaired *t*-test). This is in agreement with a previously reported 3-fold enhancement in a mismatch-provoked MutH endonuclease assay [64]. While some linearization occurred within the reaction of unmethylated DNA circles (e.g. Figure 3.10, lane 6) gels containing the hemimethylated circle did not show any linear constructs (e.g. Figure 3.10, lane 11). These results cannot be compared to nicking rates observed in 3.1.4 as other reaction conditions were used.

Table 3.2: Nicking rates of the MMR for un- and hemimethylated DNA substrates
The reduction of uncleaved cc during the MMR reaction was fitted and nicking rates were determined according to the un- and hemimethylated DNA substrates. The error derived from $n = 3$ independent experiments.

DNA	$t_{1/2}$	k_1
unmethylated GT932	250 ± 100 s	0.004 ± 0.002 s^{-1}
hemimethylated GT932	60 ± 4 s	0.017 ± 0.001 s^{-1}

Purified GT932 DNA circles were visualized by scanning force microscopy (SFM) (Figure 3.11). SFM is able to detect objects on silica by an increase in height which is illustrated by a change in color.

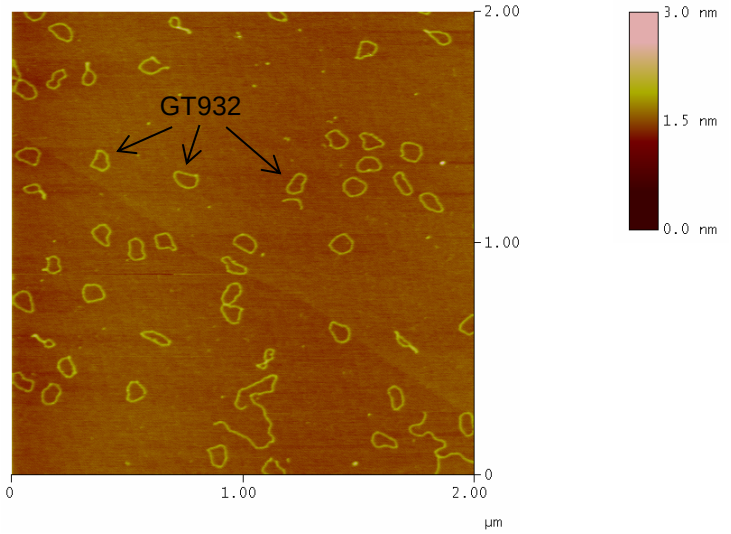

Figure 3.11: GT932 visualized by scanning force microscopy (SFM)
Hemimethylated GT932 DNA circles were immobilized on a mica surface (see experimental procedures 2.7.2.2). GT932 are visible as yellow rings while the background is orange. Imaging was performed with a Nanoscope III (Digital Instruments, Santa Barbara, CA, USA) in tapping mode. The scan size was 2.000 µm, scan rate 1.969 Hz and the data scale 3.000 nm. (M. Cristovao, unpublished data)

The immobilized GT932 can be seen as rings (yellow) in Figure 3.11. They caused an increase in height compared to the background (orange).

3.2.2 Generation of fluorescent dye labeled DNA circles (1GATC[a])

In order to observe site-specific binding of proteins to a DNA, it was necessary to generate DNA substrates that optionally possess a mismatch and a fluorophore. Those circles were called 1GATC[a] as they only contain a single GATC site and the generation process was performed after a protocol from Baerenfaller *et al*. [59]. The protocol was modified (Nicolaas Hermans, unpublished data) to enable incorporation of a fluorophore. Further modifications of the protocol were performed in this thesis to replace the usage of phages for the production of single-stranded DNA by enzymatic reactions. 1GATC[a] circles enable the observation of DNA binding characteristics of fluorescence labeled MutH proteins. The generation of the substrate required five sub-steps which are schematically illustrated in Figure 3.12.

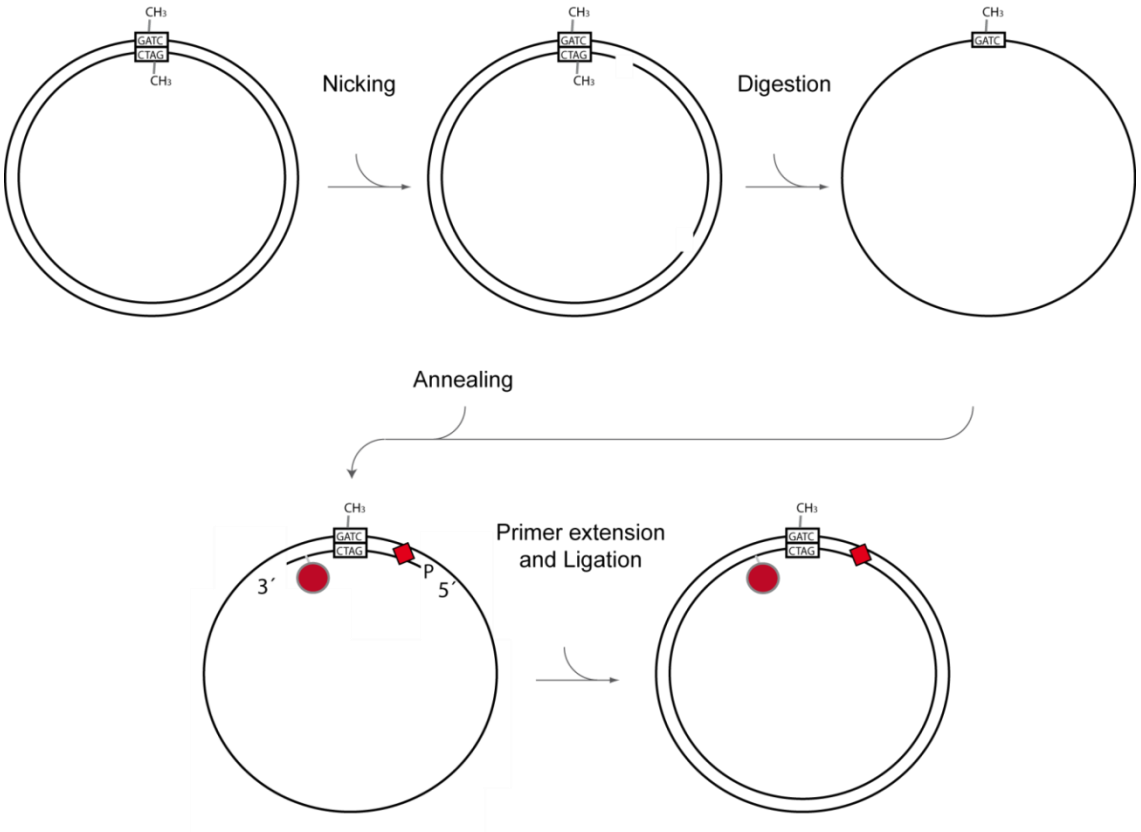

Figure 3.12: Schematic view of the generation of 1GATC[a] fluorescent DNA circles
Nicking One DNA strand in the 1GATC plasmid was nicked with Nt.BspQI in two positions. **Digestion** The nicked DNA strand was digested with Exonuclease III leaving a single-stranded DNA circle. **Annealing** A fluorescence labeled oligonucleotide could be annealed to the newly formed single-stranded DNA circle which also allowed the introduction of a mismatch. **Primer extension and Ligation** Primer extension and ligation generated the double-stranded 1GATC[a] circle. Exonuclease treatment digested residual oligonucleotides which were used in the annealing step (not shown). The fluorophore is indicated by a red circle, the mismatch by a red diamond, and the GATC site is framed by black boxes.

Intermediates in 1GATC[a] generation were nicked 1GATC plasmids and a single-stranded DNA circle (ss) after exonuclease digestion. Both can be seen in Figure 3.13 (lane 3 and 4).

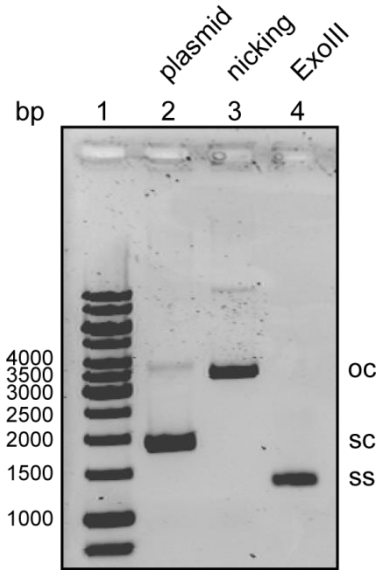

Figure 3.13: Generation of single-stranded DNA circles
A stepwise generation of single-stranded DNA is demonstrated on a 1.25% agarose gel stained with ethidium bromide. The process started with 1GATC plasmid DNA (lane 1). By nicking the bottom strand with Nb.BstQI the plasmid was transferred into an open circular form (lane 2). Addition of ExonucleaseIII led to digestion of the bottom strand. Therefore a single-stranded DNA circle was generated which ran faster in the agarose gel compared to plasmid-DNA (lane 3). The marker is GeneRuler 1 kb DNA ladder.

Further processing of ssDNA circles led to double-stranded, closed DNA circles containing a fluorescent dye. The final 1GATC[a] circle is shown in Figure 3.14, A, lane 5 and its fluorescence in Figure 3.14, B, lane 5.

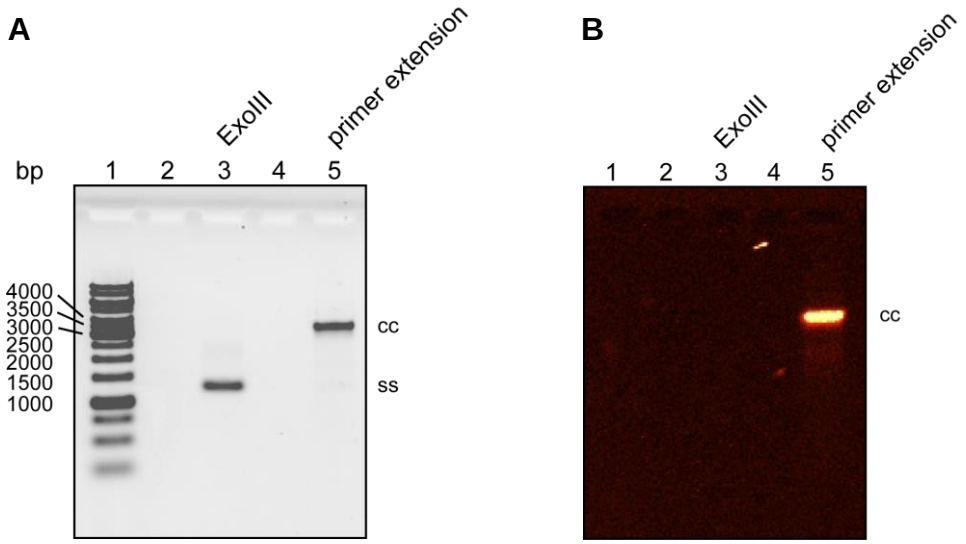

Figure 3.14: Introducing modifications into circular DNA by annealing modified oligonucleotides to single-stranded DNA circles
The conversion of a single-stranded circular DNA (from Figure 3.13) to a closed circle containing a fluorophore is visualized in a 1.25% agarose gel. **A** A single-stranded DNA circle (lane 3). Annealing of a fluorescent dye attached oligonucleotide, followed by a primer extension and ligation reaction led to the formation of a closed DNA circle (lane 5). **B** The unstained gel was analyzed in a *VersaDoc* system and shows the fluorescence of the closed DNA circle, the final 1GATC[a] circle. The marker is GeneRuler 1 kb DNA ladder.

The faster-migrating band (in Figure 3.14, A, lane 3) at 1300 bp marker length represents the ssDNA circle and disappeared after primer extension and purification (Figure 3.14, A, lane 5). Successful conversion to the final 1GATC[a] circle is visible in Figure 3.14, A, lane 5 as this band migrates slower in the gel, at the expected length of the final circle. Fluorescence labeled primers which were used for the primer extension were used in excess to the ssDNA circles. Digestion of unused primers and purification of the 1GATC[a] circles was complete. This can be seen in the *VersaDoc* fluorescence setup (Figure 3.14, B, lane 5) in which residual primers would be visible as a faster-migrating fluorescence band.

3.3 Visualizing complex formation in MMR

During this thesis, different assays were followed to visualize sub-steps in MMR. The assays are described in the following chapters, starting with MutS binding the mismatch and ending with MutH forming the incision complex. An overview of the assays is shown in Figure 3.15. Different fluorophore combinations were used in varying fluorescence setups. The nomenclature in experimental procedures 2.2 describes the abbreviations used for the fluorescence signals in the following chapters.

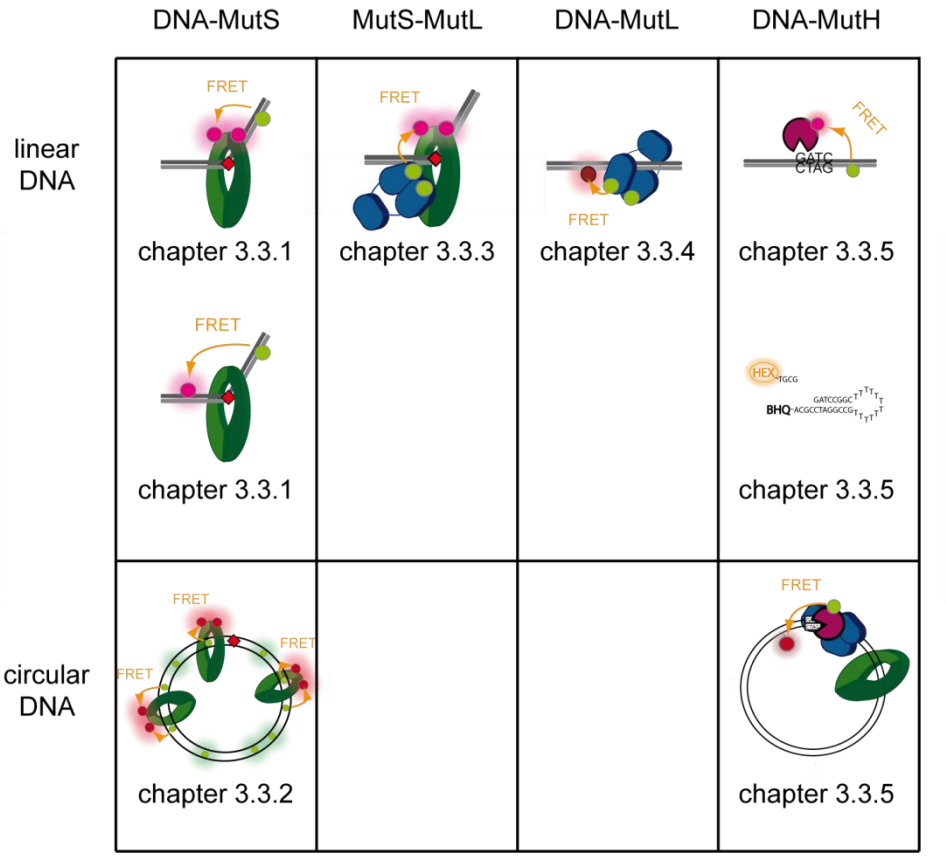

Figure 3.15: Overview of FRET assays to visualize sub-steps in MMR
The top line indicates the complex formation of two components of the MMR which was visualized by FRET. Sequences and modifications of the DNA can be seen in Table 2.6 and 2.8 (experimental procedures). Detailed information about a certain sub-step can be found in the corresponding chapter and additional assays are shown in the Appendix.

3.3.1 MutS binding DNA

The initial step in MMR is the recognition of the mismatch by MutS. To visualize and analyze this event two assays were developed. The first assay used a fluorescence labeled MutS and a DNA which carried a fluorophore next to a G:T mismatch (3.3.1.1). Binding of the labeled MutS to the mismatch generated a FRET. The second assay was based on a double fluorescence labeled DNA wherein one fluorophore was positioned at each side of the mismatch (3.3.1.2). Binding of MutS to the mismatch caused bending of the DNA and thus decreased the distance between the fluorophores. This decrease in distance led to an increase in FRET. Changes in anisotropy of the fluorophores during the DNA-bending assay were used to determine MutS binding orientations at different mismatches in DNA (3.3.1.3).

3.3.1.1 Site-specific DNA binding of MutS

A fluorophore close to a G:T mismatch acted as a FRET donor in combination with an acceptor fluorophore on MutS[a]. A FRET arose during binding of the mismatch by MutS[a]. With MutS[a] leaving the mismatch the FRET vanished.

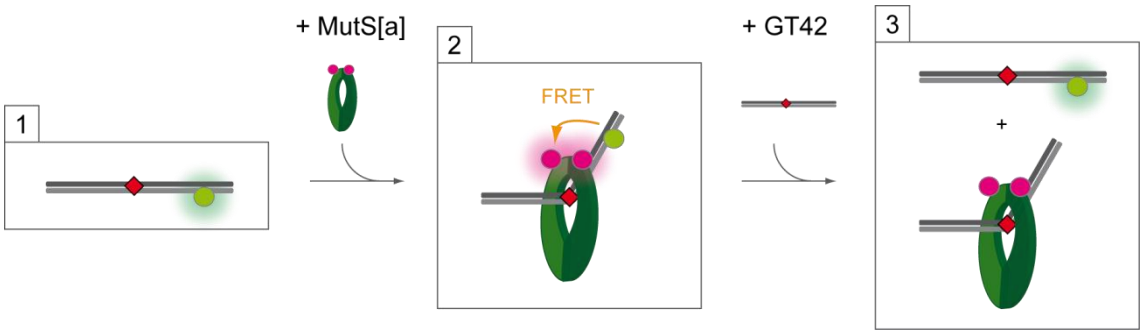

Figure 3.16: Schematic view of events during site-specific DNA binding of MutS
Excitation of donor labeled DNA resulted in fluorescence emission of the donor fluorophore (green dot) coupled to a 42 bp long oligonucleotide containing a G:T mismatch (red diamond). After addition of acceptor labeled MutS (MutS[a]), MutS[a] bound to the mismatch on the DNA and brought the acceptor fluorophore in proximity to the donor which generated a FRET (orange arrow). Excess of unlabeled 42 bp oligonucleotide containing a mismatch (GT42) acted as a competitor in the reaction. Most labeled MutS[a] did bind to the unlabeled GT42 and was therefore no longer available as a FRET partner.

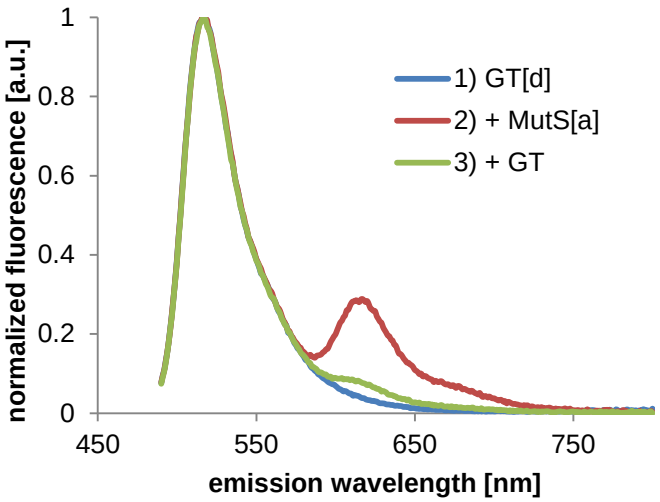

Figure 3.17: Site-specific DNA binding of MutS visualized by FRET
Excitation of donor labeled oligonucleotide GT42[d] led to a fluorescence signal which reflected donor emission (blue line). Addition of acceptor labeled MutS[a] generated FRET by binding the DNA (red line). Addition of unlabeled GT42 oligonucleotide competed within the reaction, as it was also a substrate for MutS. The FRET decreased (green line). Fluorescence spectra were normalized for the donor fluorescence to be 1 at its maximum 517 nm. FRET effects were observed in the strength of acceptor fluorescence at 617 nm. In this reaction, Alexa 488 served as a donor and Alexa 594 as an acceptor fluorophore. 50 nM of GT42[d], 100 nM MutS[a] variant R449C-D835R, and 2 µM of GT42 were used together with 1 mM ADP. K_D for DNA binding of MutS in this system was at 20 nM MutS (data not shown).

Fluorescence spectra obtained during the reaction visualized the binding of MutS by an increase in FRET. The blue graph shows the donor emission which was normalized to 1. Addition of MutS[a] resulted in a FRET which can be seen in the high accepter fluorescence emission at 617 nm. Addition of excess unlabeled GT42 DNA acted as a competitor in the reaction as the majority of MutS[d] did bind to it and there was not much MutS[a] available anymore to generate a FRET with GT42[d]. Quantitative analysis of the reaction (Figure 3.18) confirmed the occurrence of FRET in the assay.

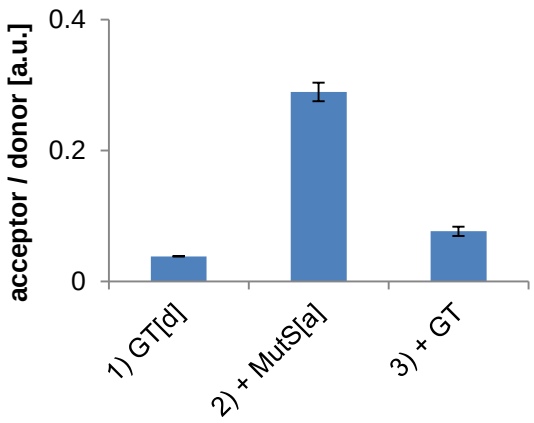

Figure 3.18: Quantitative analysis of FRET changes during site-specific DNA binding of MutS
Columns represent intensity ratios between acceptor and donor fluorescence. Changes in these ratios were caused by FRET effects during the assay and were calculated by dividing maximal acceptor emission through maximal donor emission. The reaction was repeated three times and observed ratios were averaged. The height of the columns represents the intensity ratio in each phase of the assay. Error bars indicate the standard deviation of $n = 3$ independent experiments. **1)** ratio of 0.04 **2)** ratio of 0.29 **3)** ratio of 0.08.

The ratio between acceptor and donor fluorescence emission started with a value of 0.04 which represents only the fluorescence donor at GT42[d] (signal Fd). With addition of MutS[a] the ratio reached a value of 0.29 caused by FRET and dropped to 0.08 upon addition of competitor DNA. The final ratio of 0.08 lay above the initial ratio of 0.04 in the experiment and resulted from spectral crosstalk as the acceptor fluorophore Alexa 594 was partially directly excited by the exciting light (signal Fb). Furthermore, some MutS[a] may have remained bound to GT[d] after competition which would have additionally increased the intensity ratio.

3.3.1.2 MutS bending DNA

A hallmark of DNA mismatch recognition is the bending/kinking of the DNA by MutS which has been observed for both, bacterial and eukaryotic MutS proteins at all mismatches investigated [28] [29] [65] [66]. DNA-bending can be monitored as a change in distance and hence by using FRET. In this assay, a double fluorescence labeled DNA was used. The FRET donor was attached to the DNA close to the mismatch while the acceptor was attached to the DNA beyond the mismatch.

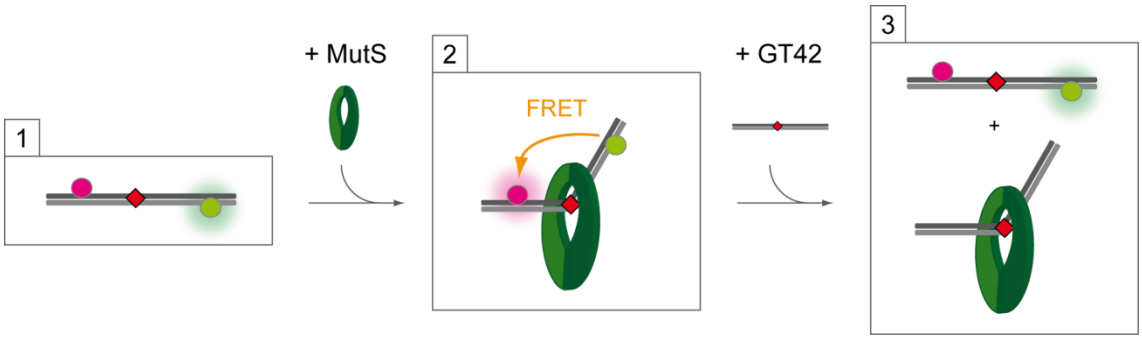

Figure 3.19: Schematic view of events during DNA-bending assay
A linear DNA containing a G:T mismatch (red diamond) was bound and bent by MutS. A donor fluorophore on one side of the mismatch (green dot) would come closer to an accepter fluorophore on the other side (magenta dot) during the bending process. The excited donor fluorophore therefore could transfer more energy to the acceptor (orange arrow). Addition of unlabeled GT42 acted as competitor in the reaction.

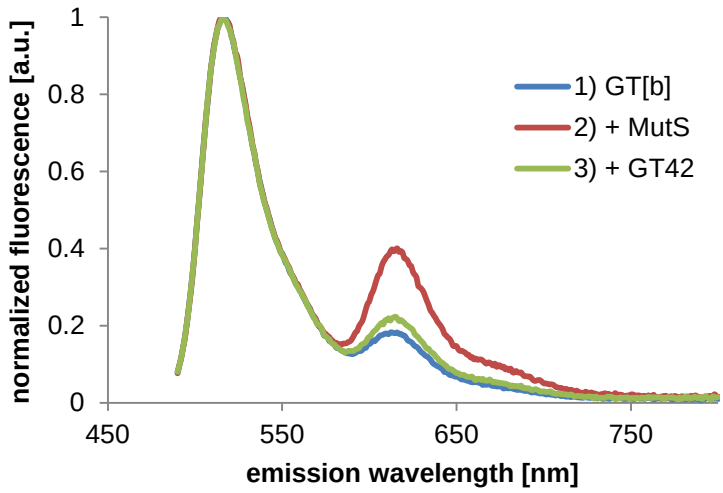

Figure 3.20: DNA-bending assay
Excitation of the donor fluorophore within the GT[b] led to a weak FRET signal, indicated by low acceptor fluorescence at 617 nm (blue line). Addition of MutS led to DNA-bending and an increase in FRET (red line). This was observed in the high acceptor fluorescence. Addition of unlabeled GT42 as competitor inhibited MutS from bending the GT[b] which led to a decrease in FRET (green line). Fluorescence spectra had been normalized for the donor fluorescence to be 1 at 517 nm. FRET effects were observed in the strength of acceptor fluorescence at 617 nm. In this reaction, Alexa 488 served as donor and Alexa 594 as acceptor fluorophore. 50 nM of GT42[b], 200 nM MutS variant R449C-D835R, and 2 µM of GT42 were used together with 1 mM ADP. K_D for DNA binding of MutS in this system was at 20 nM MutS (data not shown).

A quantitative analysis of the reaction is shown in Figure 3.21. Calculation of FRET effects were performed by dividing maximal acceptor emission through maximal donor emission.

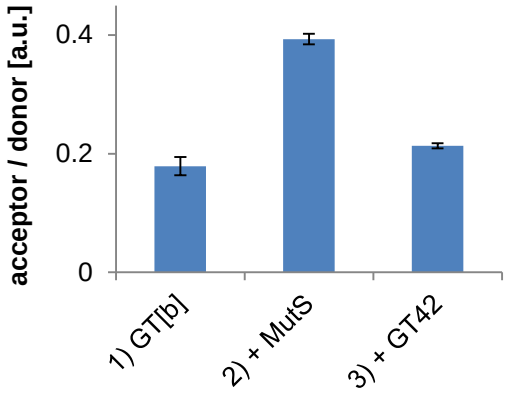

Figure 3.21: Quantitative analysis of the DNA-bending assay
Columns represent intensity ratios between acceptor and donor fluorescence. Changes in these ratios were caused by FRET effects during the DNA-bending assay and were calculated by dividing maximal acceptor emission through maximal donor emission. The height of the columns represents the intensity ratio in each phase of the assay. Error bars derived from the standard deviation of $n = 3$ independent experiments. **1)** ratio of 0.18 **2)** ratio of 0.39 **3)** ratio of 0.21.

MutS bending GT[b] was indicated by an increased intensity ratio (from 0.18 to 0.39) between acceptor and donor fluorescence which derived from FRET effects. Addition of competitor DNA GT42 caused a decrease in FRET and was observed in a drop of the ratio to 0.21. The final value of 0.22 lies above the initial value of 0.19 in the experiment, as it was already observed in 3.3.1.1. Here the slightly higher final level of intensity ratio only originates from residual MutS remaining bound to GT[b] as the acceptor fluorophore was already present in the first experimental step (signal Fb), in contrast to the experiment in 3.3.1.1 (signal Fd).

3.3.1.3 Directional MutS binding to mismatched bases in DNA

MutS crystal structures [28] [66] revealed that a phenylalanine at position 36 of MutS subunit A intercalates into DNA during mismatch recognition which generates an asymmetry in the MutS homodimer. With the intercalation, the phenylalanine stacks on one of the mismatched bases being either in the top or bottom strand. Thereby, MutS can bind a mismatch in two possible orientations (Figure 3.22). In the crystal structures, MutS only stacked on thymine in the bottom strand within a G:T mismatch and on guanine in the bottom strand within a G:G mismatch. To address the question if MutS shows the same strand preference in solution, the DNA-bending assay (Figure 3.19) was used to analyze the orientation of MutS during binding a mismatched DNA. In parallel, single-molecule multiparameter fluorescence detection (smMFD) measurements were performed by our group to address the same question on the single-molecule level [36] [60].

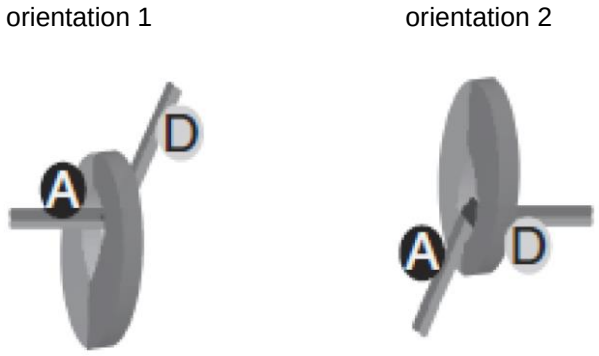

Figure 3.22: MutS binding in different orientations to DNA
Subunit A (blue) of MutS dimer intercalates into DNA and determines MutS binding orientation. MutS binding is illustrated here for a donor and acceptor fluorophore labeled DNA. The binding orientation was observed by changes in fluorescence anisotropy of the fluorophores. In orientation 1, MutS is in contact with the acceptor fluorophore [A] on the DNA, thereby increasing the fluorophores anisotropy. In orientation 2, MutS is in contact with the donor fluorophore [D].

To visualize the asymmetric DNA binding behavior of MutS the fluorescence anisotropy of the donor and acceptor fluorophore in a double labeled DNA was measured during MutS binding of a mismatched DNA. Additional experiments were performed using only a donor or acceptor labeled DNA. The DNA constructs are illustrated in Figure 3.23, A and B. Anisotropy changes of the fluorophores were observed for DNAs containing either the mismatches G:T, T:G, G:G, or the homoduplex G:C (Figure 3.23, C-E). For the T:G mismatch, strong changes in anisotropy of the donor fluorophore were observed which was not the case for the G:T construct and only small changes were observed with the homoduplex G:C. So for the T:G DNA it appears that MutS binds in an orientation which is in close proximity to the donor fluorophore. The acceptor anisotropy showed a strong increase for the G:T construct while there were only minor changes in acceptor anisotropy using the T:G mismatch DNA. Therefore MutS seems to be in proximity to the acceptor fluorophore upon binding the G:T mismatch. These results are in agreement with the crystal structure [28] and indicate phenylalanine stacking of MutS on thymine in the top strand with T:G DNA and stacking on the thymine in the bottom strand with G:T DNA. The smMFD measurements confirmed the observations of the ensemble measurements [60].

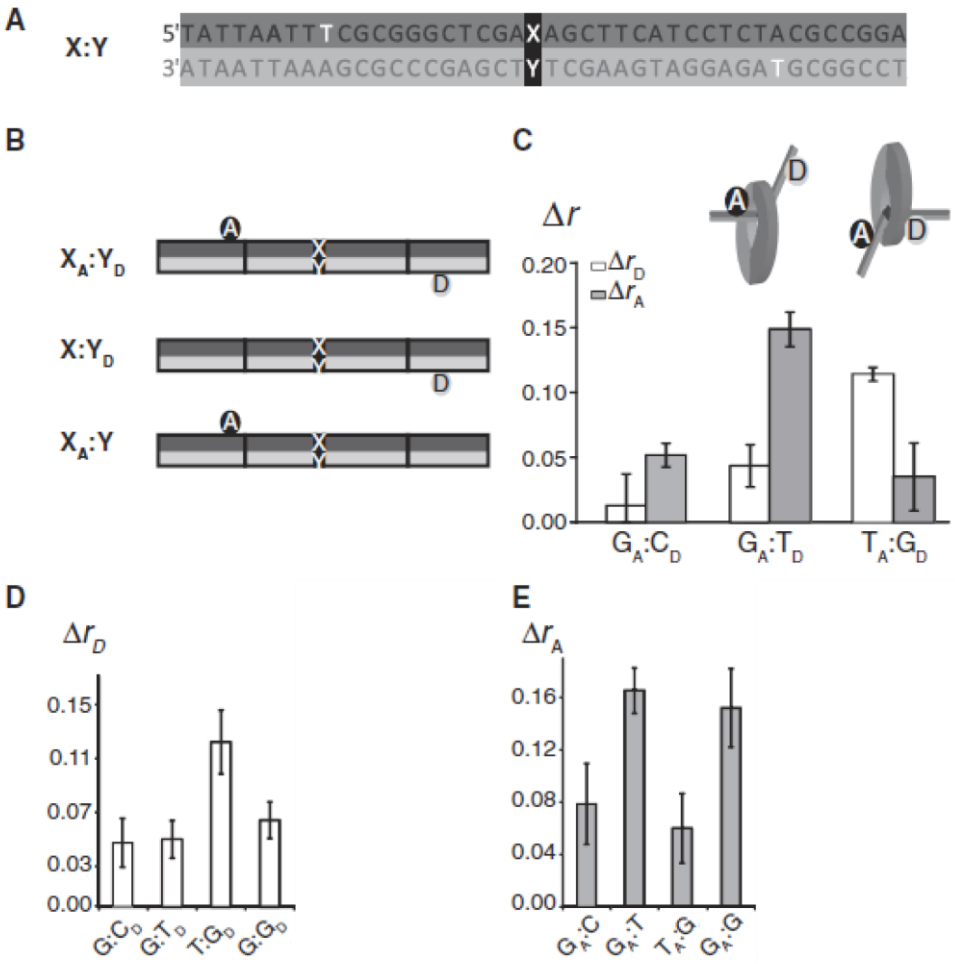

Figure 3.23: Mismatch dependence of MutS binding orientation [60] (modified)
A Sequences of the labeled DNA substrates used in the experiments. X:Y represents the varied mismatched base pair or homoduplex and can either be G:C, G:T, T:G or G:G. The T bases labeled with acceptor (top strand) and the donor dye (bottom strand) are shown in white. **B** Schematic view of the different DNA substrates. **C-E** Steady-state fluorescence anisotropy of 42 bp DNA labeled with donor and/or acceptor dyes in the presence of MutS. **C** X_A:Y_D labeled DNAs (10 nM), containing G:T, T:G or no mismatch (G:C) were incubated with MutS (250 nM) and ADP (1 mM), and changes in fluorescence anisotropy (Δr) were measured for both the donor (Δr_D, white bars) and acceptor (Δr_A, gray bars) dyes (the error bars are standard deviations from at least three independent experiments). **D** Changes in donor and **E** acceptor fluorescence anisotropy of DNA labeled with either donor (X:Y_D) or acceptor dye (X_A:Y) and the indicated mismatches.

For the G:G mismatch intermediate anisotropy changes were observed for both donor and acceptor fluorophore which indicates that MutS can bind a G:G mismatch in both orientations which was also observed in the smMFD setup [60]. These findings were not consistent with the crystal structure in which only one orientation was observed [66]. Further analysis performed by Michele Cristovao demonstrated a stacking of MutS phenylalanine on adenine within the top strand of an A:C mismatch and the adenine within the bottom strand of a C:A mismatch. Thereby, the possible influence of sequence context was also ruled out by inverting the central sequence around the mismatch which had no effect.

3.3.2 Monitoring MutS sliding clamp formation

A key step in MMR is the conversion of MutS into a sliding clamp after mismatch binding on DNA [12]. The following assay was designed to observe kinetics of this MutS sliding clamp formation. Incorporation of SYBR Green I (SG) into double-stranded DNA leads to a significant increase in SG fluorescence [52]. In a FRET setup SG can be used as a donor fluorophore [67]. In this assay, an acceptor fluorophore was attached to MutS (MutS[a]). With MutS[a] binding the DNA - SYBR Green I complex, a FRET signal was generated and could be detected in the FRET channel (Fb). This setup allowed analysis of MutS binding to any place on DNA molecules without being limited to a visualization of mismatch-specific binding. As 10 nM of a 932 bp long DNA and 100 nM SG were used in the assay, there was a dye per base pair ratio of approximately 1 dye per 93 bp. MutS can adopt a mobile conformation on DNA in an ATP-dependent manner. To avoid MutS from dissociating from DNA ends, a circular DNA containing a single G:T mismatch was used. This circular DNA was called GT932 and its generation is described in chapter 3.2.1. The reaction in the assay was started with a low concentration of ADP (1 µM), which allowed MutS[a] to bind the mismatch and thereby generate a FRET signal. As the ADP-bound MutS[a] was not able to form a sliding clamp and leave the mismatch, there was only one MutS dimer at one DNA circle (with the exception of a minor fraction of homoduplex-bound MutS[a]). With addition of excess ATP (1 mM) over ADP MutS[a] was binding ATP and transformed into a sliding clamp which enabled it to travel along the DNA. As the mismatch was no longer occupied by the initial MutS[a] dimer additional MutS[a] could bind to the DNA undergoing the same process as the initial MutS[a]. This process is called multiple loading [12] [68]. The additional MutS[a] on the DNA generated a higher FRET as there were more acceptor fluorophores close to the donor fluorophores (SG) in the DNA. The increase in FRET over time reflected the kinetics of MutS sliding clamp formation and multiple loading. A schematic view of the reaction is shown in Figure 3.24 and an exemplary time trace in Figure 3.25. Fluorescence spectra corresponding to the time trace are depicted in Figure 3.26. Kinetic rate constants determined in three independent experiments are listed in Table 3.3. Emission spectra recorded during the experiments were used for quantitative analysis of FRET effects in the assay (Figure 3.27).

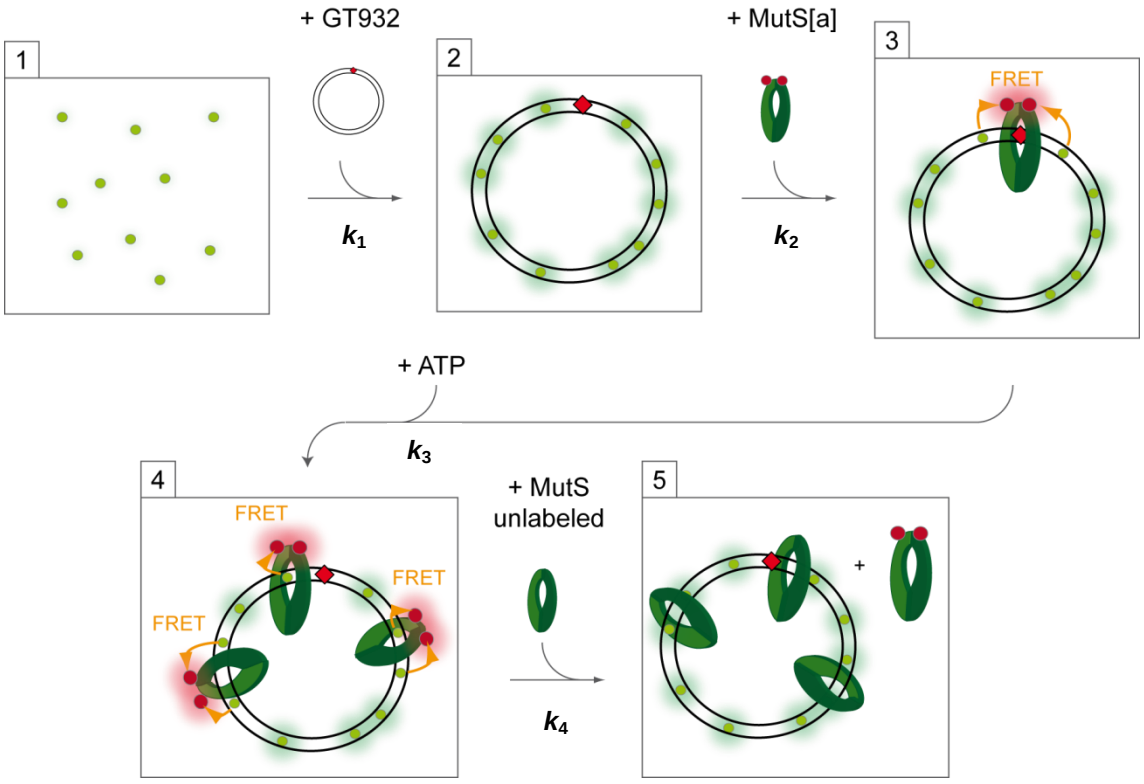

Figure 3.24: Schematic view of events during the MutS sliding clamp formation assay
SG alone (green dots) possessed a weak fluorescence. Upon incorporation into dsDNA (GT932) SG emitted a strong fluorescence. Binding of MutS[a] to the mismatch (red diamond) in an ADP-bound state generated a FRET (orange arrow) with nearby SG molecules. Binding of ATP enabled MutS[a] to transform into a sliding clamp and move along the DNA. Several MutS[a] dimers could now bind one DNA and therefore generated more FRET. Addition of excess unlabeled MutS competed the reaction by binding the DNA and therefore hindering MutS[a] from binding to DNA. The FRET vanished. $\boldsymbol{k}_{1\text{-}4}$ rates describe how fast the FRET intensity changed between two phases.

In the representative time trace which was normalized to the maximum signal (Figure 3.25), SG fluorescence itself generated a low signal of 0.01 in the FRET channel (Fd) and reflected the spectral crosstalk as no acceptor was present in the sample. Addition of DNA led to an enhanced SG fluorescence as SG incorporated into DNA. The enhanced SG fluorescence increased the signal to 0.22 which also derived from spectral crosstalk. Binding kinetics of SG to DNA (k_1) was too fast for detection in this setup. Addition of MutS[a] allowed one MutS dimer to bind the DNA at the mismatch which increased the signal (FRET) to 0.54 (k_2). Initiation of MutS sliding clamp formation was achieved by addition of ATP which further increased the signal to 1 (k_3). During competition of the reaction with 1 µM unlabeled MutS, the MutS[a] dissociation process led to a decreasing FRET (k_4). This decrease did nearly reach a plateau level of 0.62 at the end of the measurement at 1200 s. Increasing competitor concentration to 2 µM further decreased the signal to 0.40 (data not shown).

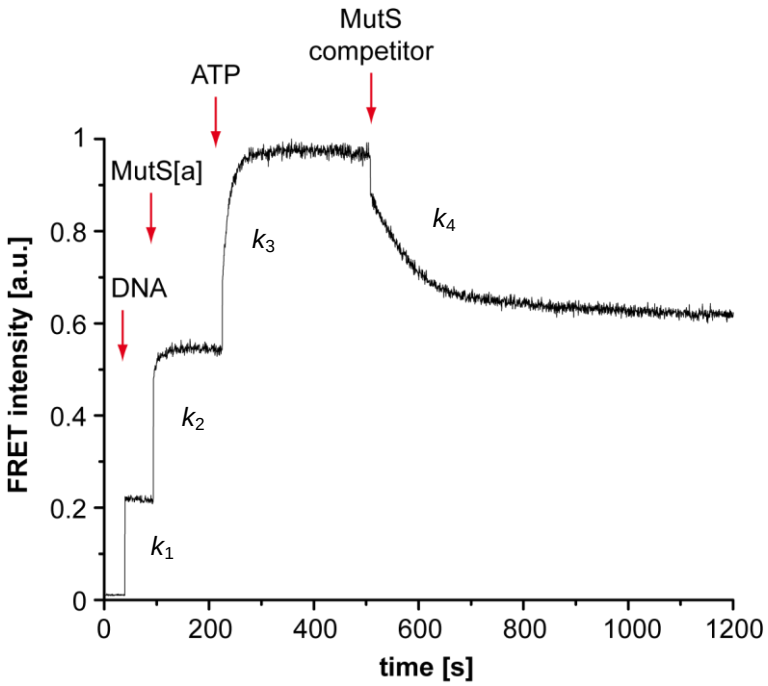

Figure 3.25: Kinetics of MutS sliding clamp formation
MutS generated a FRET upon binding a SG labeled DNA circle which was measured in the FRET channel (Fb). $\boldsymbol{k_{1\text{-}4}}$ rates describe how fast the FRET intensity changed between two phases. $\boldsymbol{k_1}$ resembles the rate of 100 nM SG incorporation into 10 nM DNA (GT932) with 1 µM ADP present. $\boldsymbol{k_2}$ binding of 100 nM MutS[a] variant R449C D835R labeled with Alexa 647 to the mismatch. $\boldsymbol{k_3}$ after addition of 1 mM ATP MutS[a] transformed into a sliding clamp which allowed more MutS[a] to bind the same DNA. $\boldsymbol{k_4}$ 1 µM of unlabeled MutS variant R449C D835R competed by hindering MutS[a] from rebinding DNA after dissociation.

Kinetic rate constants determined in the experiment are listed in Table 3.3.

Table 3.3: Kinetic rate constants of MutS sliding clamp formation assay
Kinetic rate constants for each experiment were determined and averaged. The error represents the standard deviation of $n = 3$ independent experiments.

kinetic rate	process	$t_{1/2}$	k
k_1	SG incorporation into DNA	ND	ND
k_2	MutS[a] binding DNA	4.8 ± 0.7 s	0.21 ± 0.03 s^{-1}
k_3	MutS sliding clamp formation	12.4 ± 1.6 s	0.08 ± 0.01 s^{-1}
k_4	MutS sliding clamp dissociation	54.3 ± 22.5 s	0.02 ± 0.01 s^{-1}

After each phase in the reaction, the measurement was paused and fluorescence emission spectra were determined. Representative spectra are shown in Figure 3.26 and a quantitative analysis in Figure 3.27.

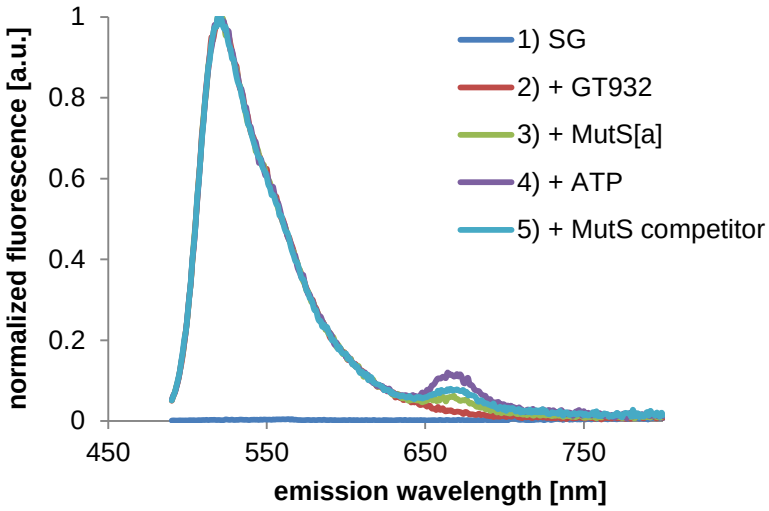

Figure 3.26: Emission spectra of MutS sliding clamp formation assay
The donor was normalized to 1 in each phase, except for 1) in which the normalization factor for 2) was used to demonstrate the difference in SG fluorescence without and with DNA. **1)** 100 nM SG with 1 µM ADP and without DNA. **2)** SG bound to circular DNA (GT932) after addition of 10 nM GT932. **3)** MutS[a] bound to the mismatch generated an intermediate FRET after addition of 100 nM MutS[a]. **4)** Multiple MutS[a] in a sliding clamp conformation bound to circular DNA generated a high FRET after addition of 1 mM ATP. **5)** Addition of 1 µM unlabeled MutS competed for DNA binding with MutS[a] and the FRET decreased.

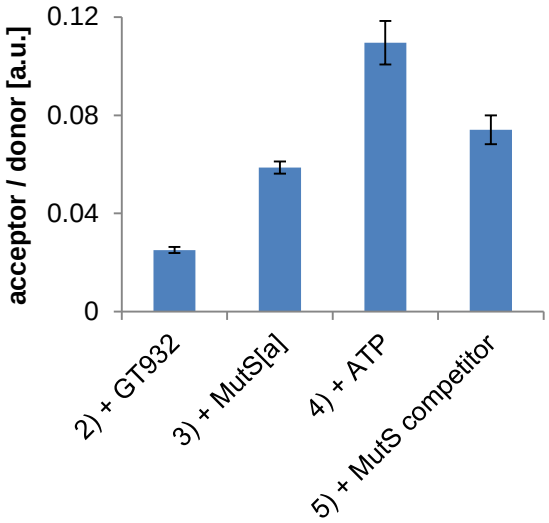

Figure 3.27: Quantitative analysis of MutS sliding clamp formation assay
Acceptor fluorescence was divided through donor fluorescence observed in the fluorescence spectra to visualize FRET effects in the assay. Ratios of three independent experiments were averaged. **1)** As SG fluorescence was hardly detectable without DNA, the acceptor / donor ratio could not be determined. **2)** Ratio of 0.03. **3)** Ratio of 0.06. **4)** Ratio of 0.11. **5)** Ratio of 0.07. Increasing competitor concentration to 2 µM further decreased the acceptor / donor ratio to 0.05 (data not shown). Error bars derived from the standard deviation of $n = 3$ independent experiments.

Taken together, this assay allowed a determination of kinetic rate constants and an observation of MutS binding to a mismatch on DNA and the following transformation of MutS into a sliding clamp. Dissociation rates of the MutS sliding clamps from DNA could be addressed as well.

3.3.3 MutS-MutL complex formation

The activated form of MutS on DNA is able to recruit MutL, the second principal component of MMR. Ternary complex formation between MutS, MutL, and DNA is addressed in this chapter. Structural information about MutS-MutL complexes were already gained in former studies by crosslinking experiments of different MutS and MutL variants [37] [35]. These crosslink experiments suggested that in the MutS-MutL complex the ATPase domain of MutL is in proximity to the mismatch binding domain and the connector domain of MutS. The data is consistent with data obtained by other groups [69].

To obtain further information about the structure of the MutS-MutL complex and the ternary complex formation, a MutS variant was labeled with an acceptor fluorophore in the connector domain (D246C) and a MutL variant was labeled with a donor fluorophore in the ATPase domain (H297C). Upon complex formation, these variants generated a high FRET (Figure 3.29, B). Another MutS variant (R449C) was labeled with an acceptor fluorophore in the clamp domain (R449C) and served as control. This variant generated a low FRET in combination with the labeled MutL (Figure 3.29, A) which was expected as the clamp domain of MutS and the ATPase domain of MutL were supposed to be further separated compared to the connector domain of MutS and the ATPase domain of MutL. The reaction of MutL[d] binding to MutS[a] is schematically illustrated in Figure 3.28 for a 484 bp linear DNA, containing a G:T mismatch (GT484). Normalized fluorescence emission spectra are shown in Figure 3.29.

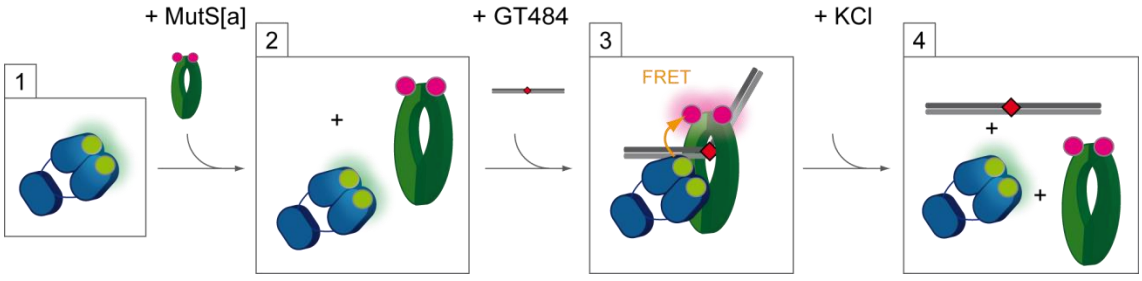

Figure 3.28: Schematic view of events during MutS-MutL complex formation on linear DNA
MutL[d] and MutS[a] were only able to form a complex after addition of mismatched DNA to the reaction (GT484). The mismatch is indicated by a red diamond, the fluorescence donor by green dots and acceptor by magenta dots. The complex formation generated a FRET (orange arrow). Increasing KCl concentration from physiological conditions of 125 mM to higher concentrations of 300 mM inhibited the complex formation and the FRET vanished.

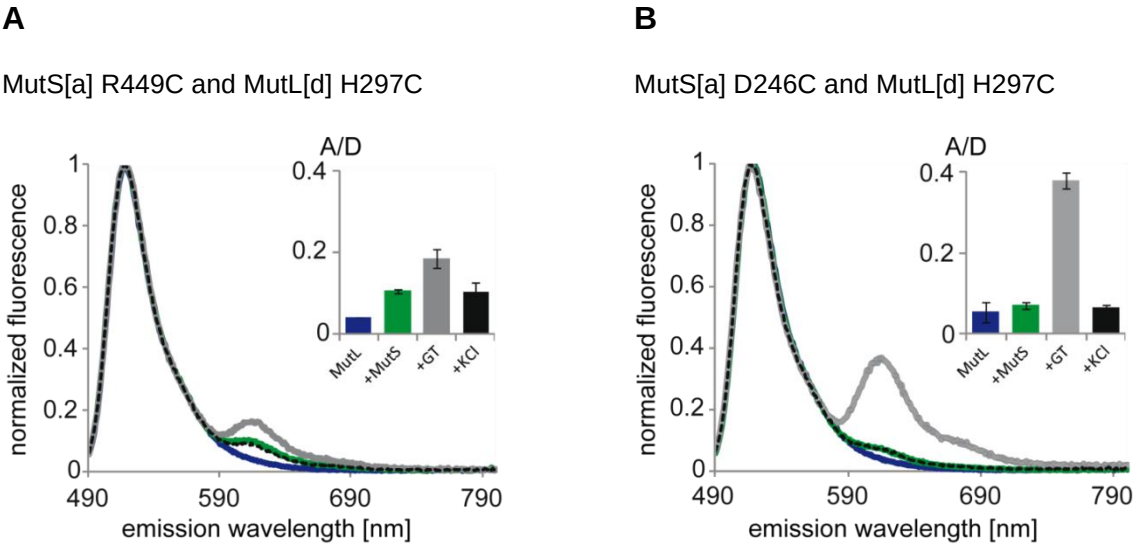

Figure 3.29: Comparing FRET intensities in the MutS-MutL complex varying the fluorophore position at MutS
Normalized emission spectra of donor and acceptor fluorophore are shown as curves. FRET effects can be seen only in acceptor fluorescence (maximum emission at 517 nm) as the donor was normalized to be 1. FRET intensities during interaction of fluorescence labeled MutS[a] and MutL[d] are indicated in the histogram. A/D is the ratio between acceptor and donor fluorescence and resembles the FRET intensity. In this reaction, Alexa 488 was used as fluorescence donor and Alexa 594 as acceptor. The reaction included 200 nM MutL[d] in the presence of 1 mM ATP (blue curves), addition of 200 nM MutS[a] green curves, addition of 50 nM GT484 (grey curves) and an increase in KCl concentration to 300 mM (black dashed curve). Averages and standard deviations (error bars) derived from n = 2 independent experiments and are plotted in the histogram. **A** MutS[a] variant R449C D835R and MutL[d] variant H297C. **B** MutS[a] variant D246C D835R and MutL[d] variant H297C.

A 484 bp long DNA was sufficient to enable MutS-MutL complex formation as FRET signals were observed. MutS variant D246C[a] generated a FRET signal of 0.38 with MutL[d] variant H297C while the R449C[a] variant of MutS generated a lower FRET signal of 0.18 (Figure 3.29, A and B). This suggests a longer distance between position 449 in MutS and position 297 in MutL compared to the distance between position 246 in MutS and position 297 in MutL.

3.3.4 MutL binding DNA

MutL can bind to both single-stranded and double-stranded DNA [70]. This effect had been observed before and its role and function is still under heavy debate. DNA binding is strongly modulated by the ionic strength and is almost absent at 125 mM KCl. The current chapter presents an assay to visualize the MutL-interaction with DNA. The assay allows measuring of the DNA binding ability of MutL in the absence of MutS either by FRET effects (Figure 3.31) or changes in anisotropy (Figure 3.32). The FRET assay was used to compare MutL binding to heteroduplex (Figure 3.31, B) with MutL binding to homoduplex DNA (Figure 3.31, A) and was performed at low ionic strength. The heteroduplex originates from deletion of an adenine in one strand generating an unpaired thymine (+T46) in the other strand after oligonucleotide annealing. The binding reaction is schematically illustrated in Figure 3.30 and fluorescence spectra are shown in Figure 3.31.

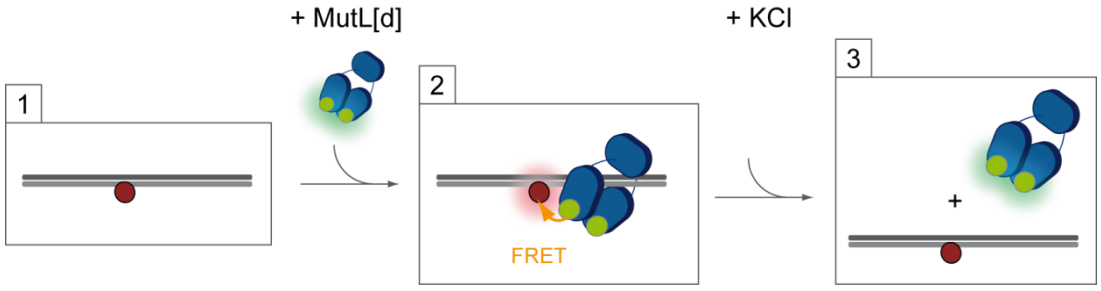

Figure 3.30: Schematic view of MutL binding linear DNA at low ionic strength
A 46 bp long linear DNA containing an acceptor fluorophore could be bound by MutL at low ionic strength. MutL carrying a donor fluorophore [d] was excited and transferred energy to the acceptor on the DNA, a FRET occurred (orange arrow). Addition of 200 mM KCl inhibited the DNA binding ability of MutL, it dissociated from DNA and the FRET effect vanished.

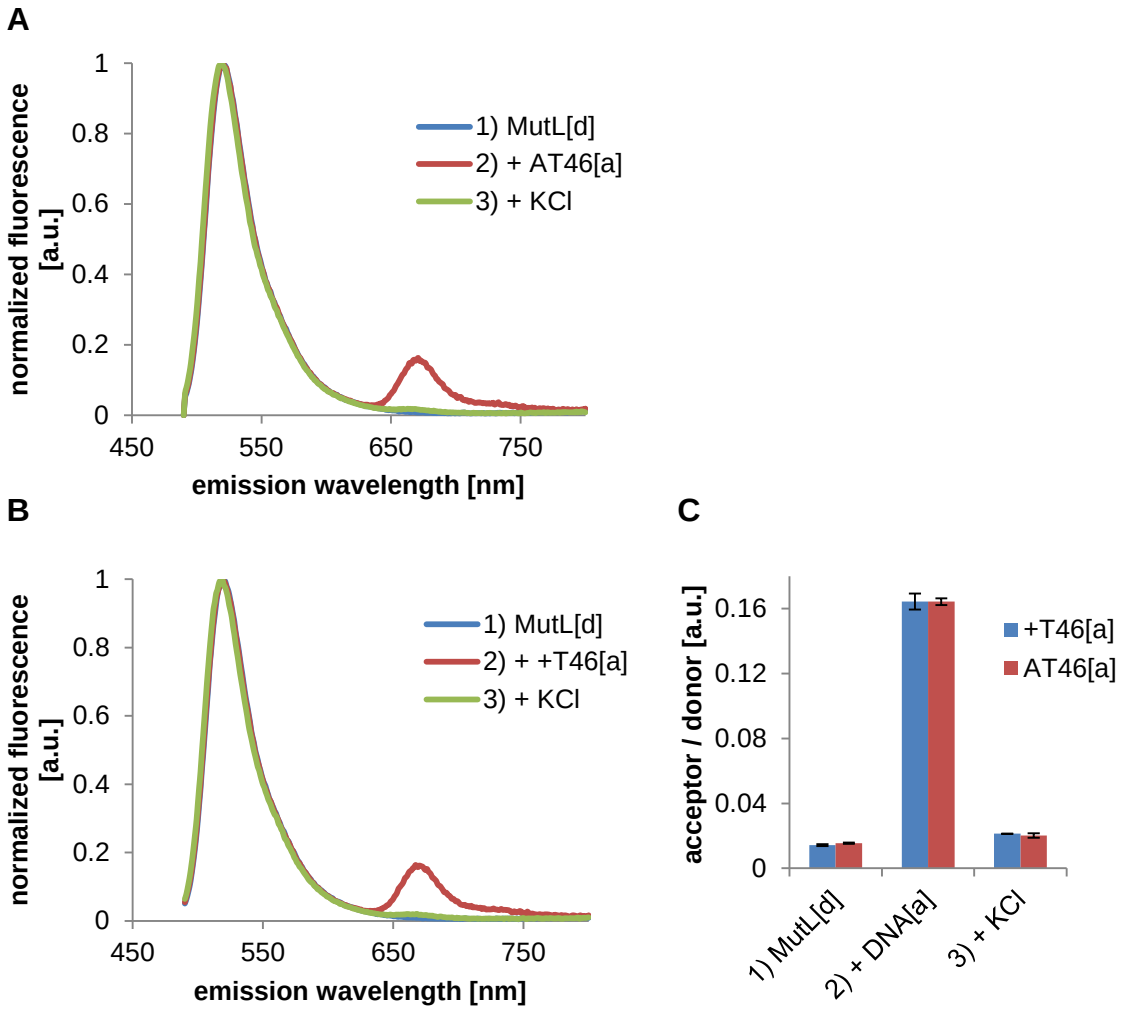

Figure 3.31: MutL binding linear DNA at low ionic strength
In the fluorescence spectra, the donor was normalized to be 1 at 517 nm. FRET effects can thereby be seen in the acceptor emission at 670 nm. In this reaction, Alexa 488 served as donor and Alexa 647 as acceptor fluorophore. 400 nM MutL[d] variant H297C and 400 nM DNA[a] were used in the presence of 1 mM ATP and low ionic strength. To inhibit MutL from binding DNA, the ionic strength was increased from 20 mM to 200 mM. Error bars indicate the standard deviation of n = 3 independent experiments. **A** MutL[d] binding to homoduplex DNA (AT46[a]). **B** MutL[d] binding to heteroduplex DNA containing an unpaired thymine (+T46[a]). **C** Comparison between homoduplex and heteroduplex binding of MutL[d]. FRET efficiencies were calculated by dividing acceptor fluorescence through donor fluorescence at the end of each phase. Homoduplex and heteroduplex acceptor to donor ratios were nearly equal and showed both in **1)** a ratio of 0.01, in **2)** a ratio of 0.16, and in **3)** a ratio of 0.02.

Normalized fluorescence spectra for both reactions (homoduplex and heteroduplex DNA[a] bound by MutL[d]) showed a high increase in FRET after MutL[d] addition (Figure 3.31, A and B). The FRET effect was reversed by addition of KCl. These changes in FRET reflected the interaction between MutL and DNA and demonstrated that it was possible to observe the interaction with this setup. Quantitative analysis of the comparison between MutL[d] either binding a homoduplex DNA[a] or a heteroduplex DNA[a] (Figure 3.31, C) did not show a significant difference (p = 0.98, unpaired t-test). It therefore revealed that a heteroduplex did not

influence the binding ability of MutL[d] under the conditions used. Binding of MutL to DNA could also be observed in the anisotropy of the fluorophore attached to DNA (Figure 3.32). This experiment contained the fluorophore Atto 488 attached to DNA and did not require a fluorophore at MutL.

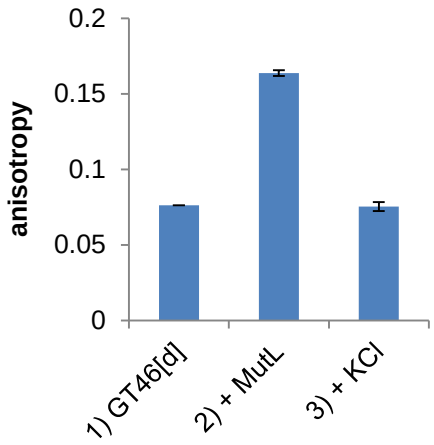

Figure 3.32: MutL binding DNA visualized by anisotropy changes (at low ionic strength)
Acceptor fluorescence was divided through donor fluorescence observed in the fluorescence spectra to visualize FRET effects. **1)** Anisotropy of Atto 488 attached to DNA (50 nM) was determined in the absence of MutL and with 1 mM ATP present. It showed a value of 0.08. **2)** After 300 nM of unlabeled MutL variant H297C were added to the reaction, it bound the DNA and thereby increased the anisotropy of the fluorophore at the DNA to a value of 0.16. **3)** Raising ionic strength from 20 mM to 200 mM by addition of KCl inhibited MutL from binding DNA and anisotropy decreased to a value of 0.08. Error bars indicate the standard deviation of $n = 3$ independent experiments.

MutL bound at low ionic strength to DNA and increased anisotropy of the fluorophore attached to the DNA from 0.08 to 0.16 (Figure 3.32, 2). Increasing the KCl concentration inhibited MutL from binding DNA and the anisotropy decreased to 0.08 (Figure 3.32, 3). Observation of these changes in anisotropy showed comparable effects to the FRET setup (Figure 3.31). Therefore, both assays were suitable to measure the DNA binding ability of MutL to short oligonucleotides.

3.3.5 MutH binding DNA

MutH possesses a weak ability to bind DNA which is inhibited at high ionic strength (125 mM KCl). The first part of this chapter (3.3.5.1 and 3.3.5.2) addresses direct DNA binding and cleavage by MutH at low ionic strength to enable the reaction. MutH did not require the active recruitment of MutS and MutL under those conditions. The second part (3.3.5.3) addresses the formation of the incision complex which is believed to be composed of DNA, MutS, MutL, and MutH [17]. This assay was performed at high ionic strength wherein MutH needs to be recruited by MutS and MutL to bind DNA.

3.3.5.1 MutH binding DNA without MutS and MutL at low ionic strength

To address DNA binding of MutH, a catalytically inactive variant was used to avoid cleavage of the DNA substrate and to generate a stable FRET. With this additional mutation (E77A), the DNA cleavage activity of MutH is disabled while its DNA binding ability is retained [47]. At low ionic strength, MutH[d] could bind a GATC site on a linear DNA[a]. A FRET signal was generated during this reaction. Increasing KCl concentration to 125 mM led to dissociation of MutH[d] and the FRET vanished. The reaction is schematically illustrated in Figure 3.33, A and representative fluorescence emission spectra are shown in Figure 3.33, B. Two different DNA constructs were used to address the influence of acceptor fluorophore positioning on DNA. In the first construct, the acceptor was located five base pairs upstream of the GATC site (1GATC-5[a]) while it was located ten base pairs downstream in the second construct (1GATC+10[a]). FRET effects represented by the ratio of acceptor to donor fluorescence are depicted in Figure 3.34 for both DNA constructs.

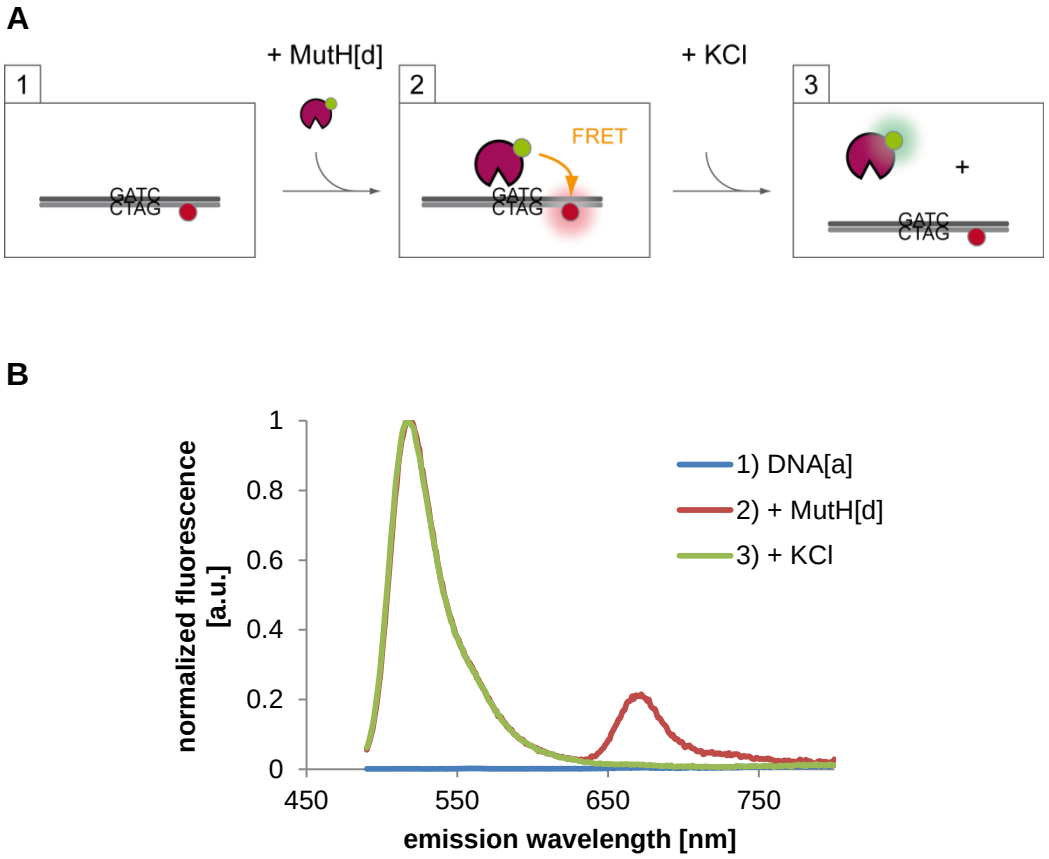

Figure 3.33: MutH binding DNA at low ionic strength
A Schematic view of MutH[d] binding a GATC site with an acceptor [a] nearby. DNA[a] was bound by MutH[d] which enabled a FRET (orange arrow) between an acceptor fluorophore [a] near the GATC site (red dot) and a donor fluorophore [d] attached to MutH (green dot). Addition of KCl inhibited the reaction as MutH[d] was unable to bind DNA at high ionic strength (125 mM KCl). **B** Normalized fluorescence spectra of an exemplary reaction of MutH[d] binding DNA[a]. Spectra of step 2) and 3) were normalized for the donor fluorescence to be 1 at its maximum 517 nm. As no donor was present in step 1) the donor value of step 3) was used for the normalization. FRET effects can be observed in the strength of acceptor fluorescence at 670 nm. In this reaction, Alexa 488 served as donor and Alexa 647 as acceptor fluorophore. 100 nM of 1GATC-5[a] oligonucleotide and 400 nM MutH[d] variant E77A S85C C96S were used and ionic strength was increased from 20 mM to 125 mM.

The representative reaction in Figure 3.33 shows a high FRET effect as the acceptor fluorescence increased upon MutH[d] binding DNA[a] (red line at 670 nm). The effect vanished after addition of KCl (green line at 670 nm). To compare FRET effects of the reaction with either 1GATC-5[a] DNA or 1GATC+10[a], the ratio between acceptor and donor fluorescence was analyzed during the different steps in the reaction (Figure 3.34).

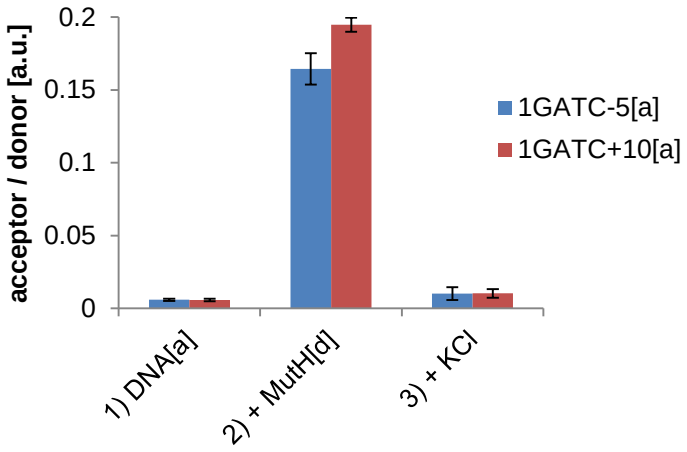

Figure 3.34: FRET effects during MutH binding linear 1GATC[a] DNA at low ionic strength
Two different DNA[a] constructs were compared regarding their FRET effects upon MutH[d] binding. The FRET effects are indicated by the ratio of acceptor to donor fluorescence intensity. In the 1GATC-5[a] DNA an acceptor fluorophore was positioned 5 base pairs upstream of the GATC sequence (blue columns) while in the 1GATC+10 DNA the acceptor was 10 base pairs downstream (red columns). FRET effects during different steps in the reaction are represented by the ratio of acceptor to donor fluorescence (height of the columns). Averaged ratios and error bars representing the standard deviation derived from n = 3 independent experiments. As no donor was present in step 1) the donor value of step 3) was used for the ratio calculation. **1)** A ratio of 0.01 for both constructs. **2)** A ratio of 0.16 for 1GATC-5[a] and 0.19 for 1GATC+10[a]. **3)** A ratio of 0.01 for both constructs.

Ratio of acceptor to donor fluorescence recorded during donor excitation represented FRET effects (signal Fb). In the reaction containing the 1GATC-5[a] DNA construct, the ratio raised from an initial value of 0.01 to 0.16 (Figure 3.34, blue columns). These effects were reversed by addition of KCl and reached a final level of 0.01. The reaction with the 1GATC+10[a] construct resulted in similar FRET values (Figure 3.34, red columns), although the acceptor to donor ratio reached a slightly higher value of 0.19. Comparison of the ratios during both reactions revealed that both DNA-constructs allowed binding of MutH[d] and generation of a high FRET. Therefore, both DNA-constructs were suitable for the generation of fluorescence labeled 1GATC circles (chapter 3.2.2) which were required for a visualization of the incision complex (chapter 3.3.5.3).

3.3.5.2 MutH cleaving DNA without MutS and MutL at low ionic strength

To observe DNA nicking activities, a catalytically active variant of MutH was incubated with a molecular beacon. The molecular beacon consisted of a short single-stranded DNA with a poly-thymine sequence in the middle region, a Hex fluorophore at the 5´-end, and a black hole quencher at the 3´-end. A partial duplex DNA was formed by the complementary ends and generated a GATC site next to the fluorophore and quencher. Nicking of the GATC site by MutH occurred either in the bottom or top strand and therefore the Hex fluorophore or the quencher did dissociate from the rest. Dividing the quencher and Hex fluorophore led to an increase in Hex fluorescence. The reaction is schematically illustrated in Figure 3.35, A and an exemplary time trace is shown in Figure 3.35, B.

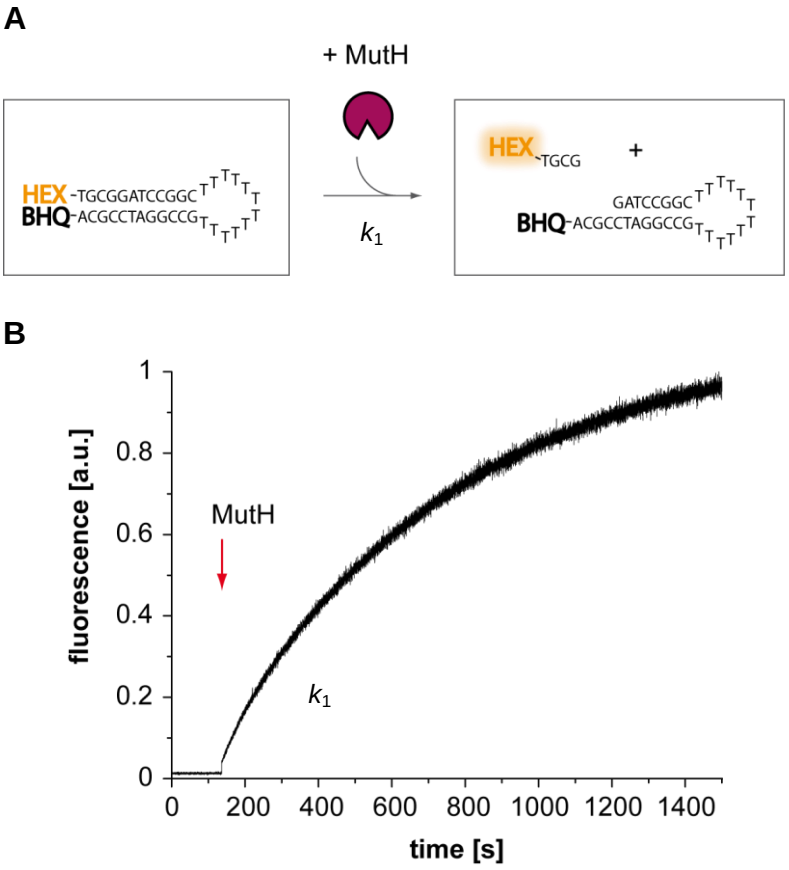

Figure 3.35: MutH nicking a molecular beacon at low ionic strength
A Schematic view illustrating the MutH nicking reaction. In a molecular beacon fluorescence of a Hex fluorophore was quenched by a black hole quencher. Low ionic strength enabled MutH binding and cleavage of a nearby GATC site which resulted in release of the fluorophore or quencher. Both cases led to a disruption of the quenching effect and an increase in Hex fluorescence (k_1). **B** The reaction started with addition of MutH (red arrow). Hex was excited at 535 nm and its fluorescence detected at 590 nm and recorded over time. 50 nM of the molecular beacon and 1 µM of MutH[d] variant S85C C96S were used at low ionic strength of 20 mM.

The Hex fluorescence remained stable at a low background level until MutH was added to the reaction (Figure 3.35, B). Increasing Hex fluorescence indicated nicking of the molecular beacon and therefore reflected MutH activity (k_1). The reaction was repeated three times. Nicking rates were determined for each experiment. The averaged nicking rate is shown in Table 3.4.

Table 3.4: Averaged nicking rate of MutH at low ionic strength
Nicking rates were determined with Origin software. Averaged nicking rate and the indicated standard deviation derived from $n = 3$ independent experiments.

kinetic rate	process	$t_{1/2}$	k
k_1	MutH nicking DNA	150 ± 20 s	0.007 ± 0.001 s^{-1}

3.3.5.3 MutH recruitment to DNA at high ionic strength (incision complex)

The incision complex is a key complex in DNA mismatch repair and is believed to consist of DNA, MutS, MutL, and MutH. It incises the newly synthesized, erroneous DNA strand and enables partial exonuclease digestion and resynthesis. Despite decades of studies in MMR, there is only little evidence for the formation of the MutS-MutL-MutH ternary complex. First evidence was provided by co-purification of MutH with MutL and a MutS affinity column [71]. Further evidence was provided by the possibility to trap the ternary complex with chemical crosslinking (Ines Winkler, unpublished data). Another heavy discussed process in MMR is the coupling of mismatch recognition by MutS with the strand discrimination of MutH (chapter 1.3). It remains controversy when MutH enters and leaves the MutS-MutL-DNA complex in time and space. Therefore, the aim of this assay was to visualize formation and dissociation of the incision complex. To achieve this, MutH[d] recruitment to DNA[a] in a MutS- and MutL-dependent manner was followed. A circular DNA, containing a mismatch and a fluorophore near a GATC site was generated (1GATC[a]). The generation process of the DNA is shown in chapter 3.2.2. Two possible fluorophore positions in this DNA were analyzed regarding their FRET efficiency upon binding of a fluorescence labeled MutH at low ionic strength in chapter 3.3.5.1. The catalytically inactive E77A variant of MutH[d], which was already used in chapter 3.3.5.1, suppresses DNA cleavage of MutH[d] and therefore may stabilize a formed incision complex. Incision complex formation at high ionic strength (125 mM KCl) requires a MutS- and MutL-dependent recruitment of MutH[d] to DNA[a]. MutS, MutL, MutH[d] and DNA[a] were pre-incubated before ATP was added to the reaction. Without ATP, the incision complex could not be formed. Therefore, the complex formation could be triggered by addition of ATP. As the complex was formed, MutH[d] bound the GATC site and came in proximity to the

acceptor fluorophore attached to the DNA[a]. A FRET was generated. Addition of unlabeled MutH acted as competitor in the reaction as it displaced MutH[d] in the complex. With this competition the dynamics of complex dissociation could be followed. A schematic illustration of the reaction can be seen in Figure 3.36. Fluorescence spectra and FRET kinetics following complex association and dissociation are shown in Figure 3.37.

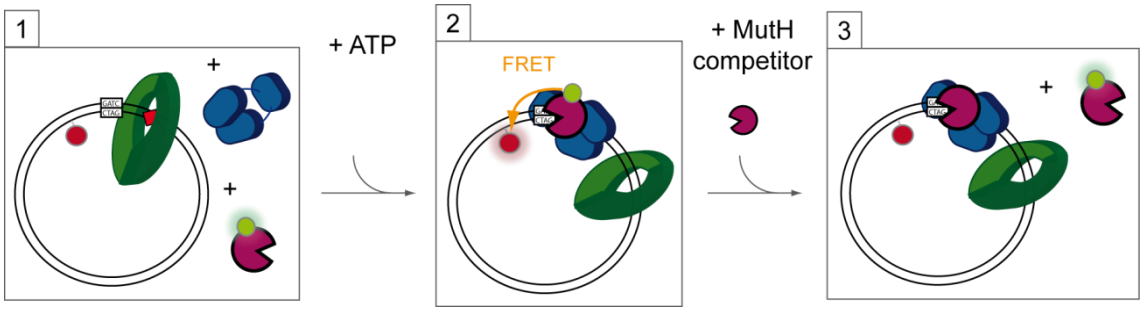

Figure 3.36: Schematic view of events during incision complex formation
1) Without ATP, the MMR proteins could not form protein complexes and MutS (green) remained bound to a mismatch (red diamond) on the DNA[a]. **2)** Upon addition of ATP, MutL (blue) and MutH[d] (magenta) were recruited to MutS on the DNA[a]. With MutH[d] binding the GATC site (black boxes) a FRET was generated (orange arrow) with a nearby acceptor fluorophore on the DNA[a] (red dot). **3)** Addition of excess of unlabeled MutH replaced MutH[d] in the incision complex and the FRET vanished.

The normalized fluorescence spectra (Figure 3.37, A) revealed binding of MutH[d] to the GATC site in the DNA[a]. Without ATP, the incision complex could not be formed which is indicated by a lack in acceptor fluorescence at 670 nm (blue line) during donor excitation at 470 nm (signal Fb). Upon addition of ATP, the incision complex was formed which included the recruitment of MutH[d] to the DNA[a] by MutS and MutL. This could be seen in the increase in acceptor fluorescence, generated by FRET (red line). To follow dissociation of the incision complex, unlabeled MutH was added to the reaction (Figure 3.38, B) and the effect became visible as a decrease in acceptor fluorescence (green line). Kinetics revealed that the dissociation was fast ($t_{1/2}$ was below 3 s) (Figure 3.38, C).

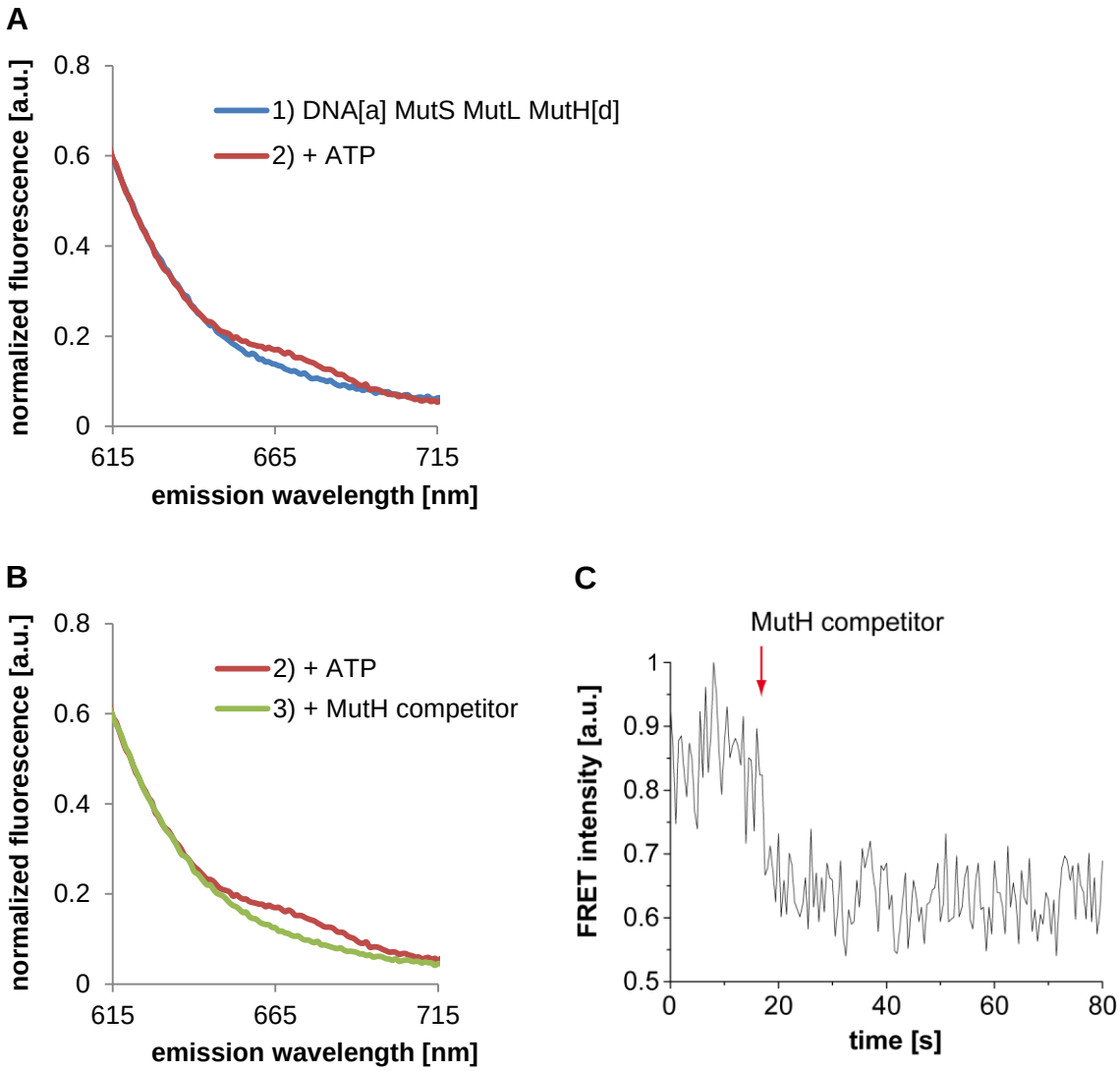

Figure 3.37: Incision complex formation and dissociation
A Incision complex formation was induced by addition of 1 mM ATP to 5 nM DNA[a] (1GATC[a]), 1 µM ADP, 200 nM MutS variant R449C D835R, 200 nM MutL variant H297C, and 200 nM of the catalytically inactive MutH[d] variant S85C E77A. In this reaction Alexa 488 served as a donor and Alexa 647 as an acceptor fluorophore. The donor was normalized to be 1 at its maximum. FRET effects can thereby be seen at the acceptor maximum at 670 nm. **B** Incision complex dissociation was induced by addition of 500 nM unlabeled MutH variant S85C E77A as competitor. **C** Time trace visualizing kinetics of incision complex dissociation.

Table 3.5: MutH dissociation from incision complex

kinetic rate	process	$t_{1/2}$	k
k_1	MutH leaving incision complex	< 3 s	> 0.3 s^{-1}

Ratios between acceptor and donor fluorescence during the different steps in the reaction are shown in the quantitative analysis (Figure 3.38). The ratio resembles unformed or formed incision complexes.

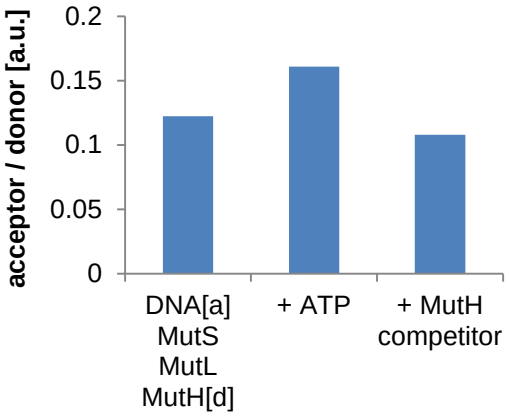

Figure 3.38: Quantitative analysis of incision complex formation and dissociation
FRET effects visualize the formation of the incision complex. Columns represent the acceptor to donor ratio during each step in the reaction. There are no error bars indicated as this experiment was performed only once.

The acceptor to donor ratio of 0.12 in step 1 corresponds to an unbound state of MutH[d] and derived from spectral crosstalk as overlapping donor emission was not subtracted from the acceptor emission (signal Fb). Addition of ATP in step 2 led to an increase in acceptor emission and to a ratio of 0.16. The increase derived from FRET effects upon MutH[d] recruitment to DNA[a] by MutS and MutL. In step 3, the acceptor emission decreased and the acceptor to donor ratio reached a value of 0.11. This was slightly lower compared to the starting value of 0.12 in step 1. Over all, the incision complex formation and dissociation could be observed with this assay although the signal changes were low.

4. Discussion

4.1 Influence of fluorescent dye labeling on protein activity

The first objective of this thesis was to find suitable positions in the MMR proteins for a possible attachment of a fluorophore. For this, single cysteine variants of the proteins MutS, MutL, and MutH were selected from a set of variants which were originally designed for protein-protein crosslinking studies in our group [33] [34] [35] [46]. A prerequisite for any FRET-based study is to exclude a possible interference of the system by the fluorophores. Fluorophores occupy a certain amount of space and may influence interactions of the proteins by steric hindrance or their charge. Therefore, variants were selected that possessed a single cysteine in an outer region on the surface of the protein. The variants R449C in MutS, H297C in MutL, and S85C in MutH turned out to be suitable for this purpose (chapter 3.1.4). Variant R449C of MutS carried an additional mutation (D835R) in the C-terminal domain of MutS to avoid a possible tetramerization of MutS. This mutation did not influence the activity of MutS in MMR [31] and represents a simplification of the system as MutS exists in a dimer/tetramer equilibrium which complicates data analysis. The fluorescence labeled variant of MutS R449C D835R was used before [36] and did not show a difference in a mismatch-provoked MutH activation assay compared to the unlabeled variant. To additionally exclude the influence of fluorophores at the selected positions in MutL and MutH on the activity of the proteins, a combination of labeled MutS, MutL, and MutH was used in a mismatch-provoked MutH activation assay and compared to unlabeled proteins (chapter 3.1.4). DNA nicking activity was addressed and revealed no significant difference in activity (150 ± 25 s for unlabeled and 130 ± 5 s for labeled proteins). MutS did carry an Alexa 647 fluorophore and MutL and MutH an Alexa 488. A DNA cleavage, only resulting from unlabeled proteins in the preparation of labeled proteins, can be excluded as the DOL of the labeled proteins was higher than 95 %. Therefore the fluorescent dye labeling with the used fluorophores did not influence protein activity.

4.2 DNA substrates for complex formation assays

Another requirement for the observation of certain complex formations e.g. MutS sliding clamp formation were circular DNA substrates to avoid a dissociation from DNA ends as MutS becomes highly mobile on DNA after turning into a sliding clamp [57] [68]. Therefore the GT932 was developed in our group [58] which contained a mismatch to allow MutS binding and initiation of the downstream MMR activities (chapter 3.2.1). This substrate furthermore possessed one GATC site to observe nicking activities of MutH. A hemimethylated status of the GATC site could be achieved via methylation of a nearby TaqI-recognition site. Nicking of

hemimethylated GT932 during the MMR reaction was 4-fold faster compared to the reaction with unmethylated GT932, which is in agreement with previously reported enhancement of 3-fold in a mismatch-provoked MutH endonuclease assay [64]. The more efficient cleavage of hemimethylated GATC sites results from a stabilization of the DNA binding pocket of MutH by the methyl group in one DNA strand [63] [41] [64].

Observation of incision complex formation required a circular DNA substrate which contained in addition to a mismatch also a fluorophore in vicinity to a GATC site. The DNA substrate is called 1GATC[a] in this thesis and originated from a protocol of Baerenfaller [59] which was modified to enable an incorporation of fluorescent dyes (Nicolaas Hermans, unpublished data). The protocol was adapted in this thesis and further modified by replacing the usage of phages to produce single-stranded DNA circles by a combination of nicking enzymes and exonucleases. The fluorophore near the GATC site acted as an acceptor fluorophore during the incision complex assay and thereby enabled observation of a donor labeled MutH[d] binding and dissociating from DNA in a MutS, MutL, and ATP dependent manner. The incorporated Alexa 647 dye further enables sensitive detection of these DNA circles in gel electrophoresis. 1GATC[a] circles were successfully generated and used to enable observation of incision complex formation of MutH[d] (chapter 3.3.5.3).

4.3 Visualizing complex formation in MMR

MutS binding a mismatch on DNA was the first MMR process to be analyzed in this thesis. Two assays were developed to allow observation of this process. The first assay combined an acceptor fluorophore labeled MutS with a donor fluorophore near the mismatch on a DNA oligonucleotide (chapter 3.3.1.1). The second assay used conformational changes in DNA which appear after mismatch binding of MutS (chapter 3.3.1.2). A donor and an acceptor fluorophore were positioned on either side of a mismatch and a FRET signal between those fluorophores was influenced by changes in distance, resulting from MutS bending the DNA. The reversible enhancement in FRET can be used as a quick control setup to test the DNA binding activity of purified MutS batches or new MutS variants. The setup of this assay was additionally used to determine binding orientations of MutS at different mismatches. It was known from MutS crystal structures [28] [66] that phenylalanine at position 36 of MutS subunit A stacks on thymine in the bottom strand of a G:T mismatch and on guanine in the bottom strand of a G:G mismatch. A combination of ensemble measurements (chapter 3.3.1.3) with single-molecule experiments now addressed MutS binding orientations at different mismatches in solution [60]. MutS showed the same preference for binding a G:T mismatch in an orientation which enables stacking on the bottom strand thymine as observed in the crystal structure [28]. For the G:G mismatch MutS showed no preference for binding the top or bottom strand, which is in contrast

to the crystal structure [66]. Further analysis performed by our group revealed that MutS also has a strong preference for binding in solution in an orientation, that allows stacking on adenine in A:C mismatches [60]. These findings were consistent with the crystal structure [66]. Taken together, the observed MutS binding orientations in solution indicate that MutS has a strong strand preference upon binding asymmetric mismatches e.g. G:T or A:C which was not observed for symmetric mismatches like G:G.

The next step in MMR to be monitored was the sliding clamp formation of MutS (chapter 3.3.2). After mismatch recognition MutS exchanges ADP for ATP which is accompanied by large conformational changes of MutS [12]. These changes result in a formation of a sliding clamp [72]. The sliding clamp remains no longer bound to the mismatch but diffuses freely along the DNA. When this thesis was started, the only assays to visualize the sliding clamp formation of MutS were based on surface plasmon resonance spectroscopy [30] and only recently several studies were able to capture the process in single-molecule FRET analysis [22] [73] [74]. The studies have in common that they all used artificially blocked DNA-ends and were performed on surface. As these conditions may influence the activity of a protein, chapter 3.3.2 in this thesis aimed on the development of an assay to detect the sliding clamp formation on a circular DNA in solution. Usage of SYBR Green I as a donor fluorophore bound to circular DNA (GT932) allowed a determination of the DNA binding of a MutS labeled with Alexa 647 as an acceptor fluorophore. In contrast to assays described in chapter 3.3.1, this assay allowed detection of MutS molecules which bound anywhere on DNA. The assay was not restricted to observe binding events at the mismatch. Preliminary kinetic data were observed in the assay (sliding clamp formation 12 s, dissociation 54 s). These data indicate a faster dissociation of MutS sliding clamps from DNA, compared to other studies (~ 600 s in Jeong *et al*., 2011 [22] for *Taq* MutS and 1800 s in Schofield *et al*., 2001 [26] for *Taq* and *E. coli* MutS). Considering the transient existence of hemimethylated GATC sites in *E. coli* cells (about 0.5 – 3.0 min in cells growing at 30 °C [75]), the observed dissociation time of about one minute for MutS sliding clamps seems to be plausible. Otherwise, a highly stable MutS sliding clamp, for more than two minutes, would lead to a state in which a majority of the GATC sites are methylated in the cell and activation of downstream repair factors like MutH would not be possible anymore. In this case activated MutS molecules would remain trapped on certain DNA areas and thus were not available for the initiation of DNA mismatch repair at other places of the genome, e.g. the site of replication. Taken together, the sliding clamp formation assay is capable of recording the dynamic processes of MutS binding a mismatch, transforming into a sliding clamp and finally dissociating from DNA in real-time and in solution.

The sliding clamp formation assay, presented in this thesis (chapter 3.3.2), can be modified by using a fluorescence dye labeled MutL. This allows an observation of a MutS-, ATP- and mismatch-dependent interaction of MutL with DNA, (chapter 6.3). A further modification of

this assay is the usage of a fluorescence dye labeled MutH, which allows the observation of a MutS-, MutL-, ATP-, and mismatch-dependent interaction of MutH with DNA and reflects the formation of the incision complex (data not shown). Kinetic data sets of both these modified assays are currently obtained in frame of a Diploma thesis.

The second principle factor in MMR is MutL. It is recruited by the activated MutS. Despite the fact, that the recruitment of MutL by MutS had been known for decades, the interaction site between the two partners remained unknown for a long time. Our group addressed the open question about the interaction site with site specific chemical crosslinking and FRET assays between MutS and MutL [37]. In this thesis, differences in FRET intensities were addressed between variants of MutS either carrying an acceptor fluorophore in the clamp domain (R449C[a]) or in the connector domain (D246C[a]) and a MutL carrying a donor fluorophore within the ATPase domain (H297C[d]) (chapter 3.3.3). The intensity of the FRET signal between the donor fluorophore at position 297 in MutL and the acceptor fluorophore at position 246 in MutS was high. In contrast to this was the intensity of the FRET signal between the same fluorescence labeled MutL and the acceptor fluorophore at position 449 in MutS low. Comparison of those intensities revealed, that the connector domain of MutS variant D246C[a] lies in proximity to the ATPase domain of MutL, within the ternary complex. Together with the site-specific crosslinking studies of Ines Winkler, it was now possible to map a potential area of interaction between MutS and MutL [37]. The results were consistent with results obtained by other groups [69]. The FRET setup of this assay can be extended to enable studies of dynamics of the ternary complex formation of MutS and MutL on DNA. For this purpose a circular DNA (GT932) was used to avoid dissociation from DNA ends and the Alexa 594 fluorophore at MutS was replaced by Alexa 647 to minimize spectral crosstalk in the FRET channel Fb. Preliminary data were collected with this extended setup, including time traces of the ternary complex formation and dissociation (chapter 6.1 and 6.2).

The assay visualizing MutL binding to DNA at low ionic strength turned out to be a new and fast setup for testing DNA binding activities of newly purified MutL variants (chapter 3.3.4). The FRET setup as well as the anisotropy setup was suitable for this purpose. An advantage of the anisotropy-based assay was that it did not require a fluorophore attached to MutL, which simplified the reaction. MutL binding did not show any difference between homoduplex DNA or a DNA containing an IDL with an extra thymine in one of the DNA strands. Bende *et al*., 1991 [70] observed similar results with a 3 nt IDL and homoduplex DNA in gel electrophoretic mobility shift assays.

Before the intricate process of incision complex formation was addressed in this thesis, the interaction of MutH with DNA was observed at low ionic strength (20 mM KCl) (chapter 3.3.5.1 and 3.3.5.2). These conditions allowed MutH to bind and cleave the DNA in a mismatch-, MutS- and MutL-independent manner. Two assays, to visualize the interaction of

either active MutH (variant S85C) or catalytically inactive MutH (variant E77A) with DNA, were demonstrated. The DNA binding assay represents a fast and robust test system for newly purified, fluorescence labeled, and catalytically inactive MutH variants. The DNA cleavage assay of MutH further represents a reliable test system for catalytically active MutH variants and does not require a fluorescence label at MutH. Taken together, both assays allow a fast analysis of the DNA binding or cleavage activity of MutH.

The final assay was the observation of incision complex formation and dissociation at high ionic strength of 125 mM KCl (chapter 3.3.5.3). These conditions resembled physiological conditions and MutS, MutL, ATP, and a mismatch were required to enable the interaction between MutH and DNA. Only little experimental evidences for the formation of the MutS-MutL-MutH ternary complex are available in literature. These evidences are mainly based on co-purification of MutH with MutL and a MutS affinity column [71]. Further evidences were obtained in our group as the complex can be trapped by crosslinking MutS to MutL and MutL to MutH (Ines Winkler, unpublished data). To monitor incision complex formation in this thesis, a FRET assay was designed, which was dependent on MutS, MutL, and ATP (3.3.5.3). The assay contained a catalytically inactive variant of MutH[d] and a circular DNA with a G:T mismatch, a single GATC site and an acceptor dye nearby the GATC site (1GATC[a]). Only minor changes of the signal in the FRET channel Fb were observed before initiation of incision complex formation. ATP dependent appearance of the acceptor peak in this assay indicated the incision complex formation. The low acceptor peak observed in the experiment may be explained by a highly dynamic incision complex. In this case MutH[d] would be only a short time in vicinity of the GATC site and therefore only for a short time in vicinity of the acceptor fluorophore. An indicator for a highly dynamic nature of the incision complex is the fast dissociation ($t_{1/2} < 3$ s). A major issue about this assay was the DNA substrate 1GATC[a], which was only available at limited amounts. Recently, the procedure was optimized in frame of a Diploma thesis.

Taken together, the assays developed in this thesis now allow an observation of the initial sub-steps in MMR. The new insights will help to understand the intricate MMR process in detail. The sub-steps in MMR which can be analyzed by the assays cover the processes of MutS mismatch recognition, MutS bending DNA, MutS sliding clamp formation, MutS-MutL complex formation, MutL interaction with DNA, MutL-MutH complex formation, and MutH forming and leaving the incision complex. These processes, with their according assays, are depicted in Figure 4.1. The obtained kinetic data sets were used for the development of a kinetic model for the whole MMR system in frame of the European FP7 project mismatch2model. Currently, the fully active, fluorescent dye labeled proteins, which were generated in frame of this thesis, are used in single-molecule studies of the MMR, e.g. in a magnetic tweezers setup combined with fluorescence detection.

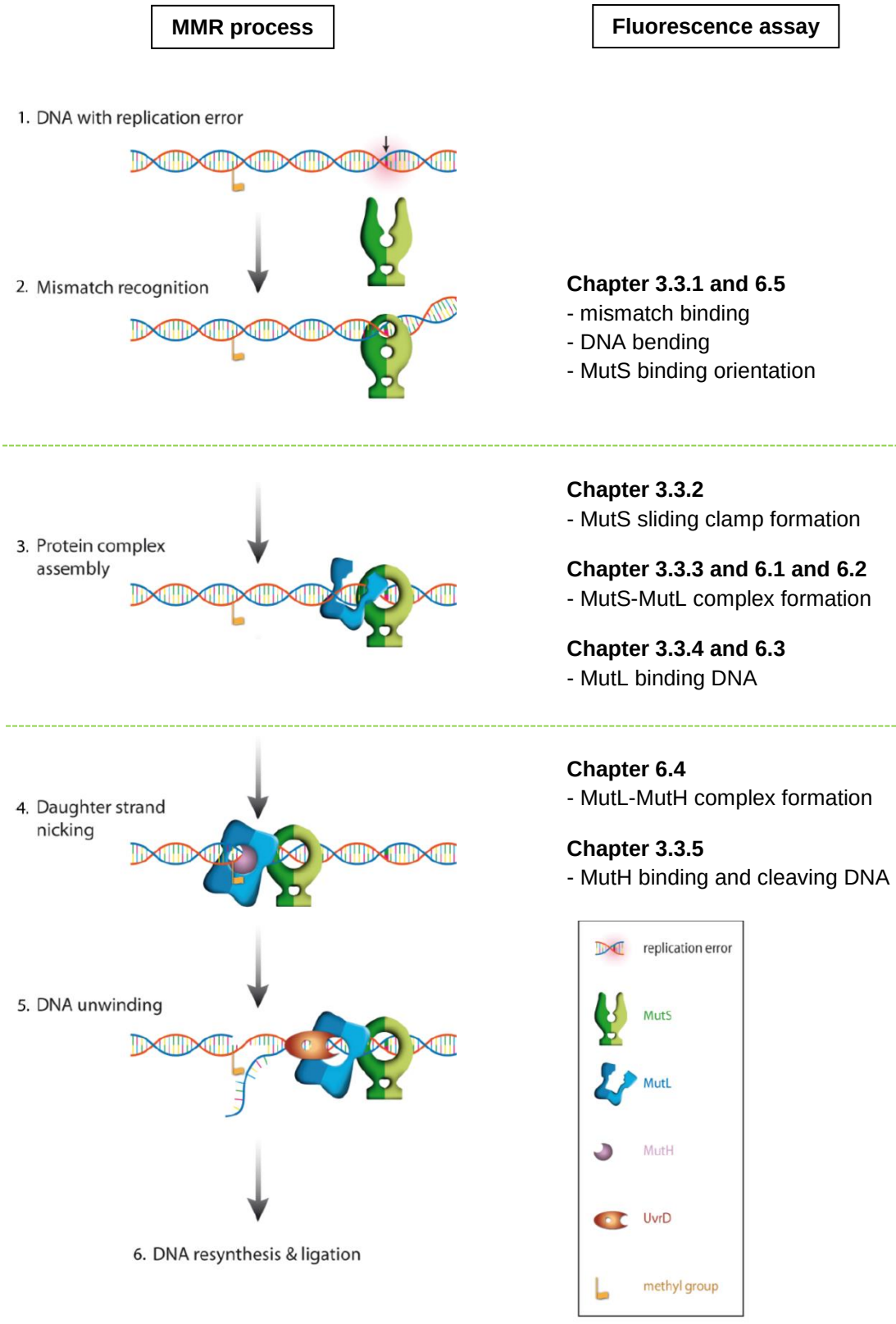

Figure 4.1: MMR processes that can be visualized by fluorescence-based assays of this thesis
Sub-steps in MMR (left side) with the according visualization assay developed in this thesis and the indication of the chapter (right side). The assays cover MutS mismatch recognition, MutS bending DNA, MutS sliding clamp formation, MutS-MutL complex formation, MutL interaction with DNA, MutL-MutH complex formation, and MutH forming and leaving the incision complex. Assays at low ionic strength were not listed here as they do not resemble the physiological situation in the cell. The illustrated MMR processes were modified after Lebbink, [19].

5. References

1. Hoeijmakers, J.H., *Genome maintenance mechanisms for preventing cancer.* Nature, 2001. 411(6835): p. 366-74.
2. Lujan, S.A., et al., *Mismatch repair balances leading and lagging strand DNA replication fidelity.* PLoS Genet, 2012. 8(10): p. e1003016.
3. Su, S.S. and P. Modrich, *Escherichia coli mutS-encoded protein binds to mismatched DNA base pairs.* Proceedings of the National Academy of Sciences of the United States of America, 1986. 83(14): p. 5057-61.
4. Parker, B.O. and M.G. Marinus, *Repair of DNA heteroduplexes containing small heterologous sequences in Escherichia coli.* Proceedings of the National Academy of Sciences of the United States of America, 1992. 89(5): p. 1730-4.
5. Jiricny, J., *The multifaceted mismatch-repair system.* Nat Rev Mol Cell Biol, 2006. 7(5): p. 335-46.
6. Larrea, A.A., S.A. Lujan, and T.A. Kunkel, *SnapShot: DNA mismatch repair.* Cell, 2010. 141(4): p. 730 e1.
7. Iyer, R.R., et al., *DNA mismatch repair: functions and mechanisms.* Chem. Rev., 2006. 106(2): p. 302-23.
8. Fishel, R., et al., *The human mutator gene homolog MSH2 and its association with hereditary nonpolyposis colon cancer [published erratum appears in Cell 1994 Apr 8;77(1):167].* Cell, 1993. 75(5): p. 1027-38.
9. Lynch, H.T., et al., *Clinical impact of molecular genetic diagnosis, genetic counseling, and management of hereditary cancer. Part II: Hereditary nonpolyposis colorectal carcinoma as a model.* Cancer, 1999. 86(11 Suppl): p. 2457-63.
10. Gradia, S., S. Acharya, and R. Fishel, *The human mismatch recognition complex hMSH2-hMSH6 functions as a novel molecular switch.* Cell, 1997. 91(7): p. 995-1005.
11. Blackwell, L.J., et al., *Nucleotide-promoted release of hMutSa from heteroduplex DNA is consistent with an ATP-dependent translocation mechanism.* J Biol Chem, 1998. 273(48): p. 32055-32062.
12. Gradia, S., et al., *hMSH2-hMSH6 forms a hydrolysis-independent sliding clamp on mismatched DNA.* Mol Cell, 1999. 3(2): p. 255-61.
13. Prolla, T.A., et al., *MLH1, PMS1, and MSH2 interactions during the initiation of DNA mismatch repair in yeast.* Science, 1994. 265(5175): p. 1091-1093.
14. Ban, C., M. Junop, and W. Yang, *Transformation of MutL by ATP binding and hydrolysis: a switch in DNA mismatch repair.* Cell, 1999. 97(1): p. 85-97.
15. Modrich, P., *Methyl-directed DNA mismatch correction.* J Biol Chem, 1989. 264(12): p. 6597-6600.
16. Sancar, A. and J.E. Hearst, *Molecular matchmakers.* Science, 1993. 259(5100): p. 1415-20.
17. Hsieh, P. and K. Yamane, *DNA mismatch repair: Molecular mechanism, cancer, and ageing.* Mech Ageing Dev, 2008. 129(7-8): p. 391-407.
18. Loh, T., K.C. Murphy, and M.G. Marinus, *Mutational analysis of the MutH protein from Escherichia coli.* J Biol Chem, 2001. 276(15): p. 12113-12119.
19. Lebbink, J.H., *mismatch2model Maintaining our genetic code.* 2008. [21.01.2013] from http://www.mm2m.eu/documents/mm2m.pdf
20. Kolodner, R.D., M.L. Mendillo, and C.D. Putnam, *Coupling distant sites in DNA during DNA mismatch repair.* Proceedings Of The National Academy Of Sciences Of The United States Of America, 2007. 104(32): p. 12953-12954.

21. Gorman, J., et al., *Dynamic basis for one-dimensional DNA scanning by the mismatch repair complex Msh2-Msh6.* Mol Cell, 2007. 28(3): p. 359-70.
22. Jeong, C., et al., *MutS switches between two fundamentally distinct clamps during mismatch repair.* Nat. Struct. Mol. Biol., 2011. 18(3): p. 379-85.
23. Hall, M.C., et al., *High affinity cooperative DNA binding by the yeast Mlh1-Pms1 heterodimer.* J Mol Biol, 2001. 312(4): p. 637-47.
24. Elez, M., M. Radman, and I. Matic, *Stoichiometry of MutS and MutL at unrepaired mismatches in vivo suggests a mechanism of repair.* Nucleic Acids Res, 2012.
25. Acharya, S., et al., *The coordinated functions of the E. coli MutS and MutL proteins in mismatch repair.* Mol Cell, 2003. 12(1): p. 233-46.
26. Schofield, M.J., et al., *Interaction of Escherichia coli MutS and MutL at a DNA mismatch.* J Biol Chem, 2001. 276(30): p. 28291-9.
27. Junop, M.S., et al., *Composite active site of an ABC ATPase: MutS uses ATP to verify mismatch recognition and authorize DNA repair.* Mol Cell, 2001. 7(1): p. 1-12.
28. Lamers, M.H., et al., *The crystal structure of DNA mismatch repair protein MutS binding to a G x T mismatch.* Nature, 2000. 407(6805): p. 711-717.
29. Obmolova, G., et al., *Crystal structures of mismatch repair protein MutS and its complex with a substrate DNA.* Nature, 2000. 407(6805): p. 703-710.
30. Galio, L., C. Bouquet, and P. Brooks, *ATP hydrolysis-dependent formation of a dynamic ternary nucleoprotein complex with MutS and MutL.* Nucleic Acids Res, 1999. 27(11): p. 2325-31.
31. Manelyte, L., et al., *Structural and functional analysis of the MutS C-terminal tetramerization domain.* Nucleic Acids Res, 2006. 34(18): p. 5270-9.
32. Mendillo, M.L., C.D. Putnam, and R.D. Kolodner, *Escherichia coli MutS tetramerization domain structure reveals that stable dimers but not tetramers are essential for DNA mismatch repair in vivo.* J Biol Chem, 2007. 282(22): p. 16345-54.
33. Manelyte, L., *Structural and functional analysis of MutS, a mismatch repair protein from Escherichia coli*, in *Institut für Biochemie, Fachbereich Biologie und Chemie*2006, Justus-Liebig-Universität: Gießen. p. 127 Bl.
34. Girón Monzón, L., *Structural and functional studies of the mismatch repair system from Escherichia coli*, in *Institut für Biochemie, Fachbereich Biologie und Chemie*2006, Justus-Liebig-Universität: Gießen. p. XIV, 100 Bl.
35. Winkler, I., *Funktionelle und strukturelle Untersuchungen zur ternären Komplexbildung zwischen MutS und MutL im mismatch-Reparatursystem*, in *Institut für Biochemie, Fachbereich Biologie und Chemie*2010, Justus-Liebig-Universität: Gießen. p. 134 S.
36. Cristóvão, M., *Conformational changes in DNA and MutS during mismatch repair in Escherichia coli, analyzed by fluorescence spectroscopy*, in *Institut für Biochemie, Fachbereich Biologie und Chemie*2009, Justus-Liebig-Universität: Gießen. p. 147 Bl.
37. Winkler, I., et al., *Chemical trapping of the dynamic MutS-MutL complex formed in DNA mismatch repair in Escherichia coli.* J Biol Chem, 2011. 286(19): p. 17326-37.
38. Sacho, E.J., et al., *Direct visualization of asymmetric adenine-nucleotide-induced conformational changes in MutL alpha.* Molecular Cell, 2008. 29(1): p. 112-21.
39. Giron-Monzon, L., et al., *Mapping protein-protein interactions between MutL and MutH by cross-linking.* J Biol Chem, 2004. 279(47): p. 49338-45.
40. Guarne, A., et al., *Structure of the MutL C-terminal domain: a model of intact MutL and its roles in mismatch repair.* EMBO J, 2004. 23(21): p. 4134-45.

41. Welsh, K.M., et al., *Isolation and characterization of the Escherichia coli mutH gene product.* J Biol Chem, 1987. 262(32): p. 15624-15629.
42. Marinus, M.G. and N.R. Morris, *Isolation of deoxyribonucleic acid methylase mutants of Escherichia coli K-12.* J Bacteriol, 1973. 114(3): p. 1143-50.
43. Record, M.T., Jr., et al., *Biophysical compensation mechanisms buffering E. coli protein-nucleic acid interactions against changing environments.* Trends Biochem Sci, 1998. 23(5): p. 190-4.
44. Ahrends, R., et al., *Identifying an interaction site between MutH and the C-terminal domain of MutL by crosslinking, affinity purification, chemical coding and mass spectrometry.* Nucleic Acids Res, 2006. 34(10): p. 3169-80.
45. Toedt, G.H., R. Krishnan, and P. Friedhoff, *Site-specific protein modification to identify the MutL interface of MutH.* Nucleic Acids Res, 2003. 31(3): p. 819-25.
46. Toedt, G., *Das MutHLS-MMR-System: Studien zur Interaktion der Proteine MutH und MutL,* in *Institut für Biochemie, FB 08*2002, Justus-Liebig-Universität: Giessen.
47. Wu, T.H., T. Loh, and M.G. Marinus, *The function of Asp70, Glu77 and Lys79 in the Escherichia coli MutH protein.* Nucleic Acids Res, 2002. 30(3): p. 818-822.
48. Friedhoff, P., E. Thomas, and A. Pingoud, *Tyr212: a key residue involved in strand discrimination by the DNA mismatch repair endonuclease MutH.* J Mol Biol, 2003. 325(2): p. 285-97.
49. Ban, C. and W. Yang, *Structural basis for MutH activation in E. coli mismatch repair and relationship of MutH to restriction endonucleases.* EMBO J., 1998. 17(5): p. 1526-1534.
50. Ausubel, F.M., Brent, R., Kingston, R. E., Moore, D. D., Smith, J. A., and Seidman, J. G. , *Current Protocols in Molecular Biology* 1992-2005, New York John Wiley & Sons.
51. Chiuman, W. and Y. Li, *Efficient signaling platforms built from a small catalytic DNA and doubly labeled fluorogenic substrates.* Nucleic Acids Research, 2007. 35(2): p. 401-5.
52. Dragan, A.I., et al., *SYBR Green I: Fluorescence Properties and Interaction with DNA.* J Fluoresc, 2012.
53. Berney, C.P., *Quantitative Fluorescence Resonance Energy Transfer Microscopy*, in *Swiss federal institute of technology Zurich*2003: Zurich. p. 154.
54. Gordon, G.W., et al., *Quantitative fluorescence resonance energy transfer measurements using fluorescence microscopy.* Biophys J, 1998. 74(5): p. 2702-13.
55. Lakowicz, J.R., *Principles of Fluorescence Spectroscopy*, 2006, Springer US: Boston, MA. p. 353-475 S.
56. Thomas, E., A. Pingoud, and P. Friedhoff, *An efficient method for the preparation of long heteroduplex DNA as substrate for mismatch repair by the Escherichia coli MutHLS system.* Biol Chem, 2002. 383(9): p. 1459-62.
57. Mendillo, M.L., D.J. Mazur, and R.D. Kolodner, *Analysis of the interaction between the Saccharomyces cerevisiae MSH2-MSH6 and MLH1-PMS1 complexes with DNA using a reversible DNA end-blocking system.* Journal Of Biological Chemistry, 2005. 280(23): p. 22245-22257.
58. Xiao, Y., et al., *Generation of DNA nanocircles containing mismatched bases.* BioTechniques, 2011. 51(4): p. 259-62, 264-5.
59. Baerenfaller, K., F. Fischer, and J. Jiricny, *Characterization of the "mismatch repairosome" and its role in the processing of modified nucleosides in vitro.* Methods Enzymol, 2006. 408: p. 285-303.

60. Cristovao, M., et al., *Single-molecule multiparameter fluorescence spectroscopy reveals directional MutS binding to mismatched bases in DNA.* Nucleic Acids Res, 2012. 40(12): p. 5448-64.
61. Xiao, J., *Generation of circular heteroduplex containing modified bases*, in *Institut for Biochemistry, FB 08*2008, Justus Liebig University: Giessen.
62. Strauss, S. and R.L. Lundblad, *Chemical Reagents for Protein Modification*. 2004: CRC Press.
63. Lee, J.Y., et al., *MutH complexed with hemi- and unmethylated DNAs: Coupling base recognition and DNA cleavage.* Mol Cell, 2005. 20(1): p. 155-166.
64. Au, K.G., K. Welsh, and P. Modrich, *Initiation of methyl-directed mismatch repair.* J Biol Chem, 1992. 267(17): p. 12142-12148.
65. Warren, J.J., et al., *Structure of the human MutSalpha DNA lesion recognition complex.* Mol Cell, 2007. 26(4): p. 579-92.
66. Natrajan, G., et al., *Structures of Escherichia coli DNA mismatch repair enzyme MutS in complex with different mismatches: a common recognition mode for diverse substrates.* Nucleic Acids Res, 2003. 31(16): p. 4814-21.
67. Howell, W.M., M. Jobs, and A.J. Brookes, *iFRET: an improved fluorescence system for DNA-melting analysis.* Genome Res, 2002. 12(9): p. 1401-7.
68. Jiang, J., et al., *Detection of high-affinity and sliding clamp modes for MSH2-MSH6 by single-molecule unzipping force analysis.* Molecular Cell, 2005. 20(5): p. 771-81.
69. Mendillo, M.L., et al., *A conserved MutS homolog connector domain interface interacts with MutL homologs.* Proc Natl Acad Sci U S A, 2009. 106(52): p. 22223-8.
70. Bende, S.M. and R.H. Grafstrom, *The DNA binding properties of the MutL protein isolated from Escherichia coli.* Nucleic Acids Res, 1991. 19(7): p. 1549-55.
71. Spampinato, C. and P. Modrich, *The MutL ATPase Is Required for Mismatch Repair.* J. Biol. Chem., 2000. 275(13): p. 9861-9869.
72. Lamers, M.H., et al., *ATP increases the affinity between MutS ATPase domains. Implications for ATP hydrolysis and conformational changes.* J Biol Chem, 2004. 279(42): p. 43879-85.
73. Cho, W.K., et al., *ATP Alters the Diffusion Mechanics of MutS on Mismatched DNA.* Structure, 2012.
74. Qiu, R., et al., *Large conformational changes in MutS during DNA scanning, mismatch recognition and repair signalling.* Embo J, 2012.
75. Barras, F. and M.G. Marinus, *The great GATC: DNA methylation in E. coli.* Trends in Genetics, 1989. 5(5): p. 139-43.

6. Appendix

6.1 Kinetics of MutS-MutL complex formation on circular DNA (GT932)

The MutS sliding clamp is very mobile on DNA [57] [68]. Therefore, DNA circles (GT932) were used in this assay to avoid complex dissociation via DNA ends and to observe a stable complex formation between MutS and MutL. This "stabilization" of the complexes allowed recording of time traces during complex formation and dissociation and determination of kinetic rate constants. The reaction can be divided into five phases which are characterized by the stepwise addition of new components to the system. A schematic illustration of the reaction is shown in Figure 6.1, A and a representative time trace is shown in Figure 6.1, B.

MutL[d] generated a weak background signal in the kinetic FRET channel at 0.1 a.u. which was further increased to ~ 0.3 a.u. after addition of MutS[a] (Figure 6.1, k_1). Without DNA, the labeled MutS[a] and labeled MutL[d] did not bind to each other. Addition of DNA led to an increase in FRET in a burst phase to 1.0 a.u. which reflected the complex formation of MutS[a] and MutL[d] on DNA (Figure 6.1, k_2). The burst phase was followed by an unknown process which caused a decrease in FRET to ~ 0.8 a.u. (Figure 6.1, k_3). Dissociation of the MutS[a] and MutL[d] complex was monitored after addition of unlabeled MutL as competitor (Figure 6.1, k_4). Dissociation of MutL[d] led to a decrease in FRET (to 0.4 a.u.). The FRET did not decrease to the initial level of 0.3 a.u. obtained before addition of DNA. The reason for this were residual MutL[d] molecules which remained bound to MutS[a] as only ten times excess of competitor MutL over labeled MutL[d] was used. Kinetic rate constants of MutS-MutL complex formation and dissociation are summarized in Table 6.1.

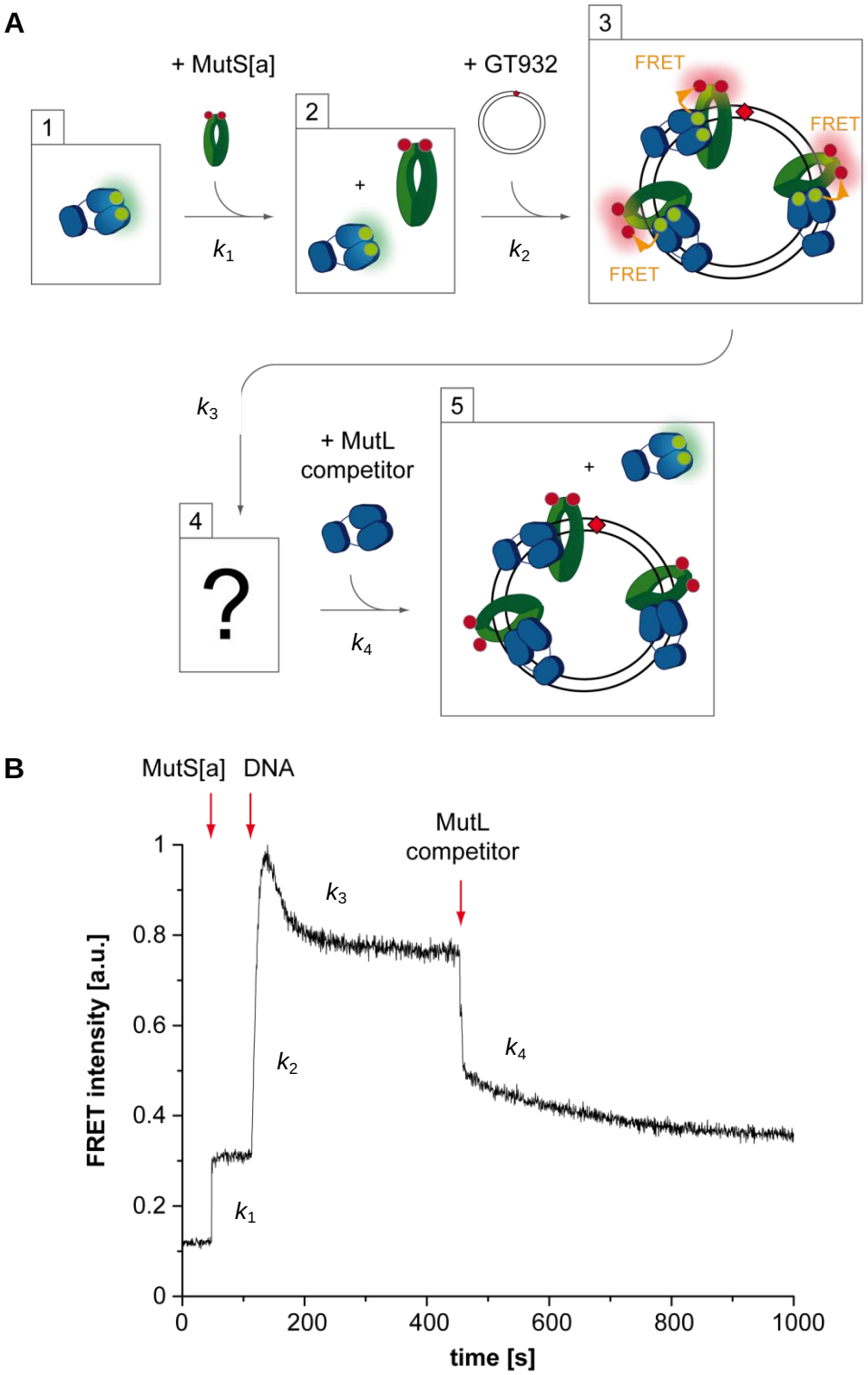

Figure 6.1: MutS-MutL complex formation on circular DNA
A Schematic view of events in the assay. $k_{1\text{-}4}$ Kinetic rate constants describe how fast the FRET intensity changed between two phases. k_1 Addition of 100 nM MutS[a] variant D835R R449C to 100 nM MutL[d] H297C in solution with 1 mM ATP and 1x buffer FB125. k_2 A FRET (orange arrows) arose during MutS[a] MutL[d] complex formation on DNA induced by addition of 10 nM GT932. k_3 An unknown process led to a decrease in FRET to a lower plateau. k_4 Competition of MutS[a] MutL[d] complex by addition of 1 µM unlabeled MutL variant H297C. The fluorescence donor [d] was Alexa 488 and was excited at 470 nm while emission of the fluorescence acceptor [a] Alexa 647 was measured at 670 nm (Fb signal). **B** Recorded FRET intensity of an exemplary time trace.

Table 6.1: Kinetic rate constants of the MutS-MutL complex formation
Kinetics rate constants of changes in FRET intensity during each phase of the MutS-MutL complex formation assay were analyzed with the software Origin and fitted using the function ExpDec1.

kinetic rate	process	$t_{1/2}$	*k*
k_1	MutS[a] MutL[d] in solution	3 s	0.33 s^{-1}
k_2	MutS[a] MutL[d] complex formation	10 s	0.10 s^{-1}
k_3	unknown	35 s	0.03 s^{-1}
k_4	MutL[d] dissociating from DNA	200 s	< 0.01 s^{-1}

6.2 Monitoring MutS-MutL complex formation using MutL[d] variant 480C

For this assay a single-cysteine variant with a native cysteine residue at position 480 in MutL was labeled with a fluorophore. Position 480 lies within the C-terminal domain of MutL. Position 297 which was used for fluorescence labeling of MutL in other assays lies within the N-terminal domain. Not normalized FRET intensities obtained during the MutS-MutL complex formation assay using variant 297 of MutL[d] (chapter 6.1) were compared to intensities obtained during the same assay now performed with variant 480 of MutL[d]. Differences in intensities give information about distances between position 449 in MutS[a] and the different positions in MutL[d] representing the N-terminal (position 297) or C-terminal domain (position 480).

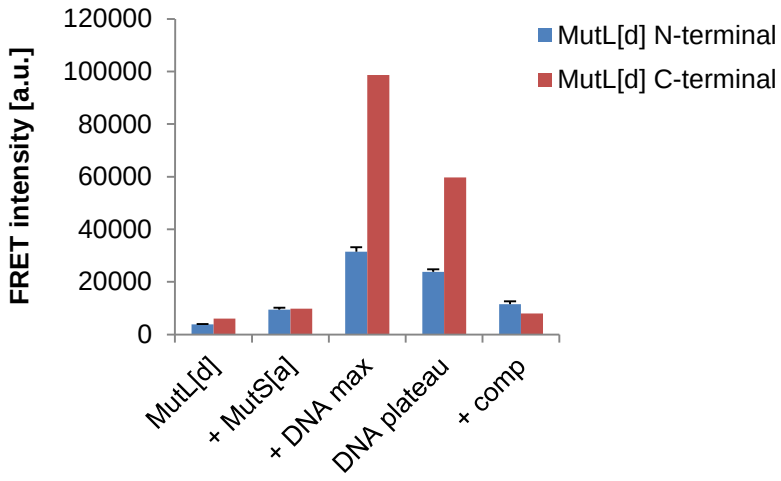

Figure 6.2: **Comparing FRET intensities in MutS-MutL complex formation using N-terminal or C-terminal fluorescence labeled MutL variants**
FRET intensities indicate complex formation between MutS[a] and MutL[d] during different Phases. Columns represent MutS[a] complex formation with either N-terminal labeled MutL[d] (blue) or C-terminal labeled MutL[d] (red). The reaction containing MutL[d] N-terminal was performed three times, the values were averaged and the error bars represent the standard deviation. The reaction containing MutL[d] C-terminal was only performed once and therefore the representing column does not show error bars.

A higher FRET signal (signal Fb) of ~ 100,000 a.u. between MutS[a] and MutL[d] 480 variant compared to ~ 30,000 a.u. observed with MutL[d] 297 variant indicated a closer distance between the C-terminal domain of MutL to position 449 in MutS compared the N-terminal domain of MutL (Figure 6.2, +DNA max). The lower final value of ~ 8,000 a.u. for the C-terminal variant of MutL (Figure 6.2, +comp, red column) resulted from Thrombin cleavage which was not used at the end of the MutS-MutL complex formation assay with the labeled N-terminal domain of MutL (Figure 6.2, +comp, blue column) in which a final value of ~ 12,000 a.u. was reached. Thrombin led to a cleavage of MutL in the linker region. Remaining MutL[d] forming a complex with MutS[a] therefore dissociated and a further decrease in FRET could be observed.

6.3 Mismatch and MutS dependent recruitment of MutL at high ionic strength

At high ionic strength MutL does not bind DNA and needs to be recruited by MutS. This assay was performed with circular DNA as the MutS sliding clamp is very mobile on DNA [57] [68].

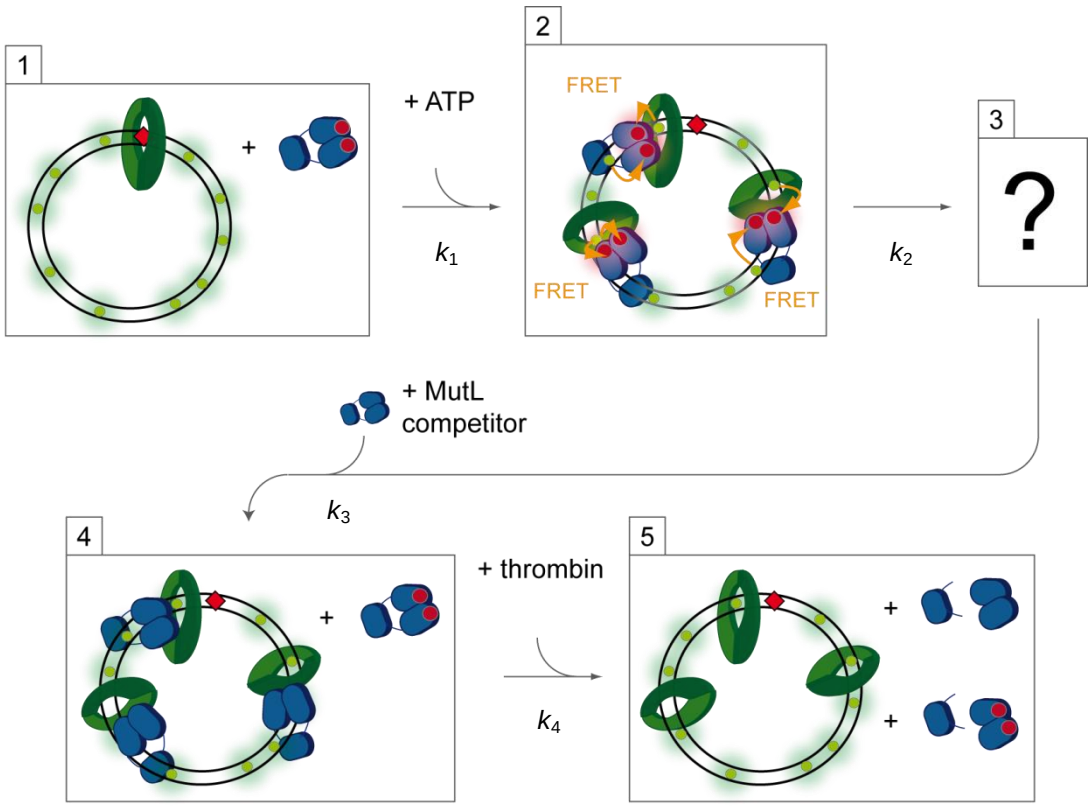

Figure 6.3: Schematic view of events during MutL recruitment to circular DNA at high ionic strength (125 mM KCl)
$k_{1\text{-}4}$ Kinetic rate constants describe how fast the FRET intensity changes between two phases. k_1 SG is incorporated in GT932 DNA circles and serves as a fluorescence donor in the reaction (green dots). MutS in an ADP bound state, remains bound to a mismatch (red diamond) on this DNA. Addition of ATP allows recruitment of MutL[a] to MutS sliding clamps on a circular DNA which generates a FRET between SG and MutL[a] (orange arrows). k_2 Unknown process following the recruitment of MutL to the DNA-MutS complex. This process decreases the FRET effect. k_3 Unlabeled MutL hinders MutL[a] from rebinding the MutS-DNA complex after dissociation. The FRET vanishes. k_4 Thrombin cleaves MutL[a] and MutL to dispose all residual MutL[a] from DNA.

The assay starts with incubation of MutS, MutL[a], ADP, SG, and GT932 DNA circles. SG will be incorporated into DNA and MutS, in the ADP bound state, will bind the mismatch. MutL is unable to bind to the ADP bound MutS and remains unbound. Addition of ATP allows the transformation of MutS into an ATP bound sliding clamp which is able to recruit MutL[a]. MutL[a] is now able to generate a FRET with nearby SG molecules incorporated in DNA. This FRET serves as an indicator in the reaction that the fluorescence labeled MutL is bound to the

DNA. Addition of excess unlabeled MutL inhibits the reaction by hindering the MutL[a] from rebinding the MutS-DNA complex after dissociating. Therefore the FRET decreases. Thrombin acts as a further inhibitor in the reaction as it cleaves MutL in the linker region and residual MutL[a] bound to the MutS-DNA complex will dissociate. The reaction is schematically illustrated in Figure 6.3. A recorded time trace gives insight into kinetics of MutL-DNA complex formations (Figure 6.4).

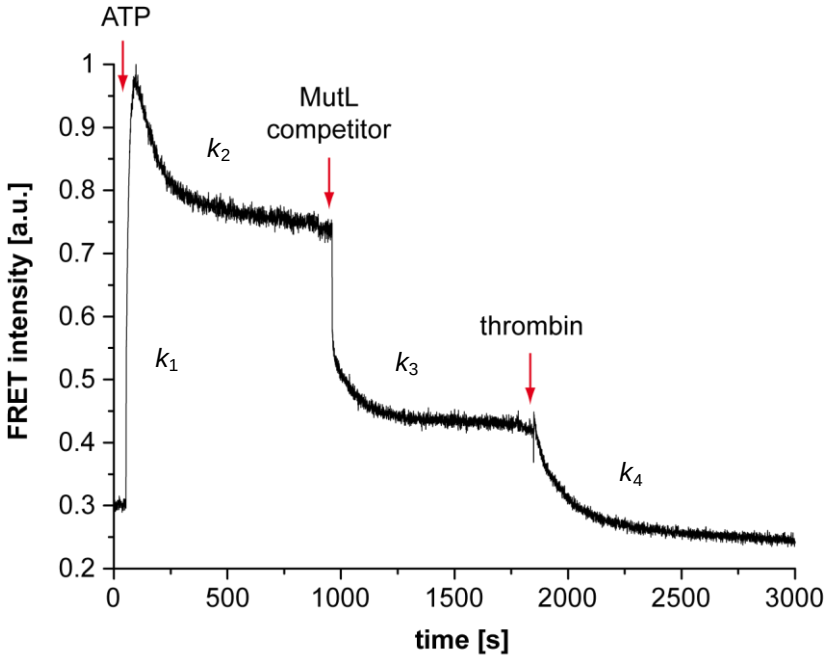

Figure 6.4: Time trace of MutL binding circular DNA at high ionic strength (125 mM KCl)
$k_{1\text{-}4}$ Kinetic rate constants describe how fast the FRET intensity changes between two phases. For a description of the different phases see Figure 6.3 or the text. The reaction began with 100 nM SG, 10 nM GT932, 100 nM MutS variant R449C D835R, 100 nM MutL variant H297C labeled with Alexa 647 (MutL[a]), and 1 µM ADP in 1x buffer FB125. The complex formation was started with injection of 1 mM ATP. Addition of 500 nM unlabeled MutL variant H297C acted as a competitor in the reaction by displacing the labeled MutL in the complex. Addition of 0.6 U Thrombin led to a cleavage of all MutL proteins in the linker connecting the N-terminal and C-terminal domain. MutL could not remain bound to the DNA and did fall off. The fluorescence donor [d] was SG and was excited at 470 nm while emission of the fluorescence acceptor [a] Alexa 647 was measured at 670 nm (Fb signal).

This assay allowed observation of the DNA binding state of MutL[a]. A high FRET state after addition of ATP in the reaction indicated that fluorescence labeled MutL (MutL[a]) was bound to DNA[d] during this phase. This phase was followed by a decrease in FRET which may resulted from dissociation of some MutL[a] from DNA[d] coupled with a delayed rebinding. Delayed rebinding could have been caused by a rate limiting step of nucleotide exchange or hydrolysis. After addition of unlabeled MutL the FRET decreased further because of a

replacement of MutL[a] by unlabeled MutL from DNA[d]. Total inhibition of the reaction was achieved by Thrombin addition and the FRET signal decreased to a level below the FRET level of the first phase which represented a not DNA[d] bound state of MutL[a]. The decrease below this starting level was due to dilution effects during the experiment. Kinetic rates are listed in Table 6.2.

Table 6.2: Kinetic rate constants of MutL binding circular DNA at high ionic strength

kinetic rate	**process**	**$t_{1/2}$**	***k***
k_1	MutL[a] binding MutS on DNA	13 s	0.08 s^{-1}
k_2	unknown	98 s	0.01 s^{-1}
k_3	MutL[a] dissociation (competition)	63 s	0.02 s^{-1}
k_4	MutL[a] dissociation (Thrombin)	148 s	< 0.01 s^{-1}

6.4 MutL-MutH complex formation

A major step in *E. coli* MMR is the activation of the endonuclease MutH. MutH is required for the formation of the incision complex which incises the newly synthesized DNA strand. Several lines of evidence suggest that MutH binds to MutL [48]. To demonstrate that it is in principle possible to visualize the recruitment of MutH to MutL, the following assay was developed. It is based on FRET which is generated between a donor labeled MutL[d] and an acceptor labeled MutH[a] and it does not require DNA. The reaction is schematically illustrated in Figure 6.5, A and fluorescence emission spectra are shown in Figure 6.5, B.

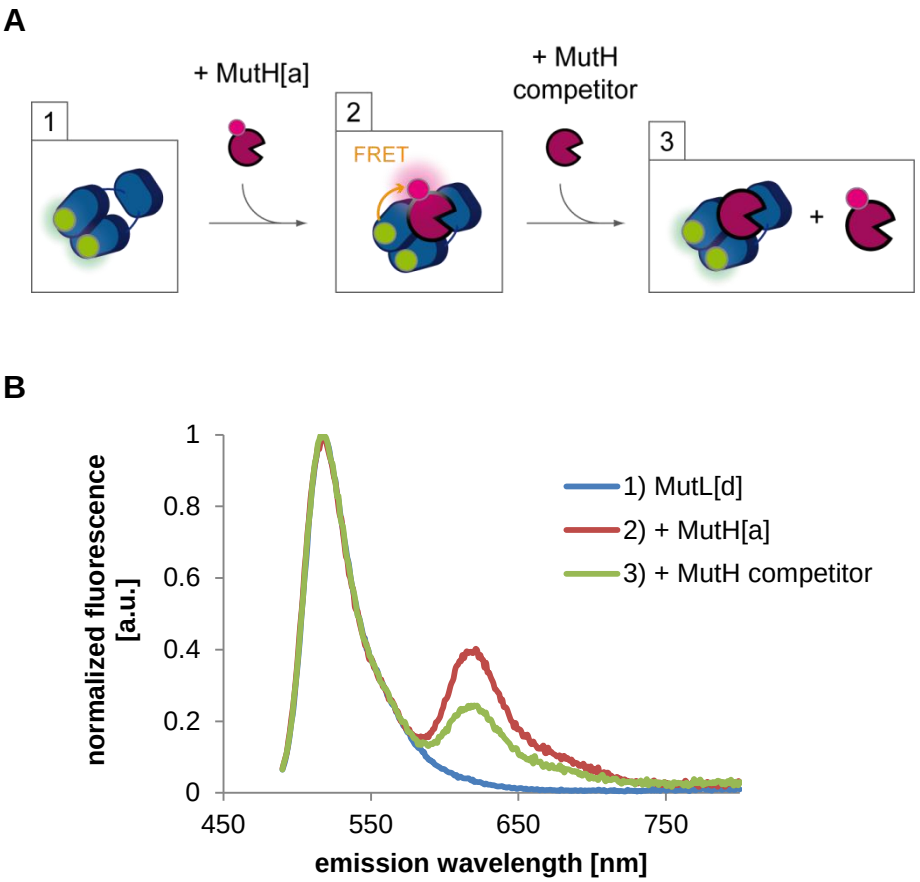

Figure 6.5: MutL and MutH complex formation
A Schematic view of events during the reaction. Binding of MutH[a] to MutL[d] generates a FRET (orange arrow). Addition of excess unlabeled MutH acts as a competitor as it competes with MutH[a] for the interaction with MutL[d]. The FRET decreases. **B** Normalized emission spectra of the reaction steps. The donor was normalized to be 1. FRET effects can thereby be seen in the acceptor emission at 617 nm. In this reaction Alexa 488 served as a donor and Alexa 594 as an acceptor fluorophore. 400 nM of MutL[d] variant H297C and 400 nM of MutH[a] variant S85C C96S were used in the presence of 1 mM ATP. 2 µM of the unlabeled MutH variant S85C C96S were used as competitor.

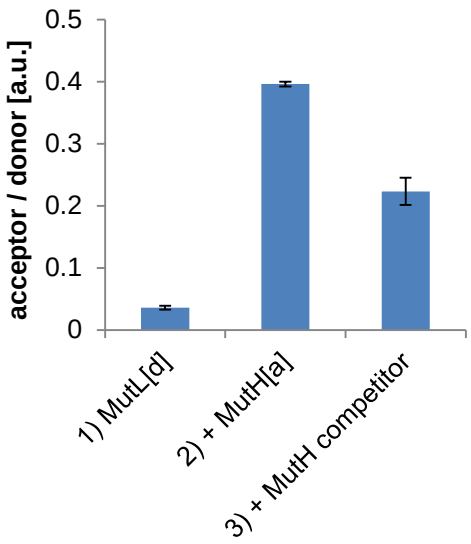

Figure 6.6: FRET efficiency in MutL-MutH complex formation
FRET ratios during the reaction steps visualize the complex formation and dissociation. They were calculated by dividing acceptor emission through donor emission. Error bars indicate the standard deviation of $n = 2$ independent experiments.

The increase in FRET ratio from 0.04 to 0.40 in step 1 to 2 (in Figure 6.6) and the following decrease in step 3 visualize the interaction between MutL and MutH. The FRET ratio decreased from 0.40 to 0.24 after competing the reaction with unlabeled MutH. The ratio did not decrease further as the acceptor fluorophore used for this assay (Alexa 594) was partially excited by the excitation light at 470 nm. It therefore generated a background signal in step 2 and 3.

6.5 Determine MutS binding orientation, varying MutS concentrations

The MutS binding orientation setup (3.3.1.3) was also used with varying MutS concentrations. Thereby only changes in anisotropy of the donor fluorophore was addressed for a double labeled DNA as well as for a donor only labeled DNA (Figure 6.7).

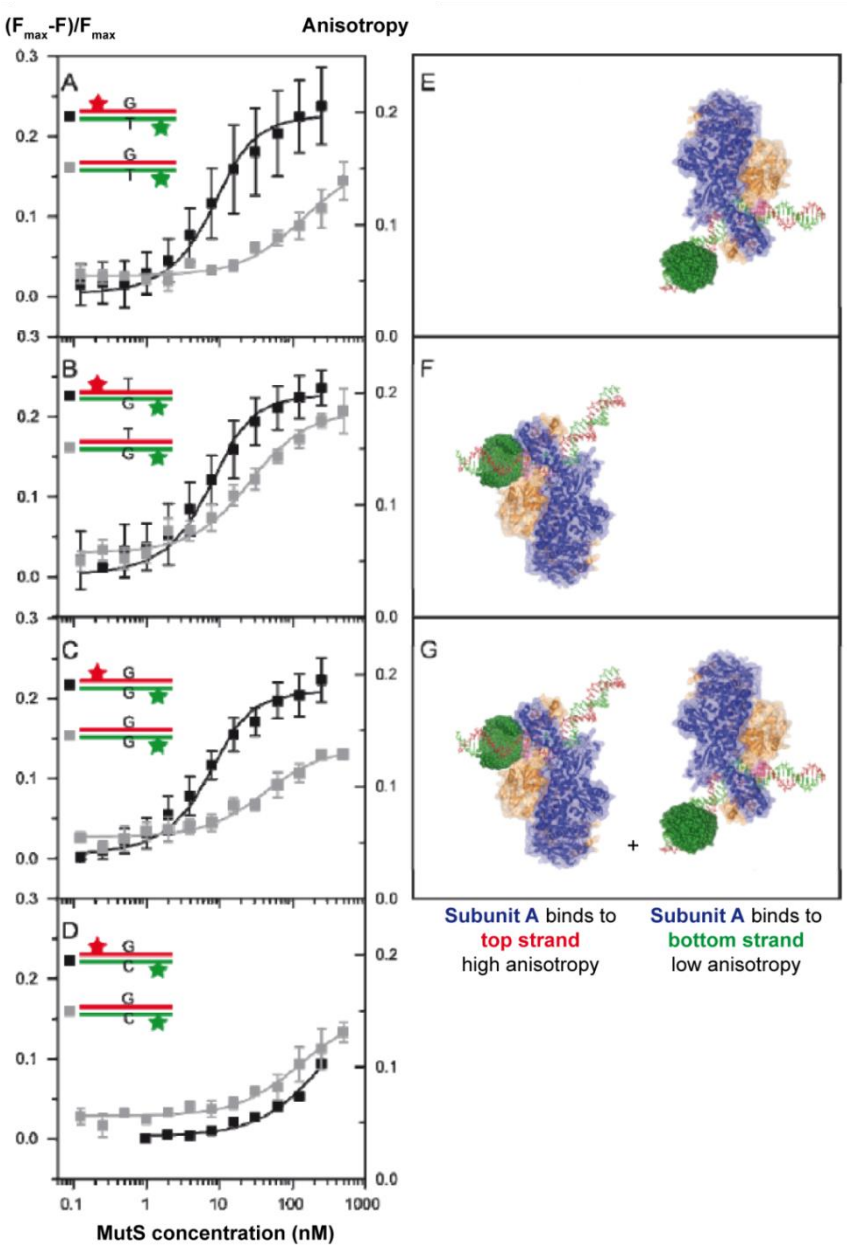

Figure 6.7: Mismatch dependent MutS binding orientation with varying MutS concentrations
A-D Quenched donor fluorescence ((F_{max}-F)/F_{max}, black squares) of a donor fluorophore at a double labeled DNA and anisotropy changes (gray squares) of the donor at a donor only labeled DNA during MutS binding different mismatches or homoduplex DNA (using MutS variant R449C D835R). Error bars derived from the standard deviation of n = 3 independent experiments. **A** G:T mismatch **B** T:G mismatch **C** G:G mismatch **D** G:C homoduplex **E-G** Illustration of MutS binding orientations on DNA. Subunit A (blue) of MutS dimer intercalates phenylalanine 36 into DNA and stacks onto thymine. **E** Subunit A binds the bottom strand at a G:T mismatch **F** Subunit A binds the top strand at a G:T mismatch **G** Subunit A adopts both possible binding orientations at a G:T mismatch.